THERMOREFLECTANCE, REFLECTANCE, AND TRANSPORT STUDIES OF GERMANIUM AND HEAVILY-DOPED n-TYPE InAs

R. R. SENECHAL

Dissertation submitted to the Faculty of the Graduate School
of the University of Ottawa in partial fulfillment
of the requirements for the degree
Doctor of Philosophy

1973

© R.R. Senechal, Ottawa, Canada, 1974.

FORWARD

This thesis reports on some of the research work which I have done as a graduate student in the Physics Department at the University of Ottawa. My initial work was the design and assembly of a versatile Faraday rotation apparatus which could be used at various temperatures with either of two magnets which were then available. This was completed in early 1969; however, I decided not to begin a long series of measurements on the apparatus because it did not look as if there was much to be gained. At this point, I decided to make a concentrated study on heavily-doped n-type InAs using several measurement techniques in order to test the validity of the Kane model at high doping levels, and to test the conclusions made in some work by Drs. C. C. Y. Kwan and J. C. Woolley on the occupancy of a second conduction band at carrier concentrations of the level of 10^{19} cm^{-3}. Because of the difficulty of making useful absorption measurements on heavily-doped material, I decided to try thermally-modulated reflectance as a method of obtaining the position of the Fermi Level in the conduction band. R. Glinski agreed to work with me in setting up an apparatus for the thermo-reflectance measurement. The techniques and equipment were fairly well developed by the summer of 1970, and late in the year I presented a statement of the particular area in which I wished to work alone, namely pure Ge and heavily-doped InAs. This was immediately accepted

by those concerned. All the work described in this thesis was conceived and executed by the author, except where otherwise indicated.

I express deep gratitude to Dr. J. C. Woolley for accepting me in his group, and for permission to follow my decisions to their conclusions, even though they were not always productive. Perhaps more important, I thank him for encouragement during a down-and-out stage of the program, and for making himself available for discussion at all times on any subject. I consider that the optical equipment and accessories, which were provided by Dr. Woolley and Dr. E. Fortin, were sufficient for a wide variety of experiments in modulation spectroscopy.

I have enjoyed my association with all the graduate students. I have benefited particularly from the very active joint program, mentioned above, with R. Glinski who made many important contributions in the development of our high quality thermoreflectance facility, from the discussion of plasma resonance and other transport measurements with G. Dionne, from the considerable advice and co-operation of A. Filion regarding the use of the superconducting magnet, and from the co-operation of A. Taylor, who, at some personal inconvenience, allowed the sharing for a few months of some optical equipment that he had set up. I have learned some procedures of the electroreflectance experiment from O. Berolo and S. Vishnubhatla.

I appreciated the careful work cheerfully done by all members of the model shop staff: N. Goodchild, D. Kingswell, W. Knott, R. Lavigueur, R. Moore and W. Laurin. I thank R. Hart for his help in the fight against imperfect vacuum systems, and A. Buser for the prompt attention he gave to frequent failures in the electronic equipment.

I have benefited from the services of the Optics Shop of the National Research Council: Mssrs. J. N. Cairns and B. Roberts advised me on mechanical polishing procedures, Mr. R. Parent explained in detail the techniques involved in evaporating silicon oxide, and other staff members provided several custom-made mirrors.

I would like to thank Mrs. L. Leroux for a careful typing of the thesis, Miss Sue Ling Kwan for many of the ink drawings, and Mrs. L. Leroux and Miss D. Dube for typing the manuscripts of the publications associated with the thesis.

Lastly, and most important, I acknowledge the financial support of the Awards Office of the National Research Council of Canada for a Post Industrial Experience Research Fellowship in the two years 1968-70, and of the Defence Research Board of Canada and Dr. Woolley for the portion of the grant money of Dr. Woolley which was alloted to me at other times.

TABLE OF CONTENTS

		page
FORWARD		i
CHAPTER 1	Introduction	1
CHAPTER 2	Preparation of and Transport and Reflectivity Measurements on Heavily-Doped n-Type InAs	14
CHAPTER 3	A Method to Facilitate the Use of the Kane Model of the Conduction Band of III-V Semiconductors	39
CHAPTER 4	Thermoreflectance Theory and Technique	54
CHAPTER 5	Thermoreflectance at the Fundamental Gap of Heavily-Doped n-Type InAs	84
CHAPTER 6	Thermoreflectance of Pure Germanium at its Lowest Direct Gap	121
CHAPTER 7	Interim Report on the Work with Germanium on Thermally-Modulated Absorption, and Thermoreflectance in a Magnetic Field	150
CHAPTER 8	Summary and Possible Directions of Future Work	168
APPENDIX A	A Derivation of the Faraday Rotation Result without Decomposition into Circularly Polarized Components	170

APPENDIX B An Attempt at a Different Application of the Kramers-Kronig Relationships 174

APPENDIX C Magnetoresistivity and Hall effect: Two Derivations. 176

APPENDIX D An Alternative Derivation of the Quantum Mechanical Expression for the Dielectric Constant 185

REFERENCES 191

Publications of material in this thesis 201

CHAPTER 1

INTRODUCTION

1.1	Rationale for the InAs Program	2
1.2	Rationale for the Ge Program	8
1.3	Outline of the Chapter-by-Chapter Presentation.	10

INTRODUCTION

This is a report of some experimental work, and of some analyses associated with the experimental results, on two semiconductors, indium arsenide and germanium.

1.1 Rationale for the InAs Program

The motivation of the work on InAs was essentially to determine the Fermi level in InAs doped with various amounts of the impurity selenium, and to compare this with an existing theory, the Kane model[1,2] for the conduction band of group III-V semiconductors, such as InAs, InSb, GaAs. Figure 1 shows the relationship between the energy of electron states and the magnitude of the wave vector, k, in the <100> and <111> crystal directions, according to Kane's theory, for the conduction and three uppermost valence bands on InAs. This figure was prepared by the author by a method which is described in Chapter 5. Spin degeneracy was assumed in making this diagram. If one refers to the abscissa in the upper right hand side of the diagram and uses the conduction band energies immediately below, one has the predicted relationship between the carrier concentration, N, and the position of the Fermi level. It is this behaviour that was tested. One might think that a better way to test the Kane model would be by some method on pure material, because a result on doped material which did not support the Kane band would be negative, in that one would not know whether the Kane model was incorrect, whether the material had

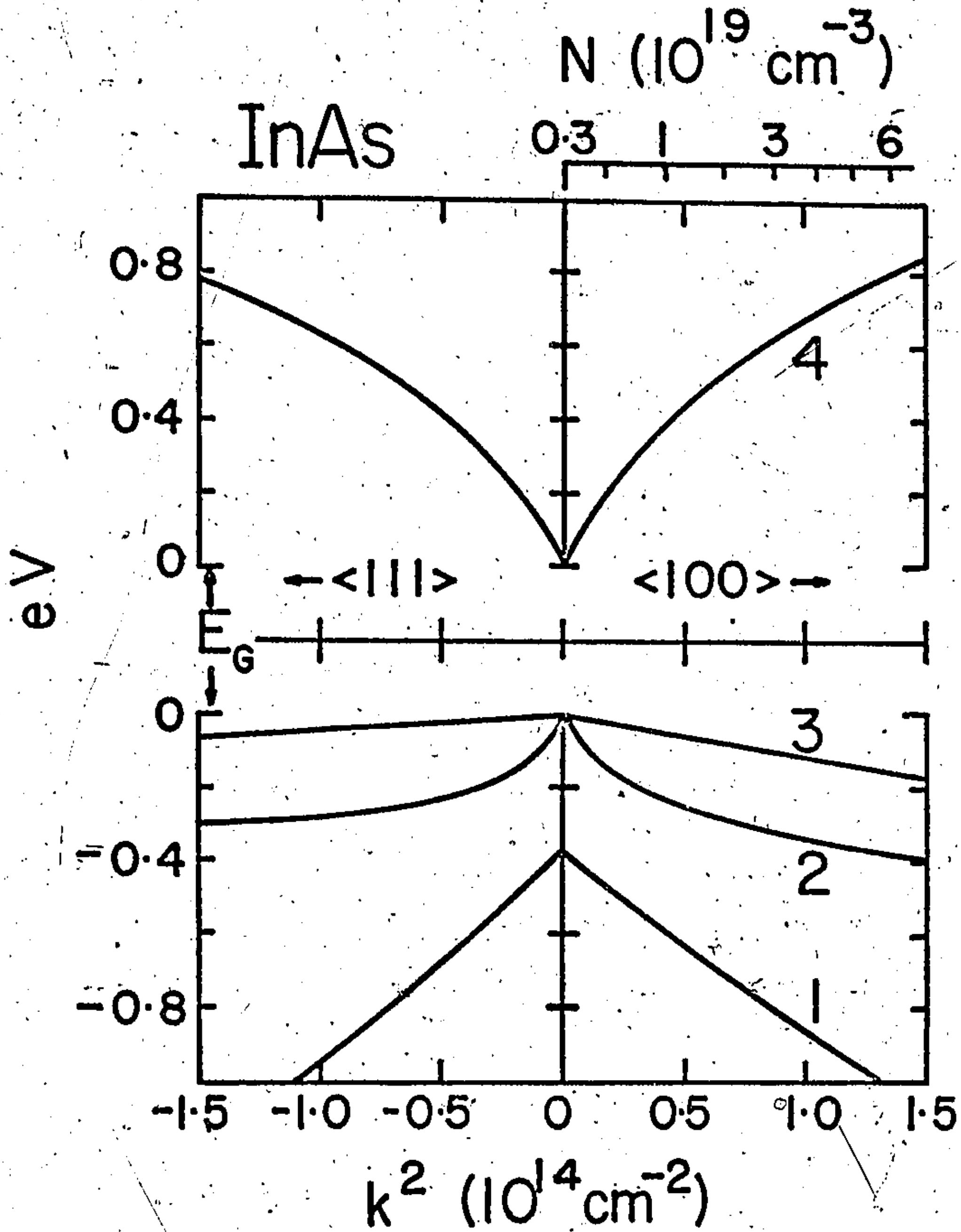

Figure 1. Energy of conduction and valence bands as a function of k^2 in the < 100> and < 111> directions as predicted by Kane's model.

been so perturbed by the doping so as no longer to be representative of the pure crystal, or both. The difficulty with an experiment such as absorption on a pure sample is that, in the interpretation, one is concerned not only with the density of states as a function of energy but also with the energy variation of transition probabilities, the energy variation of the broadening parameters associated with the transitions, with the excitonic component of the absorption[3-8], as well as with the problem of obtaining a strain-free, damage-free, parallel-faced sample. Absorption measurements on pure material have been made, for example, on InAs[9,10], and on InSb[11-13]. The slow variation of the absorption coefficient with energy above the fundamental gap suggests that although one can perhaps establish whether or not the Kane model is consistent with such results, as has been done for InSb by Johnson[14], such a conclusion is far from confirming the model. On the other hand, there have been calculations which estimate the effect of impurities on the distribution of electronic states. This has been reviewed by Bonch-Bruevich[15] and Johnson[14]. The conclusions are that although additional states are introduced near the band extrema, the density of such states is small compared to the density of the intrinsic band states, and thus should have little effect on the Fermi level vs population relation. Thus absorption measurements on doped n-type semiconductors would be expected to give a good measure of the behavior of the E vs k relationship, since absorption would begin only when the energy of the photon

was equal to the energy of separation of a direct transition (that is, between states with the same $\vec{k}$-vector) between a valence band state and an empty conduction band state. This effect of the dependence of the energy of the onset of absorption of a given semiconductor on the concentration of free carriers is called the Burstein-Moss shift.[16,17] However, the absorption result in heavily-doped n-type material, for example in InSb,[18] and InAs,[19] is broad, and does not delineate the separate contributions from transitions initiating at the two upper valence bands, bands 2 and 3 in Fig. 1. Similarly, absorption curves for heavily doped p-type material, as have been obtained and studied in detail[18] for InSb, are broad and contain complicated structures; furthermore, the analysis of the data for the InSb case assumes a conduction band estimated from absorption data on n-type material. Thus because of the lack of promise in an absorption measurement, it was decided to attempt a modulated reflectance method[20,21] which hopefully would respond with peaks in the spectral region of rapid changes in the absorption coefficient. Thermally-modulated reflectance[22,23] was selected because of the ease of its use at various temperatures, and because of the possibility of a relatively straightforward comparison between experiment and theory.

Another way of determining the shape of the conduction band is to measure the effective mass of the conduction electrons around the Fermi level. The effective mass as measured is approximately equal to $\left(\frac{1}{\hbar^2}\,\frac{1}{k}\,\frac{dE}{dk}\right)^{-1}$ at the Fermi level.[24] Thus, from Fig. 1, one would expect

to obtain a series of effective mass values from the variously doped samples. One expects also to be able to take into account the non-sphericity of the Fermi surface, so that a proper comparison can be made. There are three main measurement techniques which have commonly been used to obtain the effective mass in doped materials: infrared reflectivity,[9,25] Faraday rotation,[26] and thermoelectric power in the limit of high magnetic fields.[27] All these techniques have been used, for example, by Kesamanly et al.,[28] to study the conduction band of InAs. The difficulty with the intraband Faraday rotation for heavily-doped materials is that it is a transmission measurement and requires thin samples because the absorption coefficient is high[9]. The troube with the third technique is that high magnetic field is defined by $\mu B \gg 1$, where μ is the mobility and B the magnetic field, and this is practically unattainable in the more heavily-doped material. One is usually content to use an empirical relationship[28,29,30] to fit the magnetothermoelectric power at lower fields, from which one extracts the limiting value. A further complication is that this technique is less sensitive at higher doping levels.

When the author in 1969 had made a first series of measurements of the infrared reflectivity of InAs doped at the level of $10^{19} cm^{-3}$, no such measurements had been reported in the literature. Since that time, two detailed works on effective mass determinations in such material have appeared[28,31], with highly contradictory results. One work[31] required the existence of a second conduction band at 0.3 eV above the

first conduction band in order to reconcile the differences obtained in effective masses measured by the infrared reflectivity and Faraday rotation techniques. Since the appearance of those articles the author found a method of obtaining a good chemical polish on the InAs samples, and a complete series of reflectivity measurements was repeated so as to be more confident in the resolution of the disagreement; these were done in the fall of 1972.

A weakness that has existed in all comparisons between measured effective masses and those predicted by the Kane model is that approximations to Kane's results are always used, and, in particular, Cardona's approximation[26] is often used beyond the range for which it was developed. Furthermore there has been no, or incomplete inclusion of Kane's correction terms due to upper bands. In addition, the previous comparisons made use of values, such as that for the energy of separation of the two upper valence bands and the split-off valence band, and the momentum matrix element between the conduction and valence band states, which have since been corrected by new experiments and calculations.[32-34] Thus a careful study of the Kane form of the band was made so as to reduce the dependence on approximations.

In summary, the modulated reflectance work on InAs was directed at determining transition energies between the upper two valence bands and the conduction band, thereby tracing the variation of these band

energies in k-space. The effective mass work was used as an independent measurement of the form of the conduction band, as well as to resolve a disagreement between results in the literature. The analytical work was directed at predicting the form and magnitude of the thermoreflectance signal, as well as at avoiding the use of unjustified approximations for the Kane band.

1.2 Rationale for the Ge Program

The study on germanium was undertaken basically to test reflectance as a method for obtaining highly resolved data which could be used to compare with theoretical predictions for the variation of absorption around the fundamental gap. Although modulation techniques have been used to determine the energy of the fundamental gap of many materials, there had been no success at comparing the line shape with what was predicted. The studies of Ge and III-V semiconductors were usually interpreted with the assumption of parabolic valence band conduction bands. A detailed quantitative analysis by Aspnes and Frova[35] on their electroreflectance results on Ge revealed that the signals were much larger than predicted by such a model. They stated that a proper analysis would probably require the inclusion of excitonic effects. One expects that the interpretation of thermoreflectance (TR) data would be simpler than that of electroreflectance (ER) data. Thus a definite purpose of the present work became to see if TR data is consistent with Elliott's exciton theory.[3] Germanium is desirable for this purpose because of the following

combination of attributes: a) it can be obtained in a relatively pure state (it had been shown theoretically[36] and experimentally[37] that the addition of impurities broadens the exciton transition); b) the energy of its direct gap was in a spectral region convenient for study by the TR method (this is not true for the wavelength-modulated reflectance technique,[38] since at low temperatures the gap is in the middle of the H_2O absorption bands around 1.4 microns); c) the energy of the first indirect gap is lower in energy than the direct gap, and the absorption coefficient associated with these indirect transitions is sufficient to eliminate a spurious signal which would otherwise occur due to light reflected from the region of the back surface of the sample. Once the method was established in the absence of a magnetic field, it was considered that it would yield better results in a magnetic field than those which had been obtained by Aggarwal[39] by the piezoreflectance technique, and thus provide a tougher test for magnetooptics theories, such as that of Pidgeon and Brown.[40] Although extensive magnetothermoreflectance data has been obtained by the author, no analysis is made in the present thesis.

As part of the thermal modulation program, it was decided to try to complement the TR results with thermally-modulated absorption data. It was hoped to observe a more visual indication of the n = 2 excitonic line, which does not show explicitly in the TR results. In addition, such a measurement would give an independent value for the exciton binding energy, which would be welcome because of the significant disagreement in this value from the TR analysis, and that of recent theory.[41] At present, this project has been completed only from a tech-

nical point of view, in that a method of preparing and mounting five micron thick, damage-free Ge samples has been developed.

In summary, TR measurements were made on Ge to test the TR method itself, and to obtain, if possible the exciton binding energy and the broadening parameter associated with the transition. Some analytical development was made to permit extraction of these values from the data.

1.3 Outline of the Chapter-by-Chapter Presentation.

The following is a chapter-by-chapter outline of the material which will be presented.

Chapter 2 is a report on the work of a routine nature made on the InAs: the preparation of the Se-doped crystals, the determination of the Hall coefficient, Hall mobility, magnetoresistivity, inhomogeneity, and infrared reflectivity at room and liquid nitrogen temperatures. Included with this is a short review of the standard theoretical results required to interpret the data. In the discussion of the theory of infrared reflectivity, a simple treatment is given in terms of scattering times, rather than by the normal method of introducing a damping force.

Chapter 3 presents a simple method developed by the author whereby the Kane model for the conduction band of III-V semiconductors can be used more exactly than is the practice in its application to transport measurements. The method is exact in its use of the positive root of Kane's cubic equation and the isotropic upper band terms. Also a first order treatment of the non-isotropic upper band correction terms is made for some specific cases. The correction terms for different electron spins are

ignored. The results of the analysis are used in a comparison with the experimental effective mass results for InAs given in Chapter 2.

Chapter 4 presents the common background material needed to account for the TR results on InAs and Ge which are presented in Chapters 5 and 6. This is introduced with the theory of reflection and followed by Batz's treatment for thermal modulation at an M_o critical point. The Batz formulae are superceded in Chapters 5 and 6 by new formulae developed by the author which take into account the Kane model for the conduction and valence bands, and the excitonic contribution in a two-band picture, respectively. The techniques developed by the author associated with the TR measurements are included in Chapter 4.

Chapter 5 presents the specific experimental techniques, results and analyses connected with the TR measurements on InAs. The rather lengthy original analysis is directed at finding the quantitative predictions of a TR experiment using Kane's picture.

Chapter 6 is introduced by a summary of Elliott's treatment of the Coulombic electron-hole interaction, which results in an excitonic fundamental absorption edge. His result is developed by the author to get a Lorentzian-broadened derivative of the dielectric constant suitable for comparison with the TR results on Ge. Several new techniques associated with

the reduction of the data and the computer fit of the theoretical to the experimental curves are presented.

Chapter 7 is a cursory record of some unfinished business. The TR results on Ge at about 20K in a magnetic field are presented in a way to indicate some of the information content of the data. No analysis of that data is included in this report. This chapter also contains a statement of procedures which will provide absorption samples of Ge of thickness around 5 microns.

Chapter 8 gives a statement of what is considered to be the main results of the report, as well as a list of suggestions for further work in the general area which seem promising.

Finally, the appendices present four analyses, which occurred to the author during the course of this work, and although not used explicitly in the analysis of the data are related to the general field of interest. In any case, the author considers this a good opportunity to record them. First a derivation of the Faraday rotation effect is given which does not require the use of the usual decomposition of the linearly-polarized wave into left- and right-handed circularly-polarized waves. Secondly, a plausible observation regarding Kramers-Kronig relations is investigated; namely, if one knows, for example, only the real part of the dielectric constant over a limited spectral region, one should be able

to obtain a knowledge, although not as precise, of the imaginary part over the whole spectral region. Thirdly, some derivations are developed to improve the understanding of magnetoresistance and the Hall effect. Lastly, a quantum mechanical derivation of the dielectric constant, which is somewhat different from those found in the literature, is presented.

CHAPTER 2

PREPARATION OF AND TRANSPORT AND REFLECTIVITY MEASUREMENTS ON HEAVILY-DOPED n-TYPE INDIUM ARSENIDE

2.1	Preparation	15
2.2	Review of Theory Associated with the Transport Measurements	18
2.2.1	Conductivity and Hall effect	18
2.2.2	Infrared reflectivity	20
2.3	Measurement of Hall Voltage and Conductivity	27
2.3.1	Preparation of samples and electrical contacts	27
2.3.2	Measurement procedures	29
2.4	Measurement of Infrared Reflectivity	29
2.4.1	Sample preparation	29
2.4.2	Measurement procedures	30
2.5	Results and Comments	31
2.5.1	Electrical results and discussion	31
2.5.2	Optical results and discussion	33
2.5.3	Comments on infrared reflectivity fitting	36
2.6	Conclusions	37

All the experimental work and evaluation of data in this chapter are original works by the author.

2.1 Preparation

Indium arsenide is a crystal of two overlapping face-centered cubic lattices,[42] one with indium atoms and the other with arsenic atoms. The electron disposition in the outer shells of arsenic is $4s^2 4p^3$. The group VI elements which have the most similar outer shells are O, S, Se, and Te with outer shells of $2s^2 2p^4$, $3s^2 3p^4$, $4s^2 4p^4$, and $5s^2 5p^4$, respectively. Of these the atom Se is closest to As, and one would expect it to be the best element to use for n-type doping. The segregation coefficients for several impurities in InAs are given by Schillman[43] for atomic percent concentrations up to several millipercent. The values for Se and S are close to unity, that for Se a little higher at higher concentrations. The Te value is considerably lower.

Ingots of mass about 5 grams were prepared by heating mixtures of InAs of an impurity level of $10^{16} cm^{-3}$ with In_2Se_3 to 990°C, vibrating at about 7 cycles per second for 15 minutes, and then cooling continuously to 800°C at about 5°C/hr. Exception was made for the three most lightly-doped crystals by mixing InAs with some material from the second most heavily-doped InAs ingot. This was done because of the small amount of Se which was required. A vertical furnace was used, with a temperature variation when empty across the part which was used of 6C° over a length of 4 inches. The ingot constituents were vacuum-sealed together with some excess arsenic in quartz ampoules. Groups of

three of such ampoules were vacuum-sealed in larger pieces of quartz tubing, so as to prevent oxidation should the small ampoules break during the slow cooling. The temperature variation was accomplished by a motor-driven Variac. The vibration was accomplished by putting the rod which supported the large ampoules in spring contact with a rotating eccentric wheel. The idea for this accessory was initiated, I believe, by Dr. C. C. Y. Kwan.

The resulting ingots approximated cylinders of diameter 8 mm and length 18 mm. They consisted of a composite of single crystals, of typical dimensions from 1 to 10 mm. There was no correlation noted between the doping level and the size of the crystals. It seems that not much further effort would be required to approach a single crystal result for any such ingot.

To indicate the effectiveness of the doping, Fig. 2 shows the relationship between the effective doping achieved, as determined from the Hall coefficient, and the carrier concentration calculated assuming that each Se atom is a donor. This interpretation assumes that the Se was homogeneously distributed over the ingot. Some measurements were made to test this. On the most heavily-doped ingot, Hall measurements on two preliminary samples, one central, and the other within 1.5 mm of the outside surface of the ingot, differed by 15 percent, the higher concentration being on the outside. Figure 2 also includes a point

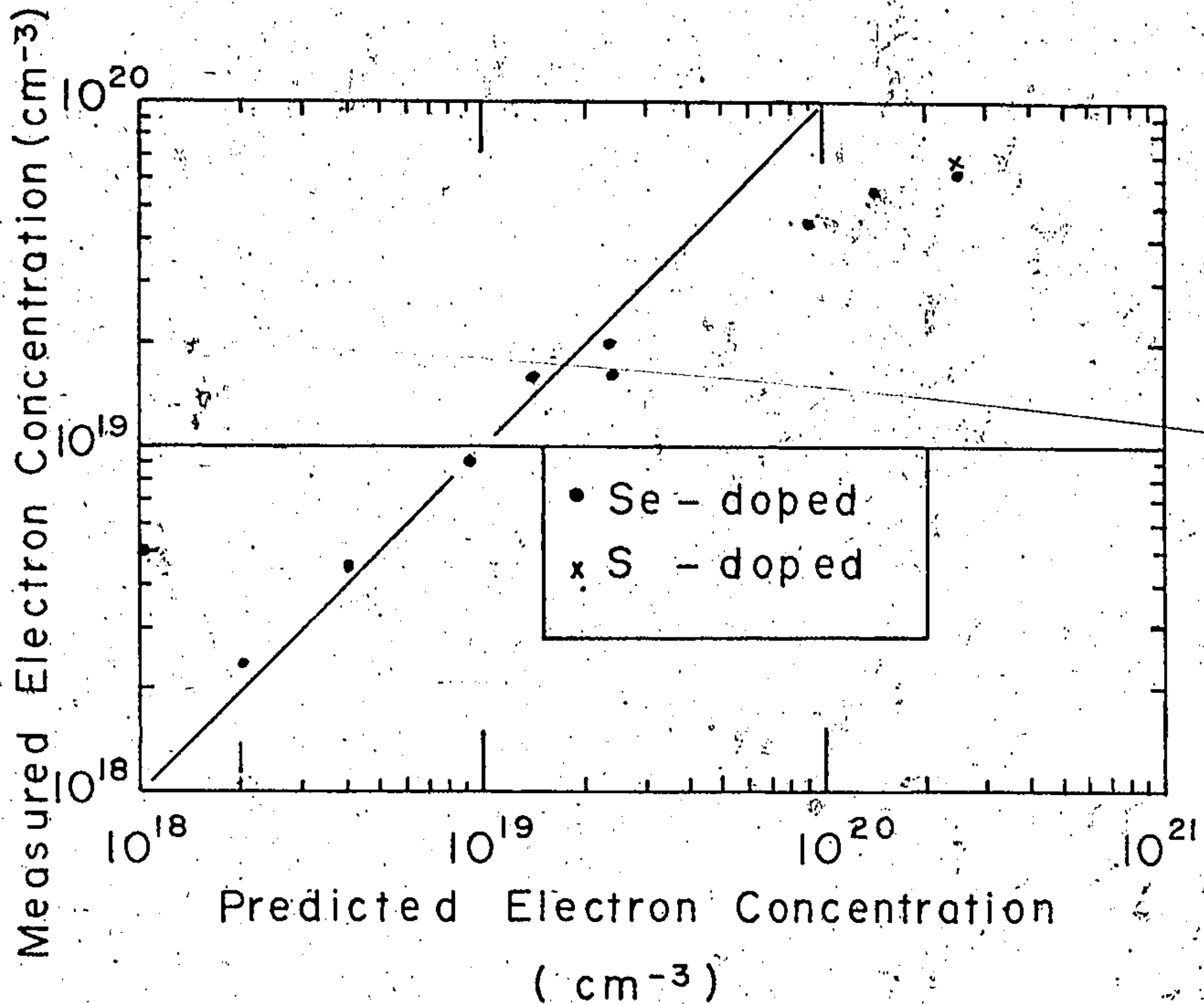

Figure 2. Measured electron concentrations in doped InAs compared to the electron concentrations predicted by assuming that each impurity atom contributes one electron to the conduction band. The diagnal line would result were there a one-to-one correspondence.

taken, for comparison purposes, with an ingot doped with InS. The only conclusion that will be made here is that the growth procedure described produces good quality material with a maximum effective doping by Se or S of the order of $6 \times 10^{19} cm^{-3}$. It is noted that InAs grown by the Czochralski method with a flux has apparently the same upper doping limit.[28]

2.2 Review of the Theory Associated with the Transport Measurements

2.2.1 Conductivity and Hall effect.

The concepts and calculations involved with simple models for the electrical conductivity can be found in many places (for example, references 44 and 24) and will not be repeated here.

The two commonly found treatments are: (1) the treatment of electrons as charged balls with energy dependent relaxation times; (2) the treatment of the perturbation of the distribution function for electrons of wave vector $\underline{k}$ in an electric field $\underline{\mathcal{E}}$. Method (2) is the Boltzmann equation method, and, in standard treatements, involves the use of relaxation times, τ, which characterize the rate of approach to the equilibrium distribution after the field is turned off. When one considers a degenerate electron gas in a band characterized by spherical energy surfaces in k-space, the conductivity is given by $Ne^2\tau/m^*$, where (τ/m^*) is evaluated at the Fermi level. In the expression for the conductivity N is the electron concentration, e, the electron charge, and m^*,

defined by $(m^*)^{-1} = (\hbar^2 k)^{-1}(dE/dk)$, is the effective mass of the electron evaluated at the Fermi level. The kinematic model of treatment (1) above will give the same result only if all the electrons are considered as having the same (τ/m^*) value.

The solution of the Boltzmann equation for the case of electric and magnetic fields (the Hall effect-case) in which the values of m^* and τ for the electrons are energy dependent is not simple. It has been carried out for the case of spherical energy surfaces in k-space by Kolodziejczak[46] following a method developed by McLure.[47] When degenerate statistics apply, this gives the same result as for carriers with a constant relaxation time and mass, namely, $R_{Hall} = (Ne)^{-1}$.

There will be no attempt to treat the magnetic effects for non-spherical energy surfaces. Perhaps such a problem would have been studied had one made measurements on an oriented single crystal. Presumably, one would follow the Jones-Zener method,[48] or the more recent approach by Allgaier.[49,50]

Some simple derivations for the Hall and magnetoresistance effects are given in Appendix C. These presentations are different from what the author has otherwise read, and are more pictorial, in that they treat orbits as well as current vectors.

2.2.2 Infrared reflectivity

The series of steps which are followed to relate the reflectivity of a vacuum-solid interface to the conductivity, σ, and the dielectric constant, ε, will be summarized here. Maxwell's equations for a homogeneous isotropic non-magnetic medium with no net charge can be combined to produce an equation for the spacial variation of an electric field of angular frequency ω of the form[51]

$$\nabla^2 \underline{\mathcal{E}} + (1 + \frac{i\sigma}{\varepsilon\omega}) \mu_o \varepsilon \omega^2 \underline{\mathcal{E}} = 0 \qquad 2 - (1)$$

in rationalized mks units, where $\varepsilon = \kappa\varepsilon_o$, where ε_o, μ_o are the constants relating $\underline{D}$, $\underline{\mathcal{E}}$, and $\underline{B}$, $\underline{H}$, respectively, in vacuum. Linearly polarized plane wave solutions of 2-(1) which include the time factor, are

$$\underline{\mathcal{E}} = \mathcal{E}_o \vec{1}_y e^{2\pi i (kx - \nu t)} \qquad 2 - (2)$$

where

$$k^2 = \mu_o \varepsilon_o \kappa \nu^2 (1 + \frac{i\sigma}{\varepsilon\omega}), \qquad 2 - (3)$$

$\omega = 2\pi\nu$, and, where, for definiteness, the wave is propagating along the x-direction with its electric field along the unit vector, $\vec{1}_y$, in the y-direction. It is straightforward to show also that $\underline{H}$ associated such an electric field is

$$\underline{H} = \frac{k}{\omega\mu_o} \vec{1}_x \times \underline{\mathcal{E}} . \qquad 2 - (4)$$

Expressing k in its real and imaginary parts

$$k = \sqrt{\mu_o \mathcal{E}_o}\ \nu (\kappa (1 + \frac{i\sigma}{\omega \varepsilon}))^{\frac{1}{2}} = \frac{\nu}{c} (n_1 + in_2) = \frac{\nu}{c} \tilde{n} \qquad 2 - (5)$$

where $c = (\mu_o \varepsilon_o)^{-\frac{1}{2}}$ is the velocity of light in a vacuum, and n_1 and n_2 are the real and imaginary parts of the index of refraction. Eq. 2- (2). in these terms becomes

$$\underline{\mathcal{E}} = \mathcal{E}_o \vec{1}_y\, e^{2\pi i [x(\frac{n_1}{\lambda}) - \nu t]}\ e^{\frac{-2\pi n_2 x}{\lambda}} \qquad 2 - (6)$$

where $\lambda = c/\nu$ is the vacuum wavelength of a wave with frequency ν.

Consider now what happens when such a wave is incident on a solid from a vacuum. Normal incidence is treated to show the idea, and the Fresnel equations for non-normal incidence are developed in detail in many places (e.g., Ref. 52). Maxwell's third and fourth equations require that the electric field and magnetic field intensity be continuous at the surface. Thus indicating by $\mathcal{E}_i$, $\mathcal{E}_r$, and $\mathcal{E}_t$, the values of the electric field along the y-direction at the inter-

face for the incident, reflected, and transmitted waves, respectively, one has

$$\mathcal{E}_i + \mathcal{E}_r = \mathcal{E}_t$$
$$\mathcal{E}_i - \mathcal{E}_r = \tilde{n}\mathcal{E}_t \qquad 2-(7)$$

where $\tilde{n}$ characterizes the solid. Solving one gets

$$\frac{\mathcal{E}_r}{\mathcal{E}_i} = -\frac{\tilde{n}-1}{\tilde{n}+1} = -R^{\frac{1}{2}}e^{i\phi} \qquad 2-(8)$$

having chosen the convention that $\phi = 0$ for metallic reflection. The fraction of the energy reflected, R, is equal [51] to the square of the absolute value of Eq. 2-(8).

$$R = \frac{(n_1 - 1)^2 + n_2^2}{(n_1 + 1)^2 + n_2^2} \qquad 2-(9)$$

Now, how are these n_1, n_2 values related to the currents and charge displacements in the solid? Maxwell's fourth equation states[51]

$$\underline{\nabla} \times \underline{H} = \underline{j}_{true} + \frac{\partial \underline{D}}{\partial t} \qquad 2-(10)$$

where j_{true} relates to the movement of unbound charges. For a time dependence $e^{-i\omega t}$

$$\begin{aligned}\underline{\nabla} \times \underline{H} &= \sigma \underline{\mathcal{E}} e^{-i\omega t} - i\omega\varepsilon \underline{\mathcal{E}} e^{-i\omega t} \\ &= (\sigma - i\omega\varepsilon) \underline{\mathcal{E}} e^{-i\omega t}\end{aligned} \qquad 2-(11)$$

Since this last equation on the right hand side just expresses the total current, the unbound charge current + polarization current + vacuum displacement current, we are at liberty to define σ_1 as the total real part (i.e. the in-phase conductivity) of the bracketed expression, and σ_2 as the imaginary part; that is,

$$\tilde{\sigma} = \sigma_1 + i\sigma_2 = -i\omega\tilde{\varepsilon} = -i\omega(\varepsilon_1 + i\,\varepsilon_2)$$

$$= -i\omega\,\varepsilon_o\,(\kappa(1 + \frac{i\sigma}{\varepsilon\,\omega})) = -i\omega\,\varepsilon_o\tilde{n}^2 \qquad 2 - (12)$$

where now a complex dielectric constant $\tilde{\varepsilon}$ has been defined. Finally one has

$$\varepsilon_1\varepsilon_o^{-1} = n_1^2 - n_2^2$$

$$\varepsilon_2\varepsilon_o^{-1} = 2n_1n_2 \qquad 2 - (13)$$

Now the complex conductivity will be related to the effective mass m*, the carrier concentration, n, and the relaxation time, τ. As in the treatment of the dc conductivity, there are two approaches, the kinematic and the distribution approach. Since we may expect, as in the dc case, that the result from the kinematic model will be the same as the Boltzmann equation results for a band with spherical energy surfaces, in k-space when the electron gas is degenerate, and since the author believes to have a very clear way of presenting the kinematic model, it will be treated in more detail than the correct Boltzmann procedure.

First the component of $\mathcal{E}$ due to unbound electrons will be considered.

One often (for example, Refs. 53-56) comes across derivations of the a.c. conductivity of solids which make use of a damping force term, $-\gamma \underline{v}$ in the equation of motion for unbound electrons. This approach is justifiable since it gives the same result for the complex conductivity as a statistical treatment for the movement of electrons which are subject to collisions. The results are the same if γ is put equal to $m^* \tau^{-1}$, where τ^{-1} is the proportionality constant in the expression for the probability of collision in a time increment, Δt. However, the author is not aware of a presentation of a justification of the damping force approach prior to the solution stage, which, albeit short and simple, is given here.

Consider a population of electrons such that their movement between collisions is determined by the force $-e\underline{\mathcal{E}}_o \cos \omega t$. For simplicity, it is assumed that the collisions are randomizing, that is, the average velocity of electrons after collision is zero. Thus in a time increment, Δt, all electrons will have their velocity $\underline{v}$ varied according to

$$\dot{\underline{v}} = -(e\underline{\mathcal{E}}_o/m)\cos \omega t \qquad 2 - (14)$$

whereas those which endure a collision will have an average additional velocity change which is equal to the average velocity of the population,

$\underline{v}_{av}$. Since the probability of collision for any electron is $\Delta t/\tau$, the average change in the velocity of the distribution due to collisions is

$$(\Delta \underline{v}_{av})_{coll.} = -(\Delta t/\tau)\underline{v}_{av} \qquad 2-(15)$$

Since the change of an average equals the average of a change, Eq. 2-(15) becomes, as $\Delta t \rightarrow 0$

$$(\dot{\underline{v}}_{av})_{coll.} = -\underline{v}_{av}/\tau \qquad 2-(16)$$

Thus it is clear that the scattering model can be represented with regard to the average effect of field and collisions by

$$m^*\dot{\underline{v}}_{av} + (m^*/\tau)\underline{v}_{av} = -e\underline{\mathcal{E}}_o \cos \omega t \qquad 2-(17)$$

It may be noted that Eq. 2-(15) accounts as well for the collision effects during any transient behaviour that would follow a change in the field condition, e.g. if the field is turned on or off.

Writing the field in the exponential form so as to get the in and out of phase components of the current more directly, the solution of Eq. 2-(17) is

$$\underline{v}_{av} = \frac{-e\tau\mathcal{E}_o e^{-i\omega t}}{m^*}\left(\frac{1}{1-i\omega\tau}\right) + c_1 e^{-t/\tau} \qquad 2-(18)$$

Assuming the field turned on at $t = 0$, and $\underline{v}_{av}(t = 0) = 0$, one has

$$\underline{v}_{av} = -\frac{e\tau\mathcal{E}_o}{m^*}\left(\frac{1}{1-i\omega\tau}\right)\left(e^{-i\omega t} - e^{-t/\tau}\right) \qquad 2-(19)$$

and for $t \gg \tau$, one gets the free carrier contribution to the complex dielectric constant as

$$\varepsilon_1 = \frac{-Ne^2}{m^*}\;\frac{\tau^2}{1+\omega^2\tau^2} \qquad 2-(20)$$

$$\varepsilon_2 = \frac{Ne^2}{m^*}\;\frac{\tau}{\omega(1+\omega^2\tau^2)} \qquad 2-(21)$$

To these values must be added the contribution of the bound electrons and ionic polarizations to the complex dielectric constant (e.g. Ref. 53, p. 165). However, this is easy in the present case since it is known[57] that n_1 for pure material varies by only 3 percent and n_2 is negligible, in the spectrum of interest, 5 to 20 microns. Thus, the real part is changed to

$$\varepsilon_1 = \varepsilon_\infty - \frac{Ne^2}{m^*}\;\frac{\tau^2}{(1+\omega^2\tau^2)} \qquad 2-(22)$$

One may wonder why the bound carriers give a positive contribution to the dielectric constant whereas the unbound ones a negative contributions. This can be "explained" in a classical model with a bound charge moving with natural frequency ω_o. If one looks at the equations[56] one sees that when the driving frequency ω is greater than ω_o, the phase relationship in ε_1 is that of free charge, whereas when $\omega < \omega_o$, it is 180 degrees out of phase. In the present case $\hbar\omega_o$ would be of the order of

the excitation energies of the bound carriers.

The Boltzmann equation solution of the ac conductivity has been treated in detail by Fan[58] and Spitzer and Fan[9], and will not be treated here. It is simply noted that the result for the complex dielectric constant in the case of a spherical band with degenerate statistics is the same as that of Eq. 2-(21) and 2-(22) provided m* is interpreted as

$$\frac{1}{m^*} = \frac{1}{\hbar^2} \left(\frac{1}{k} \frac{\partial E}{\partial k}\right)_F \qquad 2-(23)$$

where the subscript F indicates evaluation at the Fermi level.

2.3 Measurement of Conductivity and Hall Voltage

2.3.1 Preparation of samples and electrical contacts

The sample for the Hall effect and conductivity measurements were typically 15 mm long, 2.5 - 3.0 mm wide and 1.0 mm thick. Line contacts were put on the sides, on one side, one in the center, while on the other side, one in the center, and one about 3 mm away on either side of the center. The ends were completely covered with contact material. This geometry essentially eliminated any geometrical effects[59-62] in the measurement of the Hall voltage[59] and the magnetoresistivity.[60-62]

Initial contacts were made to the InAs by electroplating

indium[63] through a mask. The mask was prepared as follows: the samples were dipped several times in a 20:1 methanol:resin mixture followed by drying each time under a heat lamp; lines were cut through the coating in a jig which was designed to hold the sample as well as to allow a 0.003 in. wide saw blade to cut through the coating transversely on the sides; the coating was ground off the ends on a glass lap. Electrical contact for the sample in the bath was provided by a platinum probe spring held in a teflon jig. Once electrical contact was made the contact area was coated with the resin mixture. The electroplating circuit was operated at about 0.5 ma per mm^2 during one hour. The resin was then dissolved in methanol, and the samples were heated in He or N_2 gas to 350°C in a furnace made by the author for that purpose. Finally, indium-dipped gold wires were connected to the sample contact areas by current pulsing.

The author does not recommend this procedure, without testing, for making contacts to relatively pure samples because of uncertainty of the purity of the plated indium. However, the line contacts are ideal for the application of the van der Pauw method[64] for determining resistivities and carrier concentrations. That method was verified by the author during this work on a single crystal sample of carrier concentration about 10^{16} cm^{-3}.

2.3.2 Measurement procedures

The measurements were made at 77 and 300K in a cryostat designed by Dionne.[65] The measurements were made at 7 and 30 kG in both field directions for both current directions in order to eliminate contact misalignment and thermal voltages effects. Currents of 50 and 100 ma were used. The Hall voltages between the central contacts were used to calculate the carrier concentrations. Hall voltages were also measured between center-to-off-center contacts to estimate inhomogeneity in the samples. The resistivity and magnetoresistivity voltage measurements were made between the two off-center contacts.

2.4 Measurement of Infrared Reflectivity

2.4.1 Sample preparation

Two sets of samples were prepared, one in 1969, the other in 1972. The first set was made from material which was adjacent to the Hall sample material, whereas the second set was the Hall samples themselves. The measurements were repeated so as to obtain more careful measurement of the absolute reflectivity. This was achieved by an improved spectrometer arrangement, as well as by improved chemical polishing on the samples. The samples were prepared by lapping on glass with a 5 micron Al_2O_3 - water mixture, followed by mechanical polishing with the same mixture on cloth. The first chemical polish which was used was a good GaAs polishing solution,[66] $7H_2SO_4:1H_2O_2:1H_2O$. This is not recommended because it creates a heavily-pitted surface on Se-doped InAs.

The polish used for the second set of InAs samples was a 5 percent solution of bromine in methanol. This results in pit-free, mirror-like surfaces, except for some delineation of grain boundaries. The etch rate was measured at about 30 microns per minute, and is practically independent of the Se impurity level in InAs.

2.4.2 Measurement procedures

The dispersion apparatus was a Baird Associates, Inc., double beam, double pass, prism spectrophotometer, used in single beam operation. NaCl and KBR prisms were used in the range 3 to 20 microns. All the mirror surfaces were redone and blinds were placed at critical locations to reduce scattered light. This was considered successful since absolute reflectivities of one percent and less were measured in the range 5 to 12 microns. The reference mirror was an aluminum film evaporated on glass. The inexperienced worker is cautioned not to use an aluminum film protected by a silicon or magnesium oxide film unless it has been calibrated, since this can introduce errors of the order of 10 percent.

The detection system was a platinum strip bolometer bridge with a transformer output feeding into one preamplifier tube stage; followed by input to a PAR Model 129 lock-in amplifier. The reference signal came from a CdS cell circuit placed in the 10 Hz chopped light beam ahead of the entrance slit to the prism chamber. The user of the above lock-in, the reference circuit of which automatically uses whatever reference

frequency is offered without operator tuning, is advised that the lock-in requires a clean signal, such as is not provided by standard mechanical breaker circuits, as supplied with the Baird apparatus. Of note in the detector system is the bolometer, fabricated, it seems, at NRC, in which the platinum strip is in total contact with a KBr crystal which apparently was melted onto it. This contrasts with more orthodox designs where the element is surrounded by a vacuum space.

With the first set of samples, runs were made at room and nitrogen temperatures in a cryostat which followed a design of Fortin.[67] Reflectivity minima were carefully determined in this case; however, the measurement of the absolute reflectivities was not well done. The second set of samples was measured only at room temperature, but with care to check the reproducibility and to obtain the absolute reflectivity. An upper limit on the error in these measurements in the 3 to 13 micron range is estimated at (0.5 ± 0.02R) percent where R is the measured reflectivity in percent. The measurement range for each sample was from 3 microns to the wavelength at which the reflectivity was at least 75 percent, and in most cases at least 90 percent.

2.5 Results and Comments

2.5.1 Electrical results

The electrical results are summarized in Table I. The mobilities are approximately 15 percent higher than those of Korenblit et al.[27]

Table I   Summary of the data on the InAs samples

[a] N_{300K} $10^{19}cm^{-3}$	[a] N_{77K} $10^{19}cm^{-3}$	[b] μ_{300K} $cm^2/V\text{-}sec$	[b] μ_{77K} $cm^2/V\text{-}sec$	[c] Inhomo-geneity	[d] $\frac{\rho_H - \rho_o}{\rho_o}$	[e] λ_m(300K) microns	$\frac{\lambda_m(300K)}{\lambda_m(80K)}$	[f] R_m (300K)
.242	.243	9260	11200	.03	.12	15.70	1.025	2.3
.465	.467	7060	8060	.01	.02	12.17	1.04	0.9
.499	.500	6970	8140	.03	.04	11.45	1.03	5.0
.913	.918	5240	5880	.01	.01	9.70	1.07	1.1
1.61	1.62	3850	4370	.08	.01	8.12	1.03	4.7
1.60	1.61	3800	4340	.02	.01	7.54	1.06	3.9
2.03	2.07	3140	3570	.06	.01	6.51	1.05	4.9
4.65	4.73	1610	1790	.04	.00	5.20	1.02	1.1
5.48	5.60	1312	1456	.02	.00	5.15	1.03	3.2
6.16	6.28	1202	1330	.02	.00	5.06	1.01	0.4

[a] from R_H, the Hall coefficient, at 30 kgauss; [b] Hall mobility; [c] fractional difference in R_H for sets of contacts 5 mm apart along sample; [d] fractional magnetoresistivity at 30 kgauss at 300K; [e] wavelength of reflectivity minimum; [f] minimum value of the reflectivity (in percent).

who prepared samples doped with sulphur. The mobility is almost inversely proportional to the carrier concentration for $N > 10^{19}cm^{-3}$. The magnetoresistivities were highest at lower concentrations, and one speculates that this results from inhomogeneities. There was no confirmation of the results of Kwan and Woolley,[68] and in particular $(\Delta\rho/\rho)$ values of 0.02 for the most heavily doped samples were not observed. There is no support here or in other work for their conclusions regarding the existence of subsidiary minima in the <111> directions at 0.7 eV above the <000> minimum. Rather, as will appear in Section 2.5.2 and in Chapter 5, a single Kane band[1] at <000> gives a pretty good interpretation of all other data.

2.5.2 Optical results and discussion

The room temperature reflectivity data was fitted using Eqs. 2-(9), 2-(21) and 2-(22), with m^*, τ, and ε_∞ as variable parameters. However, in no case was the value of τ the same as that calculated from $\tau = \mu m^*/e$. The optical mobilities were always between 0.5 and 0.8 of the Hall mobilities. The dielectric constant in the fits was typically 11.5 ε_o. Table I gives the wavelength values of the reflectivity minima as well as the values of the minimum reflectivities. The minimum reflectivity values are high, since for samples of the type used here where $\omega^2\tau^2 > 1000$, the minimum reflectivity, R_m, should be less than 1 percent in every case.[69] It is speculated that these high R_m values result from inhomogeneity; one can readily visualize that the super-

position of two reflectivity curves, the minima of which are slightly displaced in wavelength, would result in a higher R_m than that of either curve. The only other published data[70] for the value of R_m for a sample of InAs in the discussed doping range has R_m equal to 7 percent for $N = 9 \times 10^{18} cm^{-3}$. Rather than try to squeeze a meaningless fit, it was decided to obtain values for the effective masses at the Fermi level from the values of the wavelength, λ_m, at which R_m occurs, that is when $n_1 \approx 1$. From Eq. 2-(22)

$$m^* \approx \frac{Ne^2}{\omega_m^2 (\varepsilon_\infty - \varepsilon_o)} \qquad 2-(24)$$

where $\omega_m = 2\pi c/\lambda_m$. A value of 12.0 was used $n_{1\infty}^2$.[57,71] According to Moss et al.,[69] the approximation 2-(24) is better than one percent for homogeneous samples of the present $\omega\tau$ values. Assuming that a temperature dependence of ε_∞ for InAs determined[72] above room temperature can be extrapolated to 77K, m* decreases on the average by 4 percent between 300 and 77K. A theoretical estimate of m* vs. N has been made by the author using the exact form of the Kane model for E vs. k,[1] including upper band corrections. A simple method of making this calculation, as well as others that one commonly meets, is described in Chapter 3. Fig. 3 gives the theoretical curve as well as the present and previous[28,31,9,26,70] values for m* as determined from infrared reflectivity. m* was calculated from the λ_m values in Ref. 28 using $n_{1\infty}^2 = 12.0$. One other set of data[73] is ignored here for the reason given in Ref. 28. It is concluded from Fig. 3 that the results of Ref. 28 are correct, and that

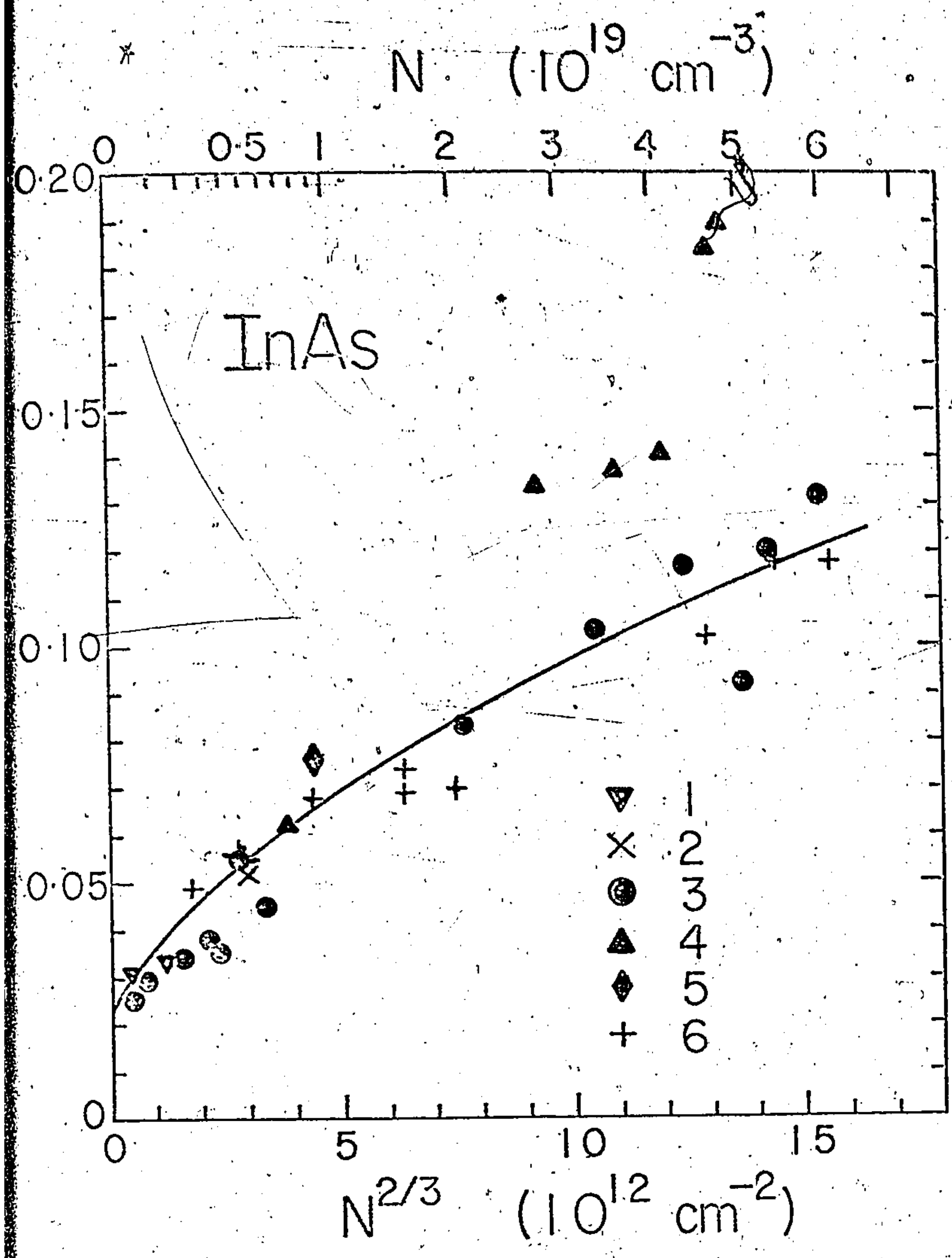

Figure 3. Comparison between calculated (smooth curve) and experimental values of the effective mass determined from infrared reflectivity as a function of $N^{2/3}$ 1),Ref. 9; 2),Ref. 26; 3),Ref. 28; 4),Ref. 31; 5),Ref. 70; 6), present data (300K).

there is no need to invoke[31] an additional band at 0.3 eV above the first minimum to explain the optical data for the effective mass. It is satisfying to note that the masses determined in Ref. 31 from the Faraday rotation experiments, fall near the theoretical curve of Fig. 3. As a cause of error in the work of Ref. 31, one can guess, from the low mobilities in the material that they used, that the inhomogeneity was much more dominant than in the present case. It is noted also that the optical gap values given in Ref. 31 are not correct, as will be seen from the thermoreflectance data and analysis of Chapter 5.

2.5.3 Comments on infrared reflectivity fitting

It seems to be accepted, especially in view of the strong statement by Moss et al.,[69] that infrared reflectivity can be used to determine (N/m^*) and τ. However, the author is aware of no case where there has been a good agreement ($\pm$ 10 percent) between the values of τ_e as determined from electrical measurements and τ_{op} from reflectivity measurements. It has been concluded from some fits[74-77] that $\tau_{op} \approx 0.5\tau_e$. But what does this mean, since the equations which are assumed say that $\tau_{op} = \tau_e$? It seems instead that the optical formulae are not completely valid, perhaps due to boundary conditions at the surface which are not taken into account in the simple theory. In order to check the invalidity of the formulae, the author fitted the results of Spitzer and Fan on InSb and InAs; they gave $\tau_{op} \sim 0.6\ \tau_e$ for InSb on the average over 5 samples, and $\tau_{op} = 0.4$, and $1.4\tau_e$ for the two InAs samples. As a further check,

the author took the prime example of Moss et al.,[69] in which N and τ were determined from λ_m and R_m. Using these values a curve of R vs λ was produced using Eqs. 2-(9), 2-(21) and 2-(22). The results are presented in Fig. 4. A useful bit of information is that, for the curves tested here, τ_{op} approaches τ_e the less one uses the part of a reflectivity curve past the minimum.

The author would like to make clear the point of disagreement with the method of Moss et al. In their paper[69] they show that equations 2-(9), 2-(21) and 2-(22) can be analyzed in a way such that from a knowledge of the value of the minimum value of the reflectivity and the wavelength of the reflectivity minimum one can obtain (N/m^*) and τ. The present author agrees with that; however, he points out that the Moss method should only be applied when equations 2-(9), 2-(21) and 2-(22) apply to the data.

2.6 Conclusions

The main original results of this chapter are considered to be:

(a) good quality, heavily-doped, n-type InAs can be prepared by slow cooling through the temperature region of the freezing point;

(b) the plasma resonance effective masses for heavily-doped, n-type InAs are in pretty good agreement with what is predicted by the Kane theory for a single band, thus settling a controversy which existed in the literature;

(c) there is no confirmation of published data on magnetoresistivity magnitudes in heavily-doped, n-type InAs, and

(d) the unquestioning application of the simple theory of infrared reflectivity to determine relaxation times is liable to lead to error.

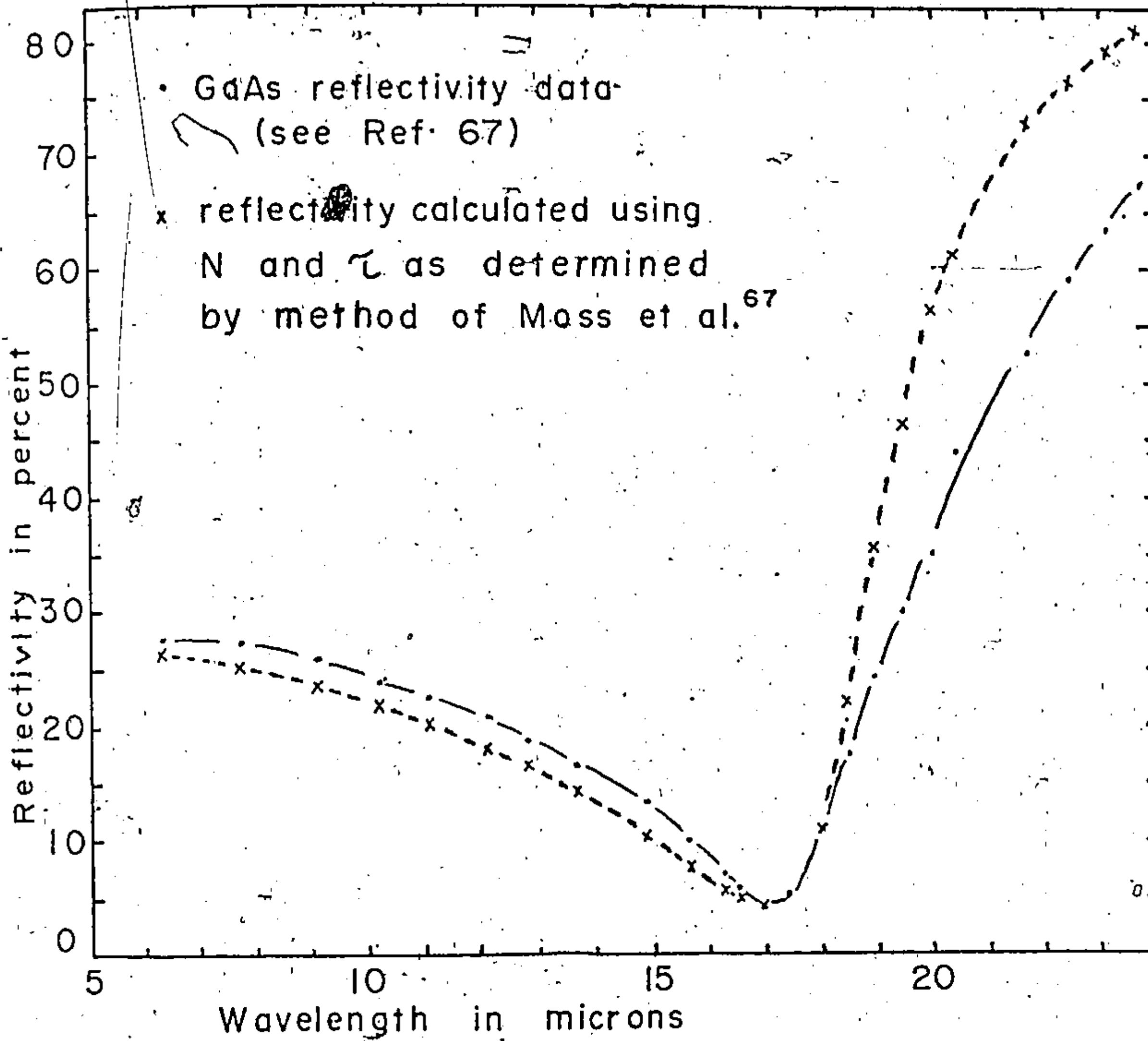

Figure 4. A demonstration of the ineffectiveness of the method of Moss et al. (Ref. 67) to extract correct values of τ from infrared reflectivity minima.

CHAPTER 3

A METHOD TO FACILITATE THE USE OF THE KANE MODEL OF THE CONDUCTION BAND OF III-V SEMICONDUCTORS

3.1	Introduction	40
3.2	Method	41
3.2.1	Arbitrary degeneracy	41
3.2.2	Special conditions on the statistics	43
3.3	Applications for the Condition of Complete Degeneracy	44
3.3.1	Relationships among E_F, m*, and N in the isotropic approximation	44
3.3.2	Relationships among E_F, m*, and N when anisotropic corrections are included	45
3.4	Approximations to the Kane Model Found in the Literature	47
3.5	Numerical Calculations for n-Type InAs in the Approximation of Complete Degeneracy for the Relations between E_F, m*, and N	48
3.6	Conclusions	53

3.1 Introduction

The Kane relationship[1,2] for the energy, E, vs wave vector, k for conduction band electrons in III-V semiconductors is usually assumed in the interpretation of transport measurements on such materials. However, the relationship is always used in an approximate form, for example, References 26 and 27. Although the approximations can be justified for small k-values, it has not been shown that they are justifiable for k-values corresponding to doping levels of $10^{19} cm^{-3}$. It is the primary intent here to show that the Kane relationship, including its isotropic first order terms for upper band contributions, can easily be used in its exact form for arbitrary degeneracy. To demonstrate the method, some specific derivations are made which relate the Fermi level, E_F, the carrier concentration, N, and the optical effective mass, m*, for the condition of complete degeneracy. A first order treatement of the effect of the band anisotropy is included in these latter relations. Some numerical calculations are made for InAs to show the relative magnitudes of the various terms which contribute to m*, as well as to compare the values of m* and E_F calculated by the present method with those calculated in Cardona's approximation.[26] The complete development in the following, from the starting point of the Kane equation, is original work by the author.

3.2 Method

3.2.1 Arbitrary degeneracy

In the determination of the intrinsic or extrinsic properties of n-type III-V semiconductor samples associated with electrons in the conduction band near k = 0 from measurements of parameters such as Hall coefficient, conductivity, magnetoresistivity, thermoelectric force, magnetothermoelectric constants and Faraday rotation and plasma resonance effective masses, one must, in the isotropic approximation, evaluate integrals of the type:[46,78,26,9]

$$I = \int g\left(k, \frac{dE}{dk}, E\right) F' \, dE \qquad 3 - (1)$$

where g is some function with a simple form, and F' is the energy derivative of the Fermi-Dirac distribution function.

The E vs k relationship derived by Kane is[2]:

$$E = E_K + sk^2 + sf_i k^2 + sf_a k^2_{xyz} \pm j(k^4 k^2_{xyz} - 9k_x^2 k_y^2 k_z^2)^{\frac{1}{2}} k^{-1} \qquad 3 - (2)$$

where E_K is the positive root of the equation

$$E_K(E_K + E_G)(E_K + E_G + \Delta_o) - sk^2 E_p(E_K + E_G + \tfrac{2}{3}\Delta_o) = 0 \qquad 3 - (3)$$

$s = \hbar^2/2m$, m is the free electron mass, sf_i and sf_a are the k-dependent coefficients of, respectively, the isotropic and anisotropic first order perturbation corrections for the effects of higher bands, k^2_{xyz} is a symbol for $(k_x^2k_y^2 + k_x^2k_z^2 + k_y^2k_z^2)k^{-2}$, the terms with j give the splitting of the Kramers doublet, E_G is the forbidden gap energy (with the condition that it includes only the lattice dilatation component of the measured gap temperature dependence[79]), Δ_o is the k = 0 spin-orbit splitting of the valence bands, and E_p is proportional to the square of the matrix element of the momentum operator between a p-like valence band state and the s-like conduction band state at k = 0. In the evaluation of I in Eq. 3 - (1), only the isotropic part of Eq. 3 - (2) will be considered, with the exception of the calculation of the plasma resonance effective mass for degenerate statistics, treated in Section 3.3.2, which includes the term with f_a.

The method used here to evaluate I is to express k, $\frac{dE}{dK}$, E and dE in terms of the variable E_K. This can be done as follows:

From Eq. 3 - (3) $\quad k^2 = Q/s \qquad$ 3 - (4)

where

$$Q = E_K(E_K + E_G)(E_K + E_G + \Delta_o)/E_p(E_K + E_G + \tfrac{2}{3}\Delta_o)$$

$$E = E_K + s(1 + f_i(E_K))k^2 = E_K + (1 + f_i)Q \qquad 3 - (5)$$

From Eq. 3 - (4)

$$\left(\frac{dE_K}{dk}\right) = \left(\frac{dk}{dE_K}\right)^{-1} = \left(\frac{Q'}{2sk}\right)^{-1} \qquad 3 - (6)$$

where Q' is the derivative of Q with respect to E_K.

From Eqs. 3 - (5) and 3 - (6)

$$\frac{dE}{dk} = 2sk \left(\frac{1}{Q'} + 1 + \left(1 + \frac{Q}{Q'} \frac{d}{dE_K}\right) f_i\right) \qquad 3 - (7)$$

From Eqs. 3 - (6) and 3 - (7)

$$dE = \left(1 + Q' \left(1 + \left(1 + \frac{Q}{Q'} \frac{d}{dE_K}\right) f_i\right)\right) dE_K \qquad 3 - (8)$$

Also F' is expressed in terms of E_K.

The method just described has some similarity to one proposed by Zukotynski and Kolodziejczak[80], where it is required that k be expressible as a function of E. Although their method could have been used directly with Eq. 3 - (3) in the approximation $E \simeq E_K$, it was not done.

3.2.2 Special conditions on the statistics

Two commonly used approximations in the evaluation of I for $(E_F/k_oT) >> 1$, where k_o is the Boltzmann constant, and T the absolute temperature, are[45]: (a) the assumption of complete degeneracy, thus making F' a δ-function, and (b) the expansion of the function g in a Taylor series about E_F, retaining only the even terms because F' is symmetrical about E_F. For the use of the method in Section 3.2.1 with (a), one has that $I = g_1(E_K)$, where g_1 is the function g after transformation of variables. In order to make use of (b), the evaluation of the derivatives of the type $d^{2n}g/dE^{2n}$ can be expressed using

Eq. 3 - (8) and the relation $d/dE = (dE_K/dE)(d/dE_K)$.

3.3 Applications for the Condition of Complete Degeneracy

3.3.1 Relationships among E_F, m^*, and N in the isotropic approximation

The effective mass, m^*, determined by the infrared reflectivity[9], and the Faraday rotation[81] techniques, is related to the band form by

$$\frac{m}{m^*} = \frac{m}{\hbar^2}\left(\frac{1}{k}\frac{dE}{dk}\right)_{E_F} \qquad 3 - (9)$$

From Eq. 3 - (7)

$$\frac{m}{m^*} = \left(\frac{1}{Q'} + 1 + \left(1 + \frac{Q}{Q'}\frac{d}{dE_K}\right)f_i\right)_{E_{KF}} \qquad 3 - (10)$$

where E_{KF} is the E_K component of E_F, which can be determined directly from Eq. 3 - (5). The carrier concentration, N, is related to E_{KF} using the uniform density of states in k-space. Thus,

$$E_F = E_{KF} + (1 + f_i)Q_F \qquad 3 - (11)$$

$$3\pi^2 N = k_F^3 = (Q_F/s)^{3/2} \qquad 3 - (12)$$

where $Q_F = Q(E_{KF})$. To see the interdependence of these quantities, a procedure is to calculate N, E_F, and m^* for different values of E_{KF}.

3.3.2 Relationships among E_F, m^*, and N when anisotropic corrections are included.

The term with f_a in Eq. 3 - (2) of Section 3.2.1 will be included in obtaining the relationship between effective mass (as determined from infrared reflectivity), E_F and N, in the approximation of complete degeneracy. The calculation for the Faraday rotation effective mass would proceed differently. To first order

$$k_F^2(\theta,\phi) = k_F^2 <100> + D\delta E_K \qquad 3 - (13)$$

where θ, φ are the usual spherical angle co ordinates, and where

$$D = (dk^2/dE_K)E_{Kav} \qquad 3 - (14)$$

To improve the approximation, the derivative is evaluated at E_{Kav}, which equals E_{KF} in a <100> direction, minus $(sf_a k_F^2<100>)/5$ which is a first order average of the anisotropic energy component on the Fermi surface. This is true since

$$\int k_{xyz}^2 d\Omega = k_F^2<100> \int h(\theta,\phi)d\Omega = \frac{4\pi}{5} k_F^2 <100>$$

$$h(\theta, \phi) = -\tfrac{1}{2}(\sin^4\theta\,(\cos^4\phi + \sin^4\phi) + \cos^4\theta - 1)$$

where dΩ is the element of solid angle. The angular function h(θ, φ) has been studied in a different context in Reference 82.

To first order

$$-\delta E_K = s k_F^2\langle 100\rangle\, f_a\, h(\theta, \phi) \qquad 3 - (15)$$

$$k_F^2(\theta, \phi) = k_F^2\langle 100\rangle\, (1 - Dsf_a(k\langle 100\rangle) h(\theta, \phi)) \qquad 3 - (16)$$

Integrating over the occupied states

$$3\pi^2 N = k_F^3\langle 100\rangle\, (1 - 0.3\, Dsf_a) \qquad 3 - (17)$$

It is easily shown from Reference 9 that

$$\frac{m}{m^*} = \frac{m}{\hbar^2} \frac{\int_{E_F} |w| \left[\frac{|\underline{w}|\,|\underline{k}|}{\underline{w}\cdot\underline{k}}\right] k^2 d\Omega}{\int_{E_F} k^3(\theta, \phi)\, d\Omega} \qquad 3 - (18)$$

where $\underline{w} = \underline{\nabla}_{\underline{k}} \bar{E}$, and the square bracket term in the numerator accounts for the area difference between the surface element in spherical coordinates, and that on a constant energy surface. It is straightforward to show that the integrand in the numerator reduces to

$$2sv\, [1 + (f_a h/v)] k^3$$

having dropped terms in $(f_a/v)^2$, where

$$v = (1/\Omega') + 1 + f_i + \frac{k}{2} \frac{d}{dk} (f_i + hf_a)$$

Expanding $(1/Q')$ about E_{Kav} and evaluating f_i, f_a and their derivatives at E_{Kav}, the result is

$$\frac{m}{m^*} = \left(\frac{1}{Q'} + 1 + \left(1 + \frac{k}{2}\frac{d}{dk}\left(f_i + \frac{f_a}{5}\right)\right)\right)_{E_{Kav}} \qquad 3 - (19)$$

The k variable can be transformed to E_K as in Section 3.2.1

3.4 Approximations to the Kane Model Found in the Literature

To permit the comparison of the results of 3.3.1 with previous methods, two commonly used approximations will be mentioned. Cardona's[26] approximation for (3), put in a convenient form for the method of Section 3.2.1, is

$$k^2 = E_{KC}(E_{KC} + E_G)/qs \qquad 3 - (20)$$

where

$$q = E_p(E_G + \tfrac{2}{3}\Delta_o)/(E_G + \Delta_o)$$

and

$$E = E_{KC} + sk^2 \qquad 3 - (21)$$

This approximation has frequently been used outside the original conditions for its application.

Another approximation, used for example in Reference 83, assumes a parabolic term for the effect of upper bands, that is,

$$f_i k^2 \simeq t k^2 , \qquad 3 - (22)$$

where t is independent of k.

3.5 Numerical Calculations for n-Type InAs in the Approximation of Complete Degeneracy for the Relations between N, m* and E_F

The quantities which determine the band form in the foregoing are E_G, E_p, Δ_o, as well as the upper band parameters, A', L', M, L, N, which are related to the present symbols by[2]

$$f_i = (a^2 A' + b^2 M + c^2 L') s^{-1} \qquad 3 - (23)$$

$$f_a = (b^2 - 2c^2)(L - M - N) s^{-1} \qquad 3 - (24)$$

$$L' = L + (E_p/E_G) s \qquad 3 - (25)$$

$$t = A' s^{-1} \qquad 3 - (26)$$

a^2, b^2 and c^2 are respectively the squares of the coefficients of the k = 0 conduction, light hole and split-off valence band states in the conduction band wave functions. The relationships between L, M, N, and the Luttinger parameters, which are determined from magneto-optical

measurements, are well known[84], the desired forms here being

$$L = -(1 + \gamma_1 + 4\gamma_2)s$$

$$M = -(1 + \gamma_1 - 2\gamma_2)s$$

$$N = -6\gamma_3 s$$

Experimental values for E_G and Δ_o at low temperatures are 0.4105 eV[85] and 0.38 eV[33], respectively. The values used for E_p and the γ's are Lawaetz's semiempirical results[34]. Although there are experimental results for some of the latter parameters[32,85], these were obtained before the new value for Δ_o[33], and the effect that this would have had on the fitting is not precisely known. A' can be determined[34] by solving for A' in Eq. 3 - (10), using the effective mass at k = 0, 0.0235m[86], determined by cyclotron resonance. With regard to the temperature dependence of the parameters, only the effect of the temperature variation of E_G on (1/Q') is considered. Since only the lattice dilatation component of measured gaps influences the band form, for the calculation it is arbitrarily assumed that this component is one-half the total change[85], that is, E_G(300K) is taken as 0.385 eV in Eq. 3 - (3).

Figure 5 shows various contributions to (m/m*) as a function of $N^{2/3}$. Curves 1 and 2 give the value of (1/Q') calculated exactly and in Cardona's approximation, respectively. Each of these curves

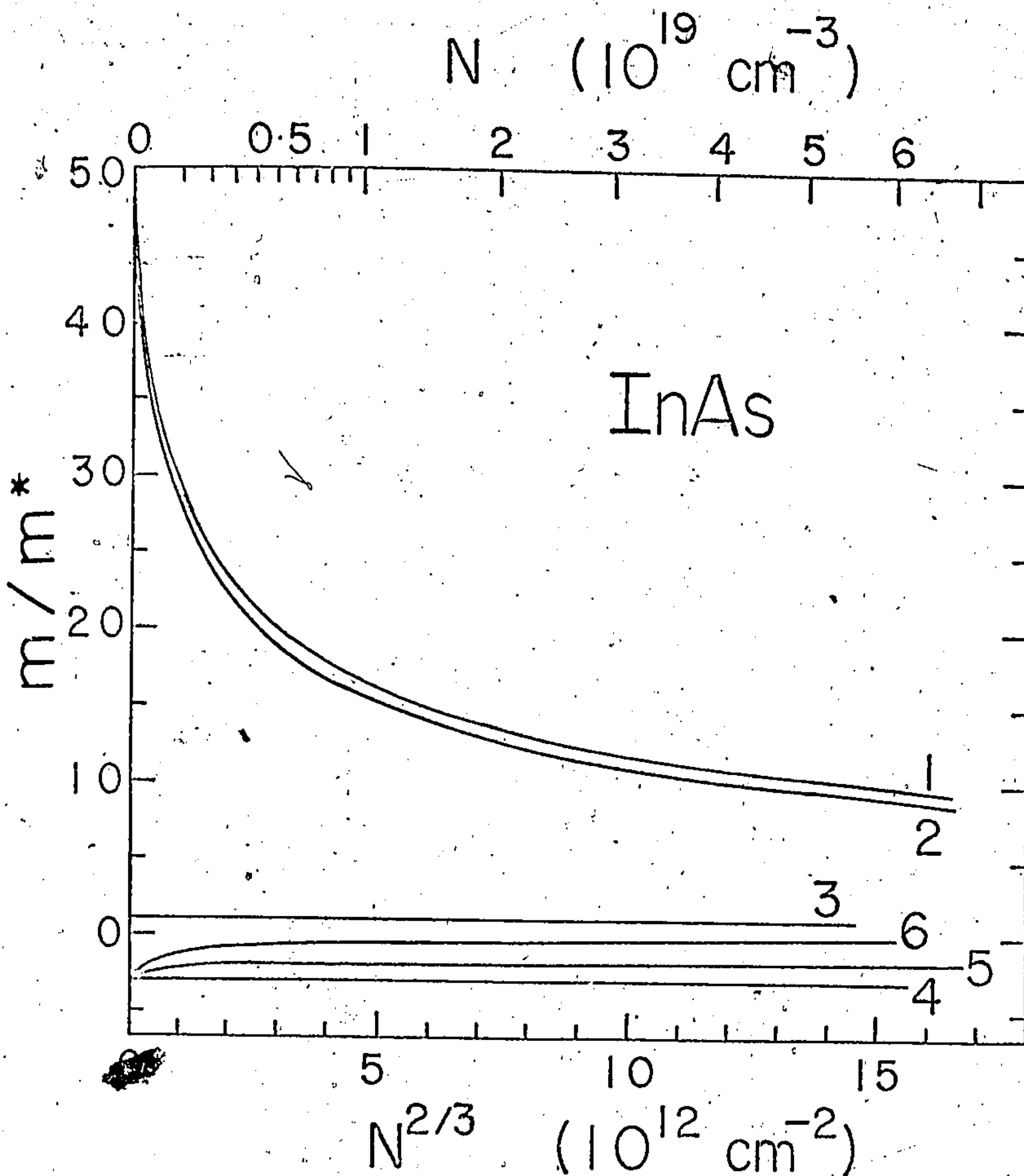

Figure 5. Calculated values of various contributions to m/m^*, for InAs, as a function of $N^{2/3}$ (see text).

is in fact two curves each, the branches for helium and room temperatures. This is hardly noticeable because the room temperature branches are higher than the others by about 6, 2, and 1 percent at N-values of 0, 10^{18} and $10^{19}cm^{-3}$, respectively. Curve 3 is the contribution from the free electron mass, curve 4 gives the contribution from A' assuming a parabolic upper band correction term ($t = A's^{-1}$ in Eq. 3 - (22)), and curve 5 gives the isotropic upper band contribution, taking into account the k-dependence of f_1. Curve 6 gives the contribution of the anisotropic term with f_a. One might think that the contribution of (1/Q') for a given value of N would depend on whether the anisotropic term is included or not; however, although the anisotropic term affects the average k-value where (1/Q') is evaluated for a given E_F, it also changes the volume of k-space enclosed by E_F, and the two effects are self-compensating. Thus, for a particular N-value, the inclusion of the anisotropic term changes the (1/Q') contribution by less than a few tenths of a percent.

Figure 6 shows the results of E_F as a function of $N^{2/3}$, for four approximations. It is not intended that Figures 5 and 6 be considered representative of all III-V compounds. They illustrate the results for a particular case. The results of Figure 5 have been used in Chapter 2, Figure 3, for comparison with effective masses determined from infrared reflectivity measurements on heavily-doped n-type InAs.

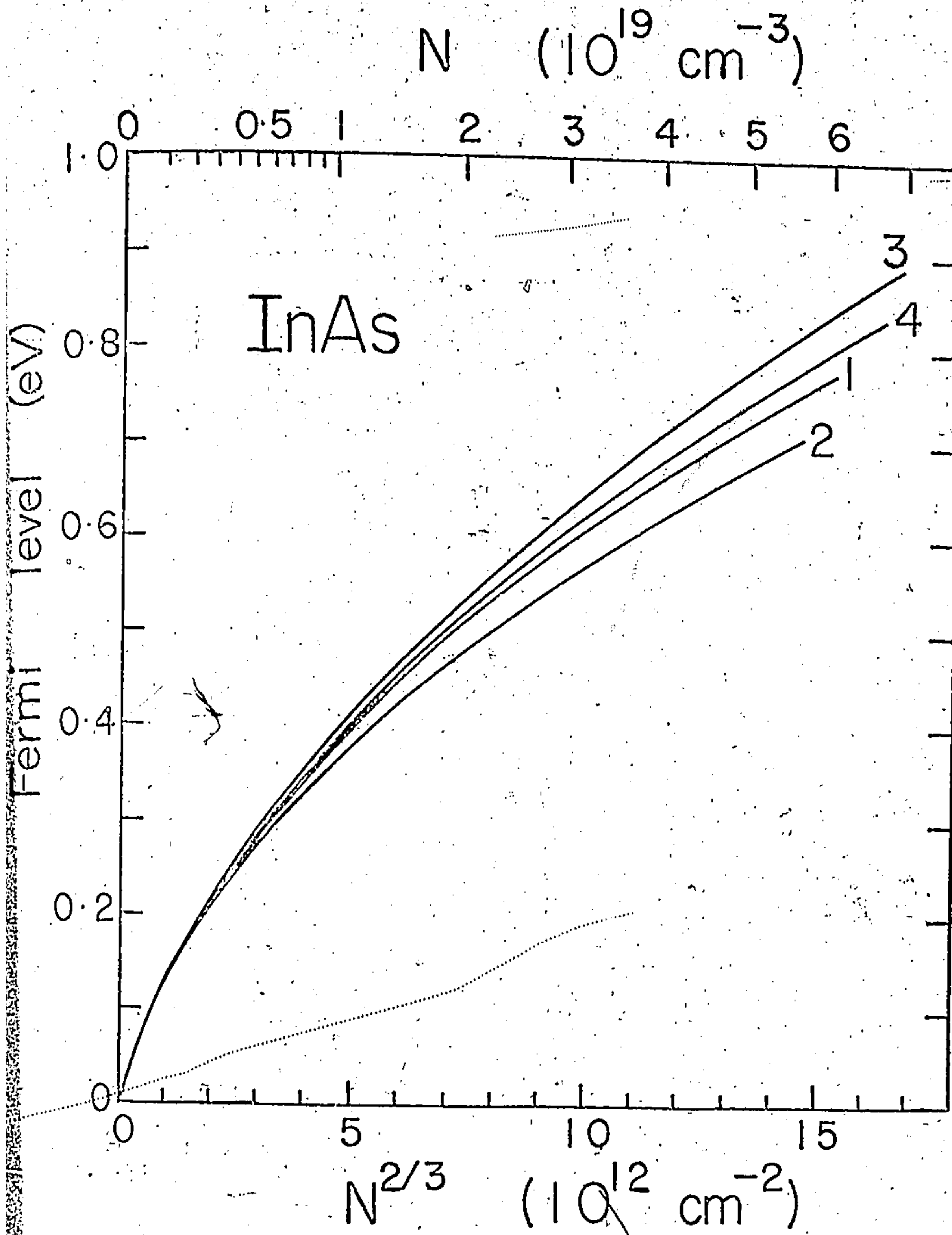

Figure 6. Calculated values of E_F at 4K as a function of $N^{2/3}$ in various approximations: 1) $E_K + s(1 + t)k^2$; 2) $E_{KC}+s(1+t)k^2$; 3) $E_K+ s(1+f_i)k^2$; 4) $E_K+ s((1+f_i)k^2 + f_a k^2_{xyz})$.

3.6 Conclusions

It is concluded that it is not difficult to achieve more accuracy than has usually been the case in the application of the Kane model to results on heavily-doped n-type III-V compounds. The Cardona approximation is fairly good for InAs well beyond the range for which it was intended.

CHAPTER 4

THERMOREFLECTANCE THEORY AND TECHNIQUE

4.1 Introduction 55

4.2 Theory of Thermoreflectance including the Calculation of ($\Delta R/R$) for Three Simple Models 57

4.2.1 Modulated reflectance in terms of changes in the dielectric constant 57

4.2.2 Contributions to the dielectric constant 60

4.2.3 Departures from the one-electron model 64

4.2.4 Calculation of ($\Delta R/R$) for three simple cases 67

4.2.4a a single transition 68

4.2.4b a step function in the joint density of states 69

4.2.4c an $(E - E_g)^{\frac{1}{2}}$ dependence in the joint density of states (the Batz problem) 70

4.3 Experimental Techniques 72

4.3.1 Sample preparation 72

4.3.2 Temperature modulation 73

4.3.2a heating elements 73

4.3.2b heat sinks 75

4.3.2c typical power levels and temperature variations 77

4.3.3 Optics 80

4.3.4 Detection 81

4.1 Introduction

Many optical measurements are made on specimens under study to locate the characteristic energies at which there are rapid changes in the absorption coefficient. Such energy values can be used in the form of "boundary conditions" in semi-empirical theories of the electronic states in the specimen, as we have seen, for example, in the case of E_G and Δ_o in the Kane theory for the energy bands in III-V compounds. Another service of such energies is to test the predictions of a theory. Examples which are related to the present work are the excitonic peaks which occur at the fundamental direct gap of pure germanium, and the shifts in the energy of the fundamental absorption edge when large numbers of impurities of particular types are put in the sample.

Typical absorption coefficients associated with the lowest energy direct transitions in semiconductors are of the order of $10^4 cm^{-1}$. Thus to get an indication of the spectral range over which this absorption becomes established, one must prepare samples with thicknesses in the range of a few microns. Higher energy transitions have coefficients of the order of $10^5 cm^{-1}$, and the preparation of absorption samples, other than evaporated films, is unimaginable, except in exceptional circumstances (such as epitaxial films on suitable substrates). Thus one looks at the possibility of locating the characteristics energies

of a crystal by reflection measurements. It is straightforward to show that a change in the absorption coefficient at E_G of $10^4 cm^{-1}$ will be associated also with the change in reflectivity of the order of 1 percent in 30 percent for an E_G value of 1.2 eV, and n_1 equal to 3.5. To identify the energy of such a change requires a fairly good reflectometer, and to determine the form of such a change requires electronic methods not in common use.[88]

Rather than attempt to measure the reflection coefficient, let us see how much one would have to change the temperature so as to shift the critical energy about 3×10^{-5} eV, which is about one hundredth of the width of a typical reflectance structure. The temperature coefficients of energy gaps is of the order of 10^{-4} eV/°K; hence, a fraction of a degree temperature modulation would do the job. Similarly, one would find that wavelength modulation of about one angstrom would reveal any normally expected structure. With respect to the signal level, the example will be given for a PbS detector circuit. One typically measures voltages resulting from chopped light incident on the sample of the order of 10-50 millivolts. With the temperature modulation indicated above, one would measure a modulated reflectance signal about 5×10^{-4} times that value, or 5-25 microvolts. Since the noise level in the detector circuit is typically 0.1 - 0.2 microvolts as measured by a phase-sensitive lock-in system for a frequency of 10 Hz, using 3 sec time constant in the output circuit, one sees that there is no

problem at all in locating critical transition energies of solids and in detailing the form using the thermoreflectance technique.

The purpose of this introduction is to show the reasonableness of approaching the optical investigation of band structure via the thermoreflectance technique. No attempt will be made to argue a great superiority over other modulation techniques. The interested reader is referred to two recent comprehensive volumes[20,21] on modulation spectroscopy as applied to solids.

4.2 Theory of Thermoreflectance-including the Calculation of (ΔR/R) for Three Simple Models.

4.2.1 Modulated reflectance in terms of changes in the dielectric constant

The procedure follows that of Yamakawa et al.[89] Two equations are repeated from Chapter 2.

$$\frac{\tilde{n} - 1}{\tilde{n} + 1} = R^{\frac{1}{2}} e^{i\phi} \qquad 2 - (8)$$

$$\varepsilon_o \tilde{n}^2 = \tilde{\varepsilon} \qquad 2 - (12)$$

where $\tilde{n} = n_1 + in_2$ and $\tilde{\varepsilon} = \varepsilon_1 + i\varepsilon_2$. Taking variations in these equations, one has

$$\frac{\Delta\tilde{n}}{\tilde{n} + 1} - \frac{\Delta\tilde{n}(\tilde{n} - 1)}{(\tilde{n} + 1)^2} = R^{\frac{1}{2}} e^{i\phi} \left(\frac{\Delta R}{2R} + i\Delta\phi\right) \qquad 4 - (1)$$

$$2\tilde{n}\Delta \tilde{n} = \varepsilon_o^{-1} \Delta\tilde{\varepsilon} \qquad 4 - (2)$$

Eq. 4-(1) is rearranged so that only $2\tilde{n}\Delta\tilde{n}$ appears on the left hand side. Equating the real and imaginary parts of that equation with the corresponding parts of Eq. 4-(2), one has

$$\Delta\varepsilon_1 = \gamma \frac{\Delta R}{2R} - \delta\Delta\theta \qquad 4-(3)$$

$$\Delta\varepsilon_2 = \delta \frac{\Delta R}{2R} + \gamma\Delta\theta \qquad 4-(4)$$

where for $z = (\tilde{n}^2 - 1)\tilde{n}$

$$\gamma = \mathrm{Re}(z) = n_1(n_1^2 - 3n_2^2 - 1) \qquad 4-(5)$$

and

$$\delta = \mathrm{Im}(z) = n_2(3n_1^2 - n_2^2 - 1) \qquad 4-(6)$$

Solving for $(\Delta R/R)$

$$\frac{\Delta R}{R} = \frac{2}{\gamma^2 + \delta^2} (\delta\Delta\varepsilon_1 + \delta\Delta\varepsilon_2)$$

$$= \alpha_1\Delta\varepsilon_1 + \alpha_2\Delta\varepsilon_2 \qquad 4-(7)$$

It is noted here that Eqs. 4-(3) and 4-(4) disagree with similar equations reported by Cardona[90,91], in that the terms with δ in the present equations are multiplied by (-1) in his. It is easy to show that this has no effect on Eq. 4-(7), and that the difference results from the definition of the phase angle, ϕ. If ϕ is defined

by the equation

$$\frac{\tilde{n}^* - 1}{\tilde{n}^* + 1} = R^{1/2} e^{i\phi} \qquad 4-(8)$$

where (*) indicates the complex conjugate, as is done by Garfinkel et al.,[92] and whose work is referred to in Cardona's book,[90] one gets Cardona's equations. However, it appears that Cardona intended[93] to use the convention of Eq. 2-(20). In any case, this difference is not relevant in the present work.

Let us suppose that $\tilde{\varepsilon}$ of the specimen is expressible in terms of several parameters $(x_1, x_2 \ldots x_n)$, with temperature dependences $(d_1, d_2, \ldots d_n)$, respectively, where $d_i = (dx_i/dT)$. Thus, if a temperature change, ΔT, is imposed

$$\frac{\Delta R}{R} = \frac{\frac{dR}{dT} \Delta T}{R} = \left[\alpha_1 \Sigma \left(\frac{\partial \varepsilon_1}{\partial x_i} d_i\right) + \alpha_2 \Sigma \left(\frac{\partial \varepsilon_2}{\partial x_i} d_i\right) \right] \Delta T \qquad 4-(9)$$

Such a result is useful when the number of unknowns in the theory whose values are to be extracted from the spectrum is small. A simplificiation of Eq. 4-(9) which, to the author's knowledge, is applicable in all cases to structures around the fundamental gap is $\alpha_2 << \alpha_1$.[94] Thus, since $|\Delta\varepsilon_1|$ is of the order of $|\Delta\varepsilon_2|$, the second part of Eq. 4-(9) can be dropped.

4.2.2 Contributions to the dielectric constant

This section summarizes Katz's treatment[95] of the dielectric constant in the one-electron approximation for energies in the range of the transition between a non-degenerate valence band and conduction band at $\underline{k} = 0$. There are other treatments in the literature,[20,96] the original work having been done apparently by Ehrenreich and Cohen.[96] Correlation effects, which introduce the exciton states,[3] will be discussed in Chapter 6.

Consider the total Hamiltonian $\mathcal{H}$ for electrons

$$\mathcal{H} = \mathcal{H}_u + \mathcal{H}_{int.} = \frac{1}{2m} \sum_j (\underline{p}_j + e\underline{A}(\underline{r}_j))^2 + V(\underline{r}_1 \ldots \underline{r}_N) \qquad 4 - (10)$$

where $\underline{A}$ is the vector potential of the light wave given by

$$\underline{A} = \tfrac{1}{2}(\underline{A}_o \exp[i(\underline{k}.\underline{r} - \omega t)] + C.C.)$$

where the wave vector of the light is taken to be real. $\mathcal{H}_u$ is the unperturbed Hamiltonian, and $\mathcal{H}_{int}$, the perturbation introduced by the light wave, is (since $\underline{\nabla}.\underline{A} = 0$) essentially

$$\mathcal{H}_{int} = (e/m) \sum_j \underline{A}(\underline{r}_j).\underline{p}_j \qquad 4 - (11)$$

where $\underline{p}_j$ is the momentum operator for the j'th electron. Using time-dependent perturbation theory, one finds that the transition probability

per unit time between the antisymmetric wave functions Ψ_o and $\Psi(ck)$, for the ground state and excited states, respectively, is

$$P_{\underline{k}}(\hbar\omega) = \frac{2\pi}{\hbar} |\langle\Psi(c\underline{k})|\mathcal{H}_{int}|\Psi_o\rangle|^2 \, \delta(E_c(\underline{k}) - E_v(\underline{k}) - \hbar\omega)$$

4 - (12)

$\Psi(ck)$ is the symbol for the state in which the electron in Bloch state $|c\underline{k}\rangle$ with wave vector $\underline{k}$ is in the conduction band, the corresponding valence band Bloch state $|v\underline{k}\rangle$ being empty. One considers here only direct transitions in $\underline{k}$-space, anticipating that the integral is essentially zero for $\underline{k}$ (valence) much different from $\underline{k}'$ (conduction). Also, the δ-function in Eq. 4-(12) states the requirement of energy conservation. Finally, simplifying the integral, and neglecting the complex conjugate in $\underline{A}$ which contributes to photon emission, Eq. 4-(12) becomes

$$P_{\underline{k}}(\hbar\omega) = \frac{\pi}{2\hbar} \frac{e^2}{m^2} A_o A_o^* |\langle c\underline{k}| \underline{a}.\underline{p}| v\underline{k}\rangle|^2 \, \delta(E_c(\underline{k}) - E_v(\underline{k}) - \hbar\omega)$$

4 - (13)

where $\underline{a}$ is a unit vector parallel to $\underline{A}_o$. The rate of energy absorption per unit volume W between the conduction and valence bands is $\hbar\omega\Sigma_{\underline{k}} P_{\underline{k}}(\hbar\omega)$. In the present gauge, $\underline{\mathcal{E}} = \dot{\underline{A}} = -i\omega\underline{A}$, so that the Poynting vector average S_{av} which is the average over a period of the power flow $\underline{\mathcal{E}} \times \underline{H}$ per unit area, can be written as $\frac{1}{2} n_1 c \epsilon_o \omega^2 A_o A_o^*$. Now, ordinarily the absorption coefficient K is looked at as the coefficient in the exponential

attenuation of the intensity I of a wave. Note however that this can be looked at from another point of view, that $(dI/dx) = -KI$, which means that K represents the fractional loss per unit of penetration. If one considers a unit of area, one sees also that

$$K = W/S_{av} \qquad 4 - (14)$$

so that, using Eqs. 2-(6) and 2-(12)

$$\varepsilon_2(\omega) = 2\pi \left(\frac{e}{m\omega}\right)^2 \sum_{\underline{k}} |\langle c\underline{k}|\underline{a}\cdot\underline{p}|\ v\underline{k}\rangle|^2\ \delta(E_c(\underline{k}) - E_v(\underline{k}) - \hbar\omega) \qquad 4 - (15)$$

where a factor of two has been added to take care of the spin degeneracy.

In order to account for lifetime broadening effects, the δ-function absorption is replaced by a peak of finite width of the Lorentzian-broadened form:

$$\delta(E - \hbar\omega) \text{ goes to } \frac{1}{\pi} \frac{\Gamma}{[(\hbar\omega - E)^2 + \Gamma^2]} \qquad 4 - (16)$$

where Γ is called the broadening parameter. One can check that the new function has a unit integral. For $\Gamma << E$, the Kramers-Kronig transform of 4-(14) can be shown to be

$$-\frac{1}{\pi} \frac{(\hbar\omega - E)}{(\hbar\omega - E)^2 + \Gamma^2} \qquad 4 - (17)$$

Thus the broadening of the δ-function has allowed the creation of an expression which represents both the real and imaginary parts of the contribution to the complex dielectric constant from a single transition, that is,

$$\varepsilon(\hbar\omega) \propto \frac{1}{(\hbar\omega - E) + i\Gamma} \qquad 4 - (18)$$

However, someone familiar with the derivation (e.g. Ref. 97) of the Kramers-Kronig relationships will see that the requirement that $\varepsilon(-\omega)$ equal $\varepsilon^*(\omega)$ is not satisfied by 4-(18). That can be fixed by multiplying the denominator by $[(\hbar\omega + E) + i\Gamma]$, and this modification has little effect on the peak forms. In fact, the development by Ehrenreich and Cohen[96] leads to that, their result being (using their symbols)

$$\varepsilon(\omega) = 1 - \frac{e^2}{4\pi^3 m} \int d^3\underline{k} \sum_{\ell\ell'} f_{\ell}(\underline{k})\, f_{\ell\ell'} \left(\omega - \omega_{\ell\ell'} + \frac{i}{\tau_{\ell\ell'}}\right)^{-1} \left(\omega + \omega_{\ell\ell'} + \frac{i}{\tau_{\ell\ell'}}\right)^{-1} \qquad 4 - (19)$$

where ℓ, ℓ' identify the bands, f_{ℓ} is the Fermi-Dirac distribution function in the empty or partially empty bands to which the transitions are made, and $\tau_{\ell\ell'}$ is the lifetime broadening parameter associated with transitions, and in general is a function of $\underline{k}$. $f_{\ell\ell'}$ the so-called oscillator strength, equals $(2/\hbar\omega_{\ell\ell'} m)$ times the square of the momentum matrix element, as given in Eq. 4-(15). It is easy to see the expected equivalence between Eqs. 4-(19) and 4-(15).

It is noted here that if, in the development for ε_2 by Batz,[95] the photon emission term had not been dropped, the two complex terms which are in the denominator of Eq. 4-(19) would also have appeared in Batz's broadened formula.

4.2.3 Departures from the one-electron model

It has been assumed in the treatment of the previous section that the optical absorption process can be described by the transition of the crystal from a state described by an antisymmetric combination of one-electron valence band wave functions to a state in which one of the $\underline{k}$-vectors is associated with a one-electron conduction band wave function. There are two important effects omitted in such a model, namely, the electron-hole interaction and the electron-lattice interaction. Elliott's treatment[3] of the electron-hole interaction is reviewed in Chapter 6, Section 6.2. The modification of the theory resulting from the inclusion of the electron-lattice interaction has been reviewed by Batz[95] and his treatment is summarized below.

The electron-lattice interaction term in the crystal Hamiltonian is

$$\mathcal{H}_{e\ell} = \sum_{\underline{q}j} [A_{\underline{q}} a_{\underline{q}} \exp(i\underline{q}.\underline{r}_j) + A^*_{\underline{q}} a^\dagger_{\underline{q}} \exp(-i\underline{q}.\underline{r}_j)] \qquad 4-(20)$$

where $\underline{q}$ is the phonon wave vector, $a^\dagger_{\underline{q}}$, $a_{\underline{q}}$ are the phonon creation and destruction operators, $\underline{r}_j$ is the coordinate of the j'th electron and

$$|A_{\underline{q}}| = \left(\frac{E_{1b}^2 q^2 \hbar}{2\omega_{\underline{q}} \rho} \right)^{\frac{1}{2}} \qquad 4 - (21)$$

where E_{1b} is the deformation potential attached to band b, and ρ is the crystal density. For a weak electron-lattice coupling, first-order perturbation theory shows that zero-order wave functions will be modified by $\mathcal{H}_{e\ell}$ according to the usual form

$$|s\rangle = |s\rangle + \sum_i |i\rangle \frac{\langle i | \mathcal{H}_{e\ell} | s\rangle}{E(s) - E(i)} \qquad 4 - (22).$$

The only non-vanishing matrix elements of $\mathcal{H}_{e\ell}$ are those connecting lattice states which differ by one phonon in a mode, and electronic states which differ by a one-electron wavefunction. These matrix elements have the form

$$\langle i | \mathcal{H}_{e\ell} | s\rangle = \langle \underline{k}'; n_{\underline{q}} \pm 1 | \mathcal{H}_{e\ell} | \underline{k}; n_{\underline{q}} \rangle$$

$$= \begin{cases} A_{\underline{q}}^* (n_{\underline{q}} + 1)^{\frac{1}{2}} \, \delta(\underline{k}' - \underline{k} + \underline{q}) \\ A_{\underline{q}} n_{\underline{q}}^{\frac{1}{2}} \, \delta(\underline{k}' - \underline{k} - \underline{q}) \end{cases} \qquad 4 - (23)$$

where $n_{\underline{q}}$, the number of modes in mode $\underline{q}$ is given by $n_{\underline{q}} = [\exp(h\omega_{\underline{q}}/k_o T) - 1]^{-1}$. The net result of the inclusion of $\mathcal{H}_{e\ell}$ in the optical calculations is that when calculating $\langle c\underline{k}' | \mathcal{H}_{int} | v\underline{k}\rangle$ one must use the perturbed wavefunctions of the form 4-(22), which results in non-zero matrix elements for $k' \neq k$; that is, aside from direct transitions, there are indirect transitions connected in

$\underline{k}$-space by the conservation rule $(\underline{k}' - \underline{k} \pm \underline{q}) = 0$ where the + and − refer to the absorption or emission of a phonon, respectively. Such indirect transitions are dominant when the direct transition at $\underline{k}$ is forbidden, as, for example, at the lowest indirect gaps of germanium and silicon. Such transitions have been studied, for example, by Berglund[98] at the indirect gap of silicon. His work is specifically mentioned here because it was also the first optical investigation of a material by a thermal modulation measurement, namely, thermally-modulated absorption.

In the treatment of the previous section, the broadening parameter Γ was introduced ad hoc to describe a line shape. This does not give the origin of Γ nor predict its variation with temperature. Batz[95] has made a study of the effect of the electron-lattice interaction on the temperature variation both of Γ and E_G, the energy gap. The increase in energy of the electron when the wave function goes from the zero-order wave function to the perturbed wave function of Eq. 4-(22) is calculated and related to δE_G and $\delta\Gamma$. After a lengthy analysis he concludes that at a direct gap in a non-polar crystal the modulation effect of Γ should be negligible compared to the modulation of the gap energy. This conclusion is supported by the relative importance of $(\partial\Gamma/\partial T)$ and $(\partial E_G/\partial T)$ found in line shape studies of $(\Delta R/R)$ of InAs and Ge by the author, and reported in Chapters 5 and 6.

4.2.4 Calculation of (ΔR/R) for three simple cases.

For the purpose of showing the main features of thermoreflectance signals, the following assumptions are made in the calculations of this section:

(i) $\alpha_2 \Delta\varepsilon_2$ is negligible compared to $\alpha_1 \Delta\varepsilon_1$,

(ii) Γ is independent of energy,

(iii) only the rapidly varying energy dependence, $(E - E' + i\Gamma)^{-1}$, is important in the calculation, and

(iv) the oscillator strength is energy independent.

These four assumptions can be summarized by saying that the contribution to ε at E from a transition at any E' is given by

$$\tilde{\varepsilon} = - \frac{c}{E - E' + i\Gamma} \qquad 4-(24)$$

Referring to Eq. 4-(9), assumption (i) means that

$$\frac{\Delta R}{R} = \alpha_1 \Delta\varepsilon_1 \qquad 4-(25)$$

More realistic models for the dielectric constant are treated in Chapters 5 and 6.

Before proceeding, we will make some observations related to the above assumptions. One may suspect that a Kramers-Kronig type of relationship may exist between $\alpha_1 \Delta\varepsilon_1$ and $\alpha_2 \Delta\varepsilon_2$ such that the local behaviour of $\alpha_1 \Delta\varepsilon_1$ is dependent on the behaviour of $\alpha_2 \Delta\varepsilon_2$ in the same spectral region.

However, this is not true. One can see this by noting first that there are Kramers-Kronig relationships between $\Delta\varepsilon_1$ and $\Delta\varepsilon_2$; one has only to take the temperature derivatives of the Kramers-Kronig expressions (given, for example, in Appendix B). On the other hand, α_1 and α_2 are not related locally to each other, being functions of ε_1 and ε_2, not $\Delta\varepsilon_1$ and $\Delta\varepsilon_2$; see, for example, equations 4-(5) to 4-(7), and Figure 16 for the values of α_1 and α_2 for InAs.

As a second observation, we note that departures of c from temperature independence would be introduced for example for (a) a term of the form $(E + E' + i\Gamma)$ (see Eq. 4-(19)) in the denominator of Eq. 4-(24), and (b) by temperature-dependent transition probabilities. It is readily verified that the extra signal added by including the term in (a) is of the order of (Γ/E') times the signal one expects when that term is neglected. If the variation of the transition probability is expressed by the form $c = c_1(E')^n$, where n is some small number, say, $|n| < 3$, then it is easily verified that the extra signal added is of the order $(n\Gamma/E')$ times the signal one expects when that variation is neglected. Since $(\Gamma/E') \ll 1$ for all cases considered in this work, the form 4-(24) is a good approximation.

4.2.4a A single transition

Taking the temperature derivative of 4-(24) and noting that $(\partial/\partial E') = i(\partial/\partial\Gamma)$

$$\Delta\tilde{\varepsilon} = - \frac{\sqrt{c}}{(E - E' + i\Gamma)^2} \left(\frac{\partial E'}{\partial T} - i \frac{\partial \Gamma}{\partial T} \right) \Delta T \qquad 4-(26)$$

Let $(E - E')/\Gamma = X$.

$$\Delta\tilde{\varepsilon} = - \frac{c}{\Gamma^2} \left\{ \frac{(X^2 - 1) - i(2X)}{(X^2 + 1)^2} \right\} \left(\frac{\partial E'}{\partial T} - i \frac{\partial \Gamma}{\partial T} \right) \Delta T \qquad 4-(27)$$

Eq. 4-(27) shows that the temperature shift in energy produces a peak form (a negative peak for $(\partial E'/\partial T)$ negative), whereas the Γ temperature dependence produces a ∿-shaped curve.

4.2.4b a step function in the joint density of states

Consider a case in which for $E' < E_s$, there are no transitions possible, whereas for $E' > E_s$, the number of transitions possible per unit energy range is N_s. Such a model would describe pretty well transitions at very low temperatures between valence and conduction bands with spherical energy surfaces and where the electron gas is degenerate.

$$\tilde{\varepsilon}(E) = - c \int_{E_s}^{\infty} \frac{N_s dE'}{(E - E' + i\Gamma)} \qquad 4-(28)$$

$$\Delta\varepsilon = \frac{cN_s}{(E - E_s + i\Gamma)} \left(\frac{\partial E_s}{\partial T} - i\frac{\partial \Gamma}{\partial T}\right) \Delta T \qquad 4 - (29)$$

$$= \frac{cN_s}{\Gamma} \left\{ \frac{X - i}{X^2 + 1} \right\} \left(\frac{\partial E_s}{\partial T} - i\frac{\partial \Gamma}{\partial T}\right) \Delta T \qquad 4 - (30)$$

where $X = (E - E_s)/\Gamma$. Thus the energy shift produces a ∿ -component in $(\Delta R/R)$ for $(\partial E_s/\partial T)$ negative, whereas a positive $(\partial\Gamma/\partial T)$ would contribute a negative peak.

4.2.4c an $(E - E_g)^{\frac{1}{2}}$ dependence in the joint density of states (the Batz problem)

Here we consider a joint density of states $g(E')$ such that for $E < E_g$, $g(E) = 0$, for $E > E_g$, $g(E) = A(E - E_g)^{\frac{1}{2}}$. Such a case is called an M_o discontinuity after van Hove.[102] Somewhat different discontinuities, called M_1, M_2, M_3, as well as the M_o type have been investigated by Batz[23,103] from the thermoreflectance vantage point. Only the M_o type is treated here, since the derivations for the others follow the same lines.

$$\tilde{\varepsilon} = -cA \int_{E_g}^{\infty} \frac{(E' - E_g)^{\frac{1}{2}}\, dE'}{(E - E' + i\Gamma)} \qquad 4 - (31)$$

A useful observation at this point is that from the point of view of $\Delta\tilde{\varepsilon}(E)$, a positive shift of E_g has the same effect on the integral as a

negative shift of E.

$$\Delta\varepsilon = -cA \left\{ \int_{E_g}^{\infty} \frac{(E' - E_g)^{\frac{1}{2}}\, dE'}{(E - E' + i\Gamma)^2} \right\} \left(\frac{\partial E_g}{\partial T} - i\frac{\partial \Gamma}{\partial T} \right) \Delta T \qquad 4 - (32)$$

The integral in 4-(32) can be performed by the method of residues.[104] Choosing the first branch and taking the contour of integration along the positive E' axis between E_g and ∞, and making the infinite circle, one has enclosed a singularity of the second order at $E' = E + i\Gamma$. Thus one must evaluate the residue of the derivative of the numerator in 4-(32). The integral becomes

$$\int = \frac{\pi i}{2} \frac{1}{(E - E_g + i\Gamma)^{\frac{1}{2}}} = \frac{\pi}{2\sqrt{2\Gamma}} \left[F(-X) + iF(X) \right] \qquad 4 - (33)$$

where $X = (E - E_g)/\Gamma$, and where[23]

$$F(X) = \left[(X^2 + 1)^{\frac{1}{2}} + X \right]^{\frac{1}{2}} (X^2 + 1)^{-\frac{1}{2}}$$

The shapes of the F(X), F(-X) functions have been given by Batz.[23]

4.3 Experimental Techniques

The techniques and the evaluation of techniques throughout Section 4.3 are the original work of the author.

4.3.1 Sample preparation

Surfaces of samples for the thermoreflectance measurement must be chemically polished. A mirror-like mechanically polished Ge surface will not produce a modulated signal at the direct gap. Even low angle ion beam etching, as described in Chapter 7, must be followed by a short chemical polish to eliminate the strain. (Perhaps annealing at a high temperature would have the same effect. In such a treatment, one would be careful about the introduction of impurities). On the other hand, highly pitted, diffuse surfaces which may result from a preferential chemical etch will give adequate signals. Neither the Ge nor InAs surfaces showed any deterioration, as measured by thermo-reflectance, when exposed to air for days. However, grease films, which may flow from behind the sample over the front surface, reduce the signal strength, and, if thick enough, produce interference effects.

Samples of heavily-doped InAs and Ge were prepared as follows. A sample of 220 micron thickness was obtained by lapping front and back surfaces of a wafer with a 5 micron Al_2O_3 - water slurry on glass. Then one surface was mechanically polished on cloth with the same slurry, but more dilute, until the surface was fairly shiny. Then about 15 microns were removed from the mechanically polished surface using the following recipes which are well known in the semiconductor field:

for Ge	5 nitric acid 4.4 glacial acetic acid 1 hydrofluoric acid saturated with iodine

(etch rate 4-6 microns/min.)

for InAs	1 bromine 20 methanol

(etch rate 25-30 microns/min.)

Masking was done by mounting the sample on glass pieces with "black wax"* (melting point, 60°C).

4.3.2 Temperature modulation

4.3.2a heating elements

There are many ways to achieve thermal modulation of a sample. One looks for one that is simple, gives a reproducible temperature variation, and, if used at low temperatures, does not strain the sample, or, at least, not in an unpredictable way.

Direct heating by current pulsing, although it requires lower power levels than indirect heating, is not a convenient method. One must make electrical contacts as a minimum in extra work. Furthermore, if one wants uniform temperature variation, the sample must be of fairly homogeneous resistivity; this is often not the case for new materials.

* Apiezon Wax, Standard 'W', Edwards High Vacuum Ltd., Crawley, Sussex, England.

If one wishes to make a temperature run, the contacts, the sample resistance and homogeneity must be suitable across the temperature range. The direct heating is not recommended.

Indirect heating can be accomplished in various ways. Some of these will be listed in what is judged as increasing order of merit:

(i) Silver paint on sapphire substrates. These are neither reproducible nor durable. They develop cracks upon drying from which is produced a large background signal during use because of the discharge across the cracked spaces.

(ii) Gold films on sapphire substrates. Two difficulties were identified here. First, the film is not durable. Secondly, in order to make contacts to the ends of the gold films, indium was built up by plating; however, the indium deposit leeched the gold in the contact area, and breaks often appeared between the contact and the rest of the film.

(iii) Sputtered tantalum with gold end contacts, on Al_2O_3 substrates. These were kindly provided upon request by Microsystems International Ltd. by Dr. K. Eastwood. Each such heater had dimensions about 15 x 6 mm^2 with resistance about 10 ohms. They are durable and are recommended for room temperature work. However, semiconductor samples mounted on these heaters are strained at low temperatures, resulting in distorted forms (see Chapter 6). If the films were sputtered onto semi-insulating GaAs wafers, perhaps one would have the ideal heater.

(iv) Semiconductor rectangular pieces with strip end contacts. All the measurements (except for the splitting of the Ge peak in Chapter 6) reported in Chapters 5, 6, and 7 were made using n-type GaAs heaters, of dimensions about 14 x 8 x 0.5 mm^3, with resistances between liquid nitrogen and room temperatures of about 8-15 ohms. The contacts were made by alloying evaporated indium strips at 475°C. Contacts were made to these areas at three places at each end using gold wires at the ends of which were attached Indalloy #1[105] balls. The contacts were made by heating to about 150°C. Such heaters are sturdy, and with reasonable precautions, endure many manipulations.

The samples were attached to the heaters by a smear of silicone-based grease, either opague white or transparent.[106] The latter is thinner and was usually used at low temperatures.

4.3.2b heater sinks

At room temperature, the heater can be mounted on a water-cooled copper block. The simplest design is perhaps a block, with holes drilled through it such that the water makes a circuit inside the block, with copper tubing soldered on the entrance and exit holes. Designs should consider a narrow width, to permit near normal incidence of the light beam, and stability against vibration. If the heater cannot be mounted directly on the sink, because of low sink-to-heater resistance, the insulation could be made with a thin sapphire wafer.

The low temperature heat sink was a copper cold finger, which was in contact with liquid nitrogen in the sample region. In order to eliminate strain in the sample, due to differential contraction between the copper and the sample, the following design was found suitable. Depending on the sample to be measured, an InAs or Ge pedestal about 1½ mm thick, with surface dimensions larger than those of the heater was put on the copper tailpiece. To ensure good thermal contact, yet little strain in the pedestal, the pedestal was coated on one side with a thin layer of silver solder, and then soldered to the copper via a thick layer of indium. The heater was separated from the pedestal by a 20 micron thickness of grease-impregnated, natural tracing paper in order to prevent excessive heat flow to the sink as well as to ensure a uniform spacing between heater and sink. This last component was essential for good results near 20K. Some modifications of this arrangement was required for the sample mount in the superconducting magnet. This is partly described in Chapter 7.

Cryostats of the Fortin type[67] were used for the experiments at liquid nitrogen and dry ice-methanol temperatures. For the experiment using liquid He, a new cryostat was designed using some ideas from the nitrogen cryostat, some of R. Glinski, and some of mine. Since it worked very well, the modifications although simple, will be described. Except for the copper in the tailpiece and in the radiation shield soldered to the liquid nitrogen reservoir, only stainless steel was used.

The He dewar, which led down to the sample region, contained about 1.5 litres. The two tubes leading to this dewar were separated from contact with the nitrogen reservoir by a length of 4 inches. The nitrogen reservoir was open at the top and covered during use with a styrofoam cap. The level of the He liquid was monitored by measuring the combined resistance of three 0.1 watt, 33 ohm, carbon resistors, in parallel, suspended at 1, 5, and 7 inches from the bottom of the dewar tank. The boil-off rate was about 0.5 litres/hr. The sample changeover time, with the help of a hot air blowing system, was 20 minutes.

4.3.2c typical power levels and temperature variations.

Power was provided by a dc power supply which was in series with a mercury-wetted relay. The relay was operated by an oscillator, which drove the relay with a duty cycle of about 0.3 at about 11 Hz, and also provided the reference signal for the lock-in in the detection circuit.

Approximate temperatures of the sample were obtained by soldering a #40 copper-constantan thermocouple to a small rectangle of sample material, and sticking this piece to the heater surface with grease. The thermocouple reference temperature was that of the lowest temperature liquid in the cryostat. From experience, it was found that this small wire thermocouple required calibration, presumably due to the presence of strain (larger wires do not need calibration). The cali-

bration was done by normalizing the measured differences between He, N_2 and ice liquid temperatures to published values.[107]

To give an indication of the power levels and temperature modulation in these experiments, Figure 7 was prepared. Of particular interest are the results near liquid nitrogen temperatures for the mounting configurations with and without the tracing paper behind the heater, as has been discussed in Section 4.3.2b. Aside from the advantage of uniformity of temperature due to a uniform spacing, one sees that one can achieve the same modulation in temperature with a reduction of a factor of 5 in power input. This latter fact also contributes to a more uniform sample temperature, since at the reduced power level the effect of hot spots in the heater would be less. It is noted that these temperature modulation measurements were made at 1 Hz; however from the quickness of response of the meter needle, it is believed that they are about the same at 11 Hz. It is believed that with a little refinement, this type of temperature measurement would permit a quantitative comparison between the experimental and theoretical ($\Delta R/R$) results. Another approach for quantitative comparison has been used in Chapter 5.

Near liquid helium temperatures, power pulses of 100-200 milliwatts were used. A slight problem in that case was that the resistance ($\sim 200\ \Omega$) of the GaAs heater was highly temperature dependent,

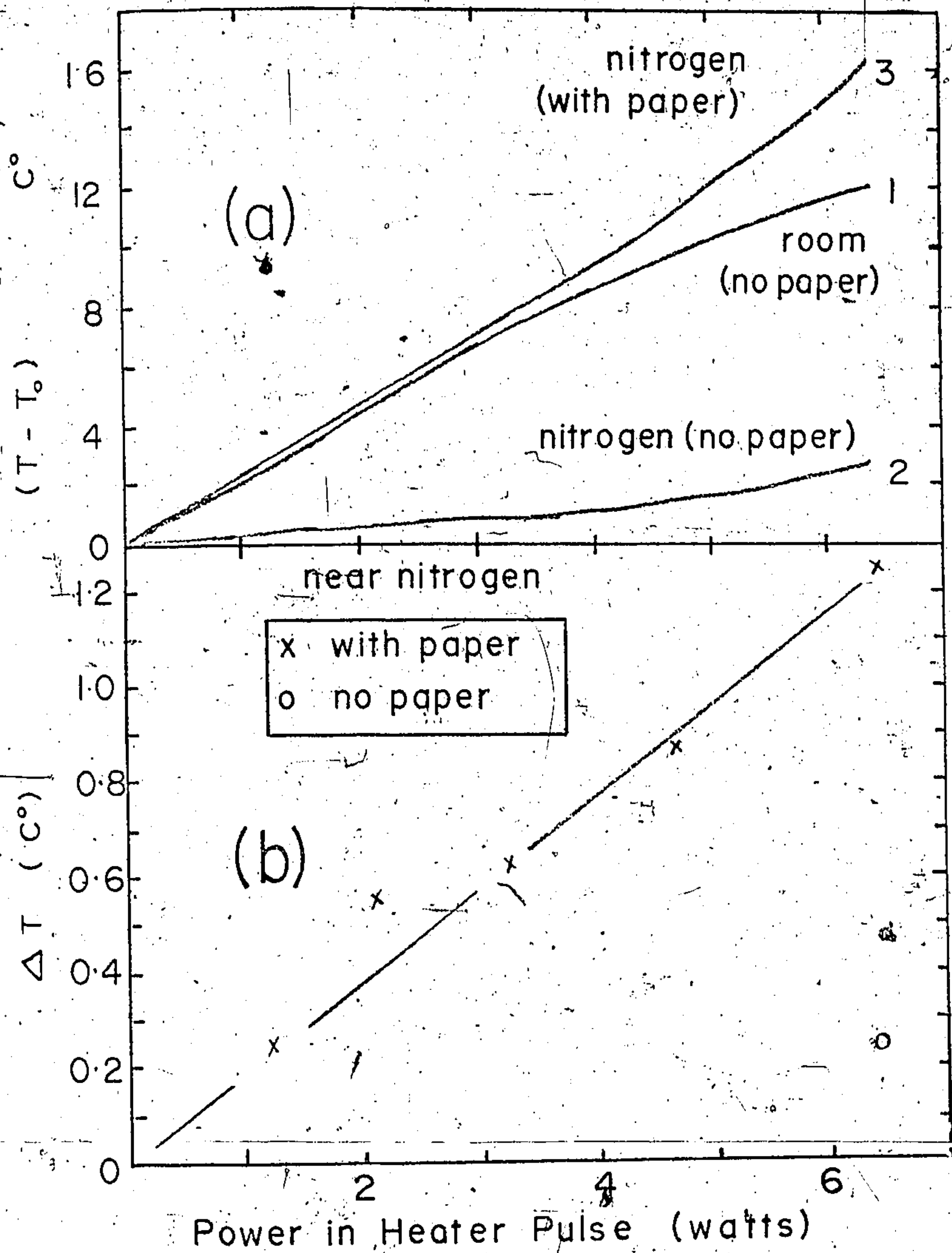

Figure 7. (a) Rise in average temperature of sample due to pulsing: (1) at 285K, at 78K, without(2) and with(3) paper behind the heater. (b) Modulation in temperature, ΔT, at 78K, as a function of power level.

and some series resistance in the relay circuit was required to prevent a runaway situation.

4.3.3 Optics

The light source was either a Sylvania DWY quartz-halogen tungsten lamp operated around 400 watts, or a Nernst filament operated around 150 watts, connected to a regulated power supply. The sources were not cooled. The source housing was made of an asbestos-base board. Adjustable rectangular blinds, which slid along vertical and horizontal tracks, were found convenient as eye protectors, as reducers of scattered light, and as controls for adjusting the aperture angle in the light beam from the exit slit. This latter use permits a less distorted slit image which may be desirable when one has a sample or detector of small dimensions. The mirrors were typically 4 inches in diameter with focal lengths suitable for f/5 optics. An eight blade chopper driven by a variable frequency motor was placed ahead of the entrance slit. Normally it was rotated around 25 cycles per second. The reference signal used in the detection of the chopped light was independent of the source, being provided by a penlight-CdS cell arrangement mounted inside the chopper housing.

The dispersion device was a Spex Model 1702 automatic scanning, grating spectrometer. The gratings used were blazed at 0.75, 1.6 and 4 microns, with typical dispersion of 20, 20, and 80 angstroms per mm.

slit width, respectively. Stain filters at 0.4, 0.6, 0.7 microns, and interference filters at 1.04, 1.9, and 3.04 microns from Optical Coatings Laboratories, Inc., served to eliminate second order contributions.

The cryostat windows were of quartz or lithium fluoride. The detectors were nitrogen-cooled PbSe cells (λ > 2.5 microns), room temperature large surface (0.8 x 1.5 cm) PbS cells (λ > 0.5 microns), and a variety of photomultiplier tubes. The PbS cell was mounted in a black box with a small opening, such that it would receive light only from the detector mirror.

Excessive precautions were not required for eliminating room light, and all experiments were done under normal room conditions with the light beam chambers somewhat shielded.

4.3.4 Detection

This section is organized as follows: first, a few comments about liquid nitrogen cooling of detectors; secondly, a statement of the equipment using in the detector circuit; and thirdly, some notes about the sources and reduction of undesirable signals.

The PbSe cells were pressed with beryllium copper springs against a metal plate attached to a cold finger. No success was made

in mounting a PbS detector on a cold finger. Although the substrates contracted closely with respect to the PbS films as was seen when the whole detector was immersed slowly through the vapor into liquid nitrogen, the films cracked in every case when mounted in several manners on the tailpiece. One guesses that the substrate cooled ahead of the film. Possible ways to avoid this would be to cool slowly, monitoring the tailpiece temperature, or to use a cryostat in which the detector could be totally immersed in liquid nitrogen.

The detector was in series with 24.3 volts of Mallory Duracell mercury batteries and a 931 K resistor. The signals were amplified and phase-sensitively detected using the following Princeton Applied Research equipment: (a) for the modulation signal, Model 213 pre-amplifier, Model 210 selective amplifier, Model 220 lock-in amplifier; (b) for the chopped light signal, Model 122 lock-in amplifier. For electronic division of the two signals in order to obtain (ΔR/R) values directly, either a home-made box containing two operational amplifiers to convert the output impedances of the lock-ins, a power supply and a Burr-Brown divider, or a PAR Model 230 multiplier-divider unit was used.

The main spurious signal present at room temperature is often the heater-sample modulated black body radiation at the modulation frequency. Some ways to reduce this are (a) to use detectors which do

not respond at wavelengths longer than the measurement range desired, and (b) to use filters which do not pass long wavelengths, for example a quartz window when using PbSe in the 2.5 - 4 micron range. This signal must be eliminated by a dc back-off if one is performing electronic division of the lock-in signals. The effect is insignificant at low temperatures. Common causes of noise in the modulation signals are source instability, vibration of optical components, faulty cables, and a varying leakage resistance at the junction of the detector leads on the cryostat.

CHAPTER 5

THERMOREFLECTANCE AT THE FUNDAMENTAL GAP OF HEAVILY-DOPED n-TYPE INAS

5.1	Introduction	85
5.2	Experiment and Data	86
5.2.1	Sample preparation	86
5.2.2	Sample mounting	87
5.2.3	Measurements	87
5.2.4	Results	88
5.3	Theory and Analysis	91
5.3.1	Outline	91
5.3.2	The Kane model	91
5.3.3	The dielectric constant	97
5.3.3a	discussion of the meaning of $\rho(E')$, the density of possible transitions at E'.	99
5.3.3b	calculation of $\rho(E')$ for band $2 \rightarrow 4$ and band $3 \rightarrow 4$ transitions.	102
5.3.4	Modulation of the dielectric constant	108
5.3.5	Line shape calculations	111
5.3.6	The possibility of broadening of the line shape by sample inhomogeneity.	117
5.4	Discussion and Conclusions	118

5.1 Introduction

This Chapter presents the thermoreflectance data and analysis for the InAs material, the preparation of which was described in Chapter 2. A small part of the analysis in Section 5.3.2 reproduces some of the ideas of Chapter 3. This has been done to make the reading easier. The measurements, techniques, and analysis described in this chapter are the original work of the author.

Although modulated reflectance techniques have been used widely during the past decade,[20,21] their application to group IV and III-V semiconductors in all but a few cases has been concerned with intrinsic optical structure, that is, the reflectance of materials with full valence bands, and empty higher bands. Some exceptions have been electroreflectance measurements by Cardona et al.[91] on some heavily-doped n- and p-type GaAs, and the field-induced, band-filling technique in n-type InSb by Glosser et al.[108] In the former work, Burstein-Moss shifts[16,17] up to 0.1 eV were observed, but the light and heavy hole bands were not distinguished. In the latter work, the variation of transition energies to and from states near the Fermi level as the surface potential was changed was used to identify the band origins of some electroreflectance structure. Another modulation technique, thermo-absorption, served to study intervalence band transitions in p-type Ge.[109] However, except for the short treatement in Reference 91, modulation techniques have not been applied to trace the conduction and valence

band energies near $k = 0$ at conduction electron or hole concentrations at the level of 10^{19} cm^{-3}. Some d.c. absorption studies of heavily-doped III-V semiconductors have been made, the most detailed of by Gobeli and Fan[18] on p-type InSb. The absorption edge in heavily-doped n-type InAs[10,19] is broad, and absent of structure which would indicate the separate onsets of transitions from the heavy and light hole valence bands.

The thermoreflectance technique has been used here to study the region of the onset of band-to-band transitions in heavily-doped n-type InAs. The experimental results are presented first in order to better identify the specific aim of the analysis section, which is to see if the signals obtained are consistent with the Kane model for the conduction, and light and heavy hole valence bands. The effect of the impurities on the band structure[110] will be ignored in the analysis. Finally, some comments will be made regarding the comparison between experiment and theory.

5.2 Experiment and Data

5.2.1 Sample preparation

The samples were cut from material central to the ingots and adjacent to the material used for the Hall measurements which were

described in Chapter 2. The sample dimensions were typically $8 \times 2.5 \times 0.20$ mm^3.

5.2.2 Sample mounting

The sample mounting and heating were as described in Section 4.3.2. In a series of measurements such as this, indirect heating is preferable so that all the samples can be more or less equally heated. This was assured by two monitoring procedures: 1) a small thermocouple was mounted via a small sample on the heater, and its reading was reproduced for each measurement; 2) samples were always mounted two at a time on the heater, one of the samples being common to all the runs, and some measurements of $(\Delta R/R)$ of the common sample were part of each run.

5.2.3 Measurements

All measurements were made at 85 ± 3K, except for one which was made at room temperature for comparison purposes. A PbS detector was used, except in the case of some measurements of $(\Delta R/R)$ in the E_1, $E_1 + \Delta_1$ region, which were made to see if these transitions were affected by the doping. In most cases, the quotient $(\Delta R/R)$ was calculated from consecutive measurements of the intensities of the a.c. component of the thermally-modulated light beam, and the total reflected beam. This procedure gave a better signal-to-noise ratio than the simultaneous electronic division of the two signals. A $(\Delta R/R)$ run was

made on a pure Ge sample under the above conditions, so that a comparison between theory and experiment could be made for the ratio of the InAs to Ge modulation of reflectance.

5.2.4 Results

The ($\Delta R/R$) results for the InAs samples are shown in Figs. 8 and 9. The main features of these spectra seem to be the following: 1) within each spectrum there are two maxima and two minima; 2) the magnitude of the changes in ($\Delta R/R$) is nearly the same for all the samples, although the higher energy peaks are noticeably weaker for the samples with lower doping; 3) there is a shift of all the peaks toward higher energies as the doping increases; 4) the separation between successive minima increases rapidly for the first range of doping increase, and then more slowly; 5) the widths of individual structures become continuously broader as the doping increases. Another aspect is the negative-going result at low energies for samples with N equal to 0.24, 0.47 and 5.60 x 10^{19} cm^{-3}. This is due to the modulation of the absorption of light which has passed through a sample and is reflected from the back surface. This component is much reduced in the more heavily-doped samples, but is evident in the sample with N = 5.6 x 10^{19} cm^{-3} because, in the preparation, both surfaces of the sample were inadvertently chemically polished, thus reducing the thickness as well as increasing the in-beam reflection from the back surfaces.

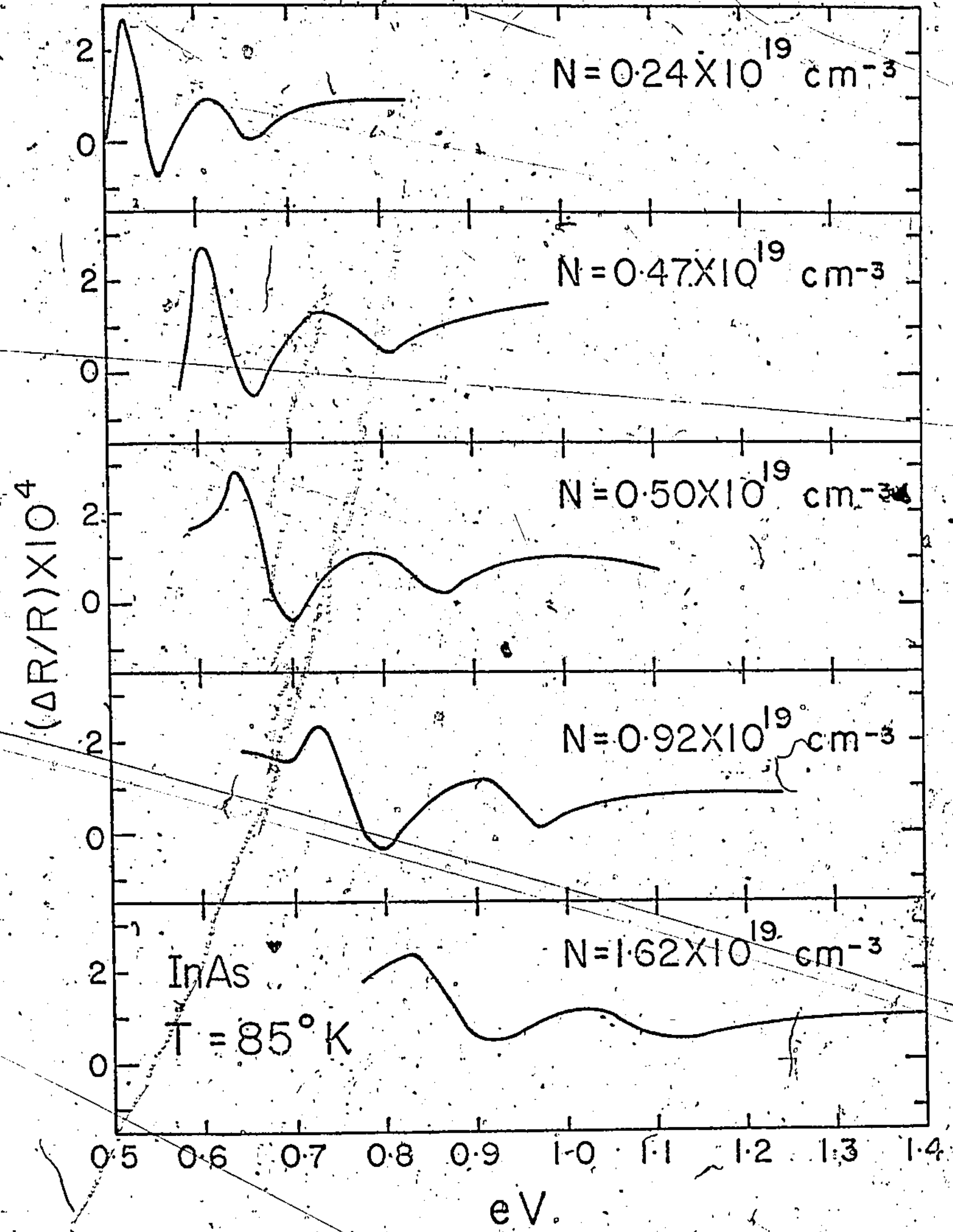

Figure 8. (ΔR/R) spectra at 85K for the first five InAs samples.

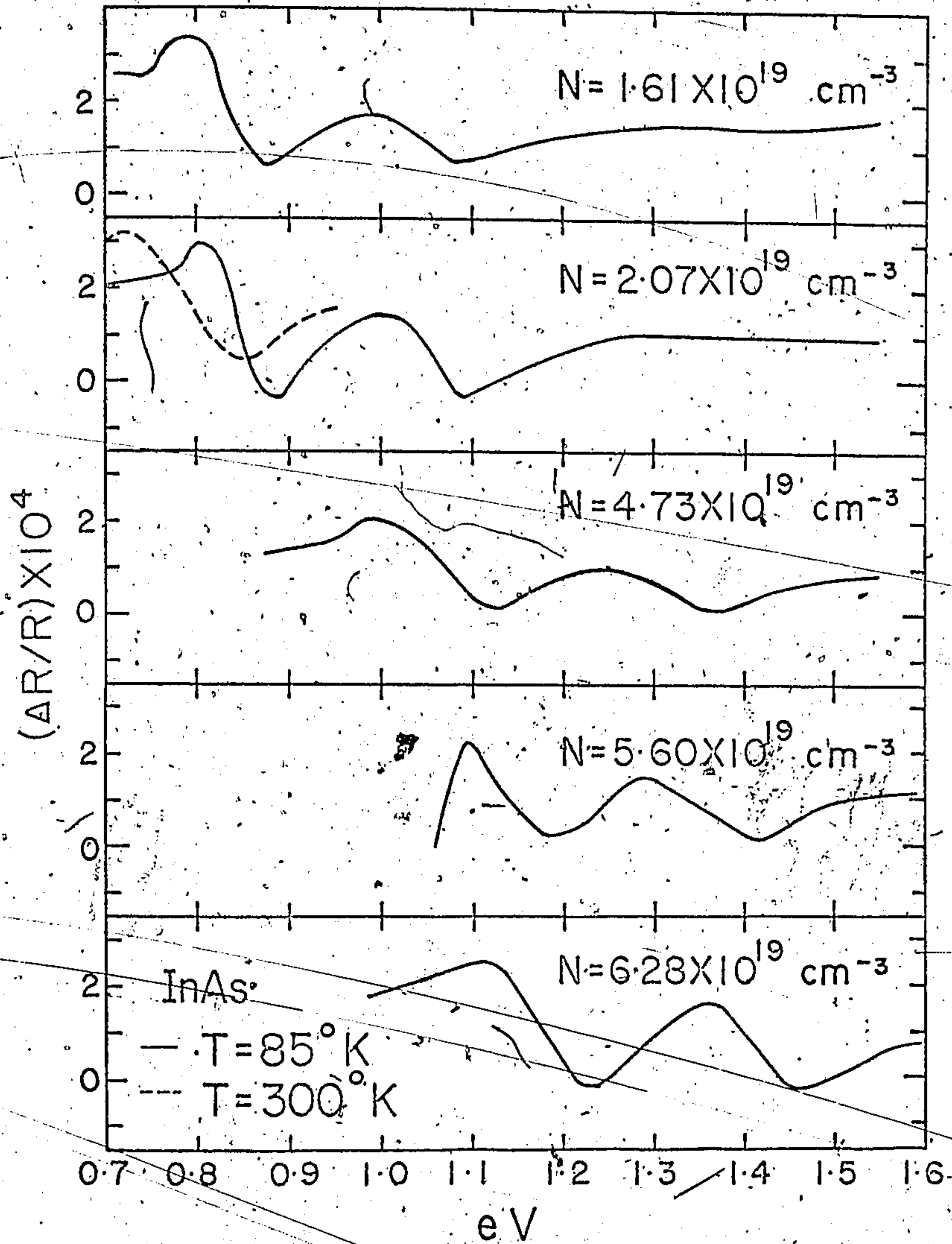

Figure 9. (ΔR/R) spectra at 85K for the remaining five InAs samples, as well as one peak at 300K for one sample.

The results of the auxilliary experiments were: 1) room temperature measurements give a structure shifted to lower energies, and considerably broadened; 2) the negative peaks of the $(E_1, E_1 + \Delta_1)$ structures for N = 0.001, 2.07 and 6.28 x 10^{19} cm^{-3} were at (2.607, 2.917), (2.591, 2.887) and (2.580, 2.890) eV, respectively; 3) the magnitude of $(\Delta R/R)$ of the negative exciton peak for Ge was 4 x 10^{-4}. The result 2) above is not discussed further.

5.3 Theory and Analysis

5.3.1 Outline

The basis of the present analysis comes from three sources: 1) the Kane model for the conduction and valence bands of III-V compounds, including the first order perturbation corrections for higher bands, but assuming spin degeneracy; 2) some experimental and semi-empirical values for the band parameters, and 3) the relationship of Ehrenreich and Cohen for the contribution of a valence-to-conduction band transition to the dielectric constant. With these, the temperature derivative of the dielectric constant is calculated and related to $(\Delta R/R)$ by Seraphin's expression.

5.3.2 The Kane model

Kane's result[2] for the E vs $\underline{k}$ relationship of the conduction and three uppermost valence bands at k = 0 is

$$E_i = E_{Ki} + k^2 \left[s + a_i^2 A' + b_i^2 M + c_i^2 L' + (b_i^2 - 2c_i^2)(L-M-N)h(\theta, \phi) \right]$$

$$i = 1, 2, 4 \qquad 5 - (1)$$

where E_{Ki} is a solution of the equation

$$E_{Ki}(E_{Ki} + E_G)(E_{Ki} + E_G + \Delta_o) - sk^2 E_p (E_{Ki} + E_G + \tfrac{2}{3}\Delta_o) = 0 \qquad 5 - (2)$$

and

$$E_3 = -E_G + k^2 \left[s + M + (L-M-N)h(\theta, \phi) \right] \qquad 5 - (3)$$

In these equations the following conventions and notation have been used: the bottom of the conduction band is the zero of energy; the subscripts 1, 2, 3, 4 correspond to the split - off, light and heavy [illegible] valence bands, and the conduction band, respectively; s equals $\hbar^2/2m$ where m is the free electron mass; a_i^2, b_i^2, c_i^2 are the squares of the coefficients of an s- and two p-type wave functions in the wave functions for bands 1, 2, and 4; the coefficients A, M, L', L, and N involve matrix elements of the momentum operator between the wave functions at k = 0 of these four bands and those of upper bands; $h(\theta, \phi)$, where θ , ϕ are the usual spherical angle co-ordinates, is defined by $k^4 h(\theta, \phi) = k_x^2 k_y^2 + k_x^2 k_z^2 + k_y^2 k_z^2$; E_G and Δ_o are the differences at k = 0 of $E_4 - E_3$ and $E_3 - E_1$, respectively; E_p is proportional to the square of the momentum matrix element between s- and p-type functions; more exactly,

$$E_p = \frac{2}{m} \left| \langle X | p_x | s \rangle \right|^2 \qquad 5-(4)$$

where X indicates the transformation properties of a p-type function, and s indicates the spherical symmetry of the conduction band s-type function.

As a first step, Eq. 5-(2) was solved for a range of E_{Ki} values, using the values of 0.40,[85] 0.38,[33] and 22.2[34] eV for E_G, Δ_o and E_p respectively.

In using 0.40 eV for E_G, half of the measured gap temperature dependence was subtracted as an approximation to retaining only dilatation component of the temperature shift.[79] a_i^2, b_i^2, c_i^2 were calculated according to Kane's paper.[2] The values for the upper band matrix elements, excepting A', were calculated using Lawaetz's semi-empirical values[34] for the Luttinger parameters (see Ref. 84 for the conversion relations). M, L' and (L-M-N) are -3.9s, 0.0, and 5.5s respectively. A' was determined to be -3.0s from the difference between the measured[86] cyclotron resonance effective mass at helium, 0.0235 m, and that calculated at k = 0 excluding upper band terms. Fig. 10 shows the result for the four bands for the <100> and <111> directions, while Fig. 11 gives a plot of a^2, b^2 and c^2 for the conduction and light hole valence bands. Fig. 10, although already seen in Chapter 1, is reproduced here for easy reference. For convenience, one abscissa of Fig. 10, and that of Fig. 11 are given in terms of N,

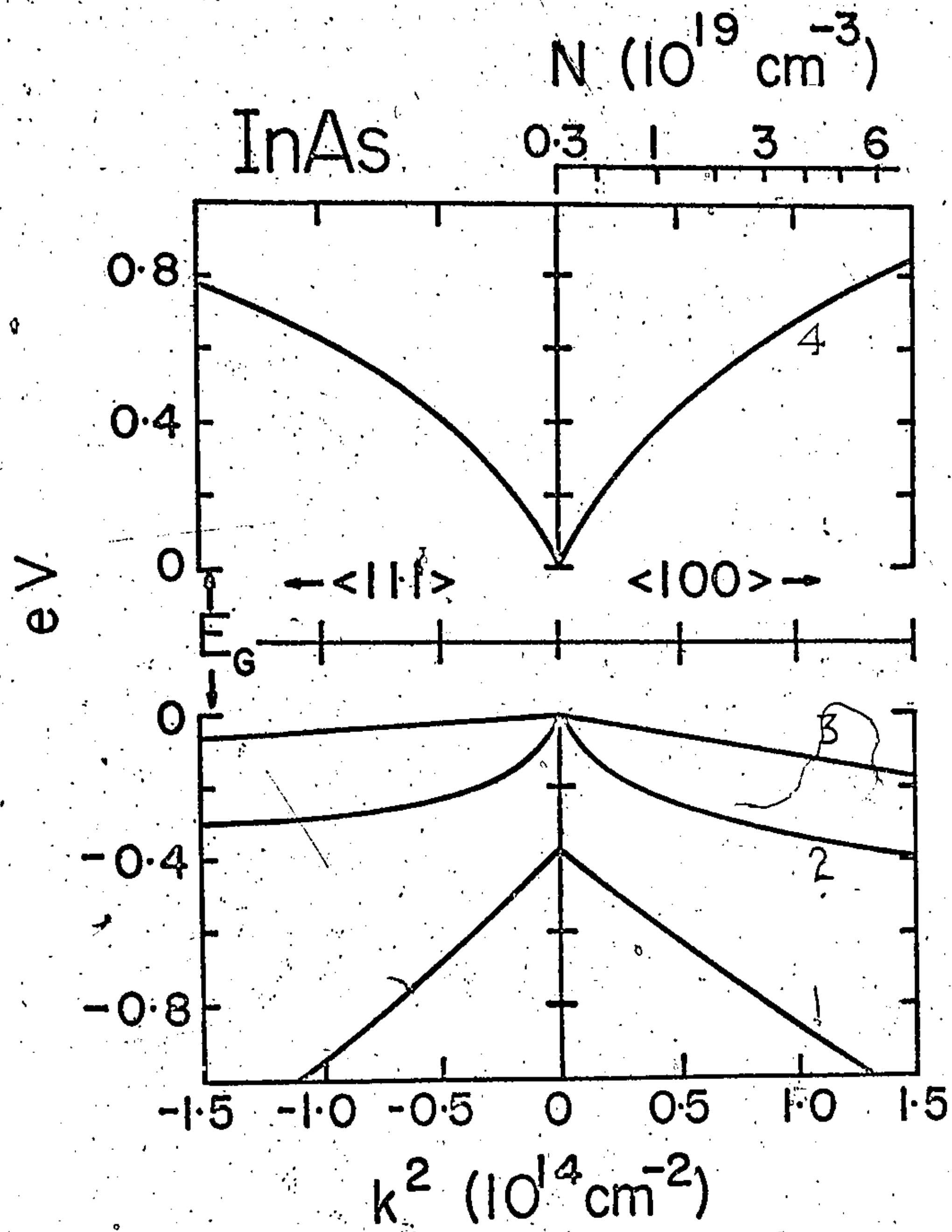

Figure 10. E vs k^2 in <100> and <111> directions for bands 1 - 4, for InAs. The upper right hand abscissa indicates the concentration electrons for $E_{Fermi} = E_4$<100>.

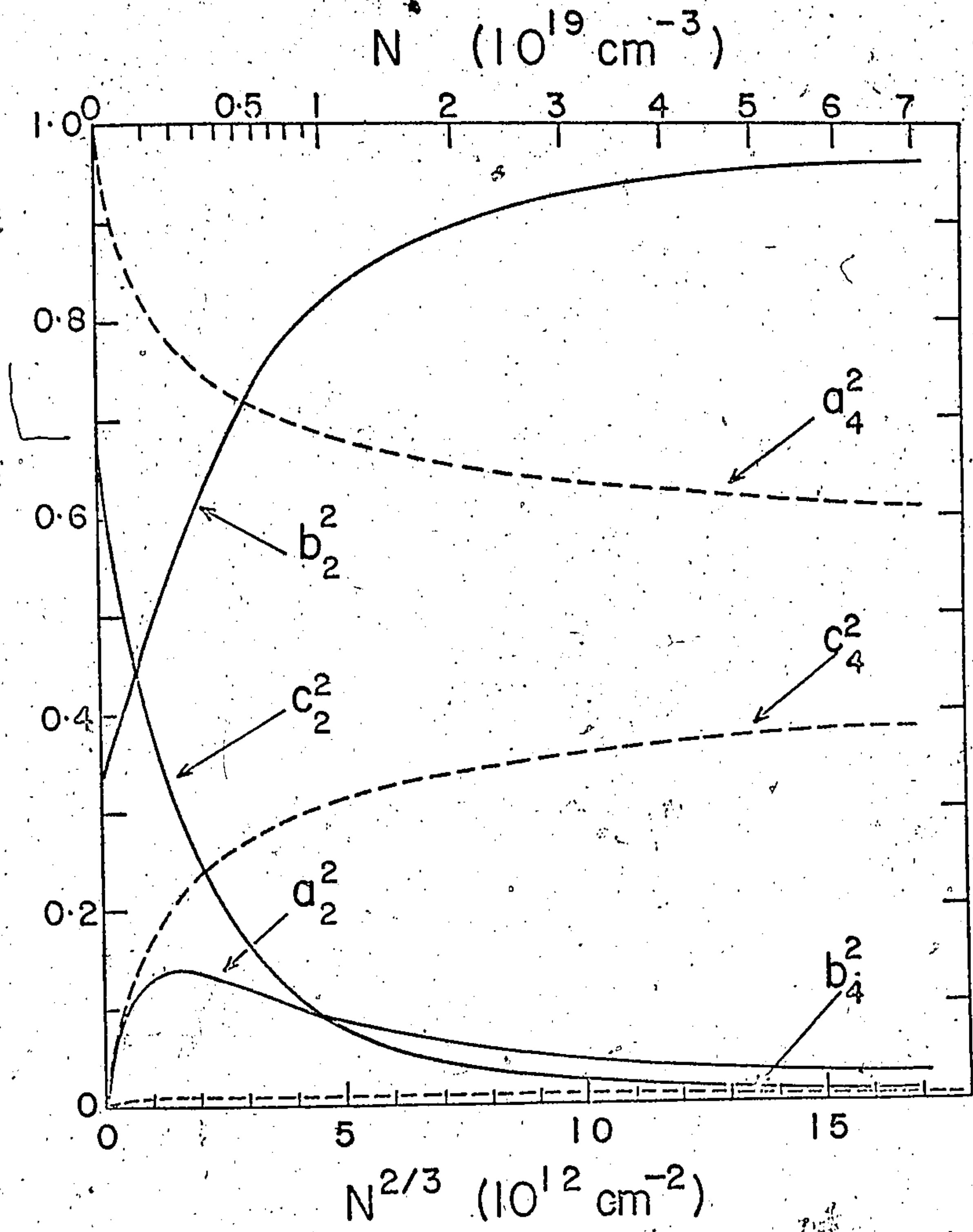

Figure 11. a^2, b^2, and c^2 at the Fermi level for the conduction and light hole valence bands as a function of $N^{2/3}$.

the electron concentration in the conduction band. The calculation assumed complete degeneracy, which is correct to the order of $(k_o T/E_F)^2$,[45] where k_o is the Boltzmann constant and E_F, the Fermi level. The procedure for finding N as a function of E_F will be outlined. Eq. 5-(2) states that $k_F^2(\theta, \phi)$ is determined by E_{K4}. Since the average value of $h(\theta, \phi)$ over all angles is (1/5), a first order approximation to $k_F^2(\theta, \phi)$ is

$$k_F^2(\theta, \phi) = k_F^2\langle 100\rangle (1 - D_4 f_a h(\theta, \phi)) \qquad 5 - (5)$$

where

$$f_a = (b_4^2 - 2c_4^2)(L-M-N)$$

and

$$D_4 = (dk^2/dE_4)_{av} \qquad 5 - (6)$$

the derivative being evaluated with Eq. 5-(2) at $E_4 = E_4\langle 100\rangle - f_a k^2/5$. Relating the concentration of carriers to the volume of occupied states in k-space in the usual way, one has a first approximation

$$3\pi^2 N = k_F^3\langle 100\rangle (1 - 0.3\, D_4 f_a) \qquad 5 - (7)$$

It is noted from Figs. 10 and 11, that for N of the order of $10^{19}\,cm^{-3}$ and higher, the light and heavy hole bands are almost equally "heavy", the behaviour in the <100> directions being $(s + M)k^2$, since b_3^2 is almost unity.

5.3.3 The dielectric constant

The contribution to the dielectric constant ε at an energy E from transitions between bands 2, 3 and band 4 is given by[96] (see Section 4.2.2)

$$\varepsilon(E) = -C \sum_{i=2,3} \int_0^\infty \frac{M_{i4}^2(E')}{E'} \rho_i(E') \frac{dE'}{(E - E' + i\Gamma)(E + E' + i\Gamma)} \qquad 5-(8)$$

where $C = 4\pi e^2 \hbar^2 E_p/3m$, e is the electronic charge in unrationalized electrostatic units, M_{i4}^2 is the square of the momentum matrix element between valence and conduction band states, normalised to unity at k = 0, ρ is the density of possible transitions at E', and Γ is the lifetime broadening parameter. There are two approximations in Eq. 5-(8) which are not made in the original expression;[96] M^2 is considered as dependent on E', and Γ is treated as a constant, whereas M^2 and Γ are more exactly functions of the k-value at which the transition takes place.

Fig. 12 shows the values of M^2 as a function of N for direct transitions from the valence bands to the neighbourhood to E_F, as calculated with Kane's formulae.[1] M^2 for band 1 to band 4 transitions are the smallest. Other factors which act against the observation of $(\Delta R/R)$ structure from the split-off band are: a) the E' denominator in the oscillator strength in Eq. 5-(8) is larger, as is the denominator in $(E + E' + i\Gamma)$; b) $\rho(1 \rightarrow 4)$ is smaller because the steep slope for

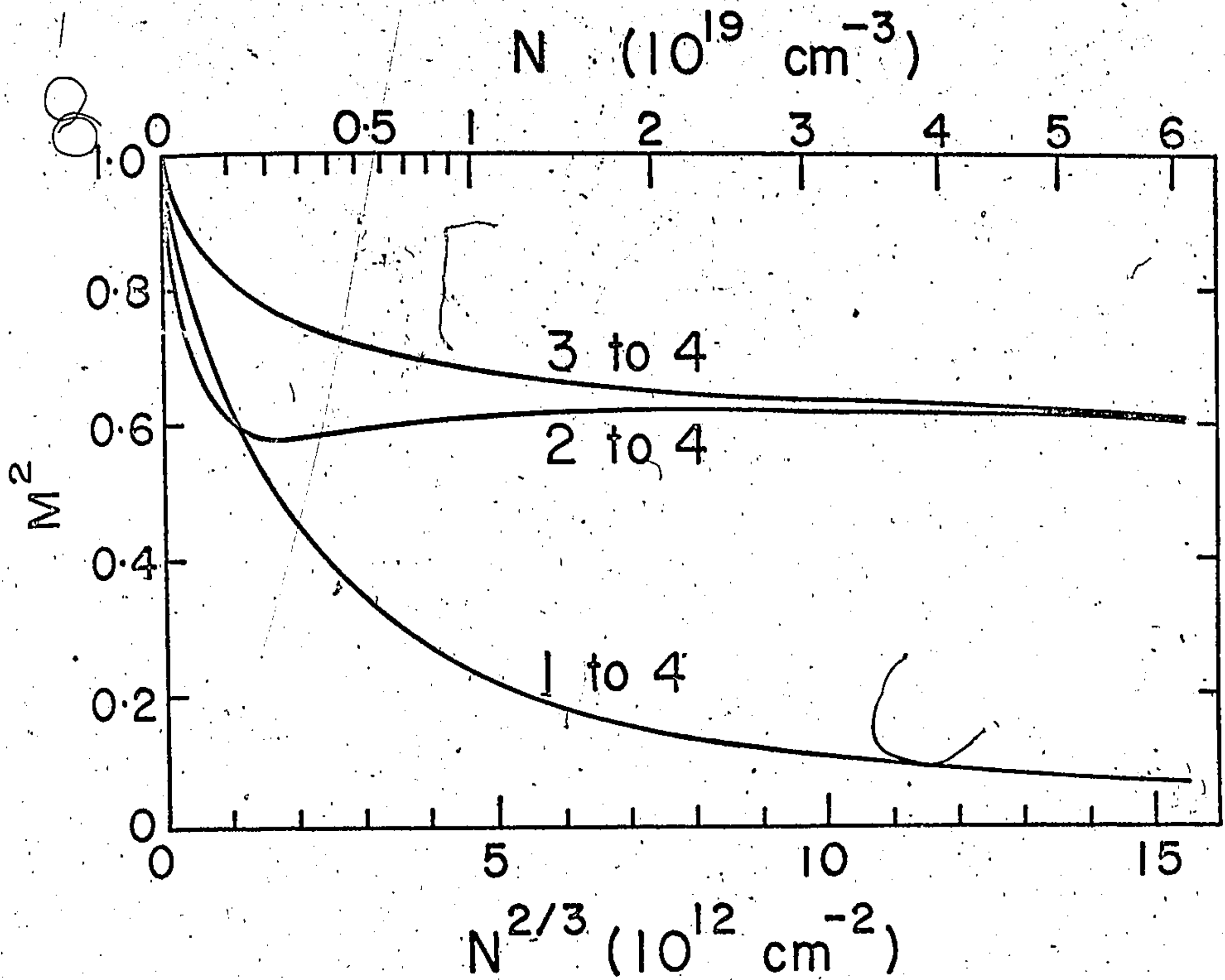

Figure 12. Relative transition probabilities for direct transitions from bands 1, 2, and 3 to E_F in the conduction band, as a function of doping level.

band 1 in Fig. 1; c) the Γ values are probably higher, as has been found in Ge for valence to conduction band transitions at $k = 0$.[111]

5.3.3a discussion of the meaning of $\rho(E')$ the density of possible transitions at E'

Before proceeding with the statement of the approximations to be made in the evaluation of 5-(8), a qualitative discussion will be made of the meaning of $\rho(E')$ in eq. 5-(8). In order to use the expression for the contribution to the dielectric constant due to transitions which occur at E', one must know how many transitions could occur in the energy range E' to $E' + dE'$. This question will be viewed for five situations of increasing order of complexity: (i) spherical constant energy surfaces in the conduction and valence bands at zero degrees Kelvin; (ii) situation (i), but at non-zero temperatures; (iii) situation (i), but with considerable anisotropy in the constant energy surfaces in the valence band; (iv) situation (iii) but with a slight anisotropy in the constant energy surfaces in the conduction band; (v) situation (iv) but at non-zero temperatures.

(i) spherical energy surfaces at zero Kelvin

At absolute zero one need only know the joint density of states $\rho_o(E')$ and the energy E'_F of a direct transition between the valence band and the Fermi level at E_F ($=E_{4F}$) in the conduction band.

(ii) case (i) at $T \neq o$

The Fermi-Dirac statistical factor applies to the occupation of

states around E_{4F}. Consider a transition which occurs between the valence band and conduction band at E' such that the energy of the final state is E_4. It is clear that if one wishes to write the statistical factor in terms of the transition energies E' and not E_4, the energy term in the distribution must be multiplied by dE_4/dE'. If one is only considering a small range of E' values, one can make the linear approximation that $(dE_4/dE') = \beta^{-1}$. Thus at finite temperatures $\rho(E')$ becomes $\rho_o(E')[1 - (1 + \exp (E' - E_F')/\beta k_o T)^{-1}]$.

(iii) anisotropy in the valence band at zero Kelvin

As an introduction to this situation, consider the distribution of energies for transitions to the constant energy surface at the Fermi level in the conduction band. If the valence band has the anisotropy given by the Kane model, the difference between the minimum energies and the maximum energies will be approximately that given by the W-values in Figure 15. This is approximate because Figure 15 also includes the effect of a slight anisotropy of the Fermi surface in k-space. The distribution of the energies for such transitions is presented in Figure 13. The peak in the distribution results from the saddle point behaviour of the anisotropic terms near the <110> directions. It is noted here that Figure 13 is an original finding.

Consider a negative anisotropy term for the valence band, such that the energy on a sphere of radius k has minima in the <111> directions. This is the behaviour of the bands 2 and 3 in Figure 10. In order to find the joint

density of states one must integrate over a constant conduction-valence band energy difference. The final states in the conduction band do not have constant k_F, E_4 values. To calculate the joint density of states one should make a sum of the sort

$$\rho_o(E_F') = \int_0^{-W} w(\Delta E)\ \text{Dens}\ (\Delta E)\ d(\Delta E) \qquad 5 - (9)$$

where ΔE is $E_4 - E_{4F}$, Dens (ΔE) is just the density of the various ΔE intervals as presented in Figure 13, normalized such that

$$\int_0^{W} \text{Dens}\ (\Delta E)\ d(\Delta E) = 1,$$

and $w(\Delta E)$ would be an appropriate weighting factor for each E_4 value. The author has been unable to obtain a workable form for w, and in this work it will be considered constant and equal to (dN/dE') evaluated in the <100> direction. This data can be obtained from Figure 10. That w is fairly constant for a particular E' value can be argued as follows. Consider the maximum and minimum energy points on the conduction band energy surface of Eq. 5-(9). They will be in the <111> and <100> directions, respectively. w would be proportional to (dN/dE') which equals $(dN/dE_4)(dE_4/dE')$. It can be shown using the data of Figure 10 that (dN/dE_4) varies by less than 10 percent, and (dE_4/dE') varies by less than 15 percent for the W-values of Figure 15.

(iv) case (iii) with slight anisotropy in the conduction band

When the conduction band is also anisotropic, energy widths and energy distributions different from situation (iii) are obtained for the transitions from a valence band to a constant energy surface in the conduction band. However, if the conduction band anisotropy is slight, the constant weighting factor of case (iii) can be assumed.

(v) case (iv) at $T \neq 0$

At finite temperatures one must weight each density component in 5-(9) by the appropriate statistical factor, which, for a general E' transition energy, is taken to be $[1 - (1 + \exp[(\Delta E + E' - E_F')/\beta k_o T])^{-1}]$. It is appreciated that the use of β in this form when applying to transitions away from the <100> directions is a simplifying approximation. It is used in this manner because β is not far from unity for the case of n-type InAs. The use of the proper expression would be very cumbersome and it is believed that its effect on the results would be to make the line shapes a little narrower.

An outline of the actual calculation will now be stated.

5.3.3b calculation of $\rho(E')$ for band 2 → 4 and band 3 → 4 transitions

The density ρ of allowable transitions at E' is determined by three factors: 1) the Fermi distribution of occupied states in the conduction band; 2) the curvatures of the bands near k_F (the relevant ones for the modulation calculation); and 3) the anisotropy of the bands. The last of these will be considered first and, as a preliminary, the

density distribution of energies associated with the function $h(\theta, \phi)$ is treated. This has been evaluated by computer by randomly selecting 150,000 values of θ and ϕ in the range 0 to $\pi/2$, and weighting by $\sin\theta$ the incidence of any particular value of h found in one of 100 equal intervals between 0 and 1/3. The result, shown in Fig. 13, with the abscissa normalized to unity, has a peak in the distribution at 0.75. Using a calculation with 500 intervals, a log-log plot was made of the density vs the distance from the peak. As shown in Fig. 14, the density goes as a minus one-fourth power in the neighbourhood of the peak. Thus, were there no anisotropy in the conduction band, direct transitions, for example, from the heavy hole band to a particular k value in the conduction band, would have a range energy of $(L-M-N)k^2/3$, and the distribution given in Fig. 13. However, $k(E_4)$ is a function of direction (see Eq. 5-(5)), and the variation $\Delta E'$ of transition energy E' with respect to E'<100> is to first approximation

$$\Delta E'_{3\to4} = -(L-M-N)k_a^2 h + (s + M)(k^2\langle100\rangle - k_a^2) \qquad 5 - (10)$$

$$\Delta E'_{2\to4} = -(b_2^2 - 2c_2^2)(L-M-N)k_a^2 h + (s + a_2^2 A' + b_2^2 M + c_2^2 L' + D_2^{-1})(k^2\langle100\rangle - k_a^2) \qquad 5 - (11)$$

where k_a^2 gives the variation of k^2 for a constant energy surface in band 4, and where D_2 is the same function as D_4, but calculated for band 2. Because of the terms in h^2, the density distribution of energies is a little different from that of Fig. 13. The widths of the distributions, W, for transitions to E_F are shown in Fig. 15.

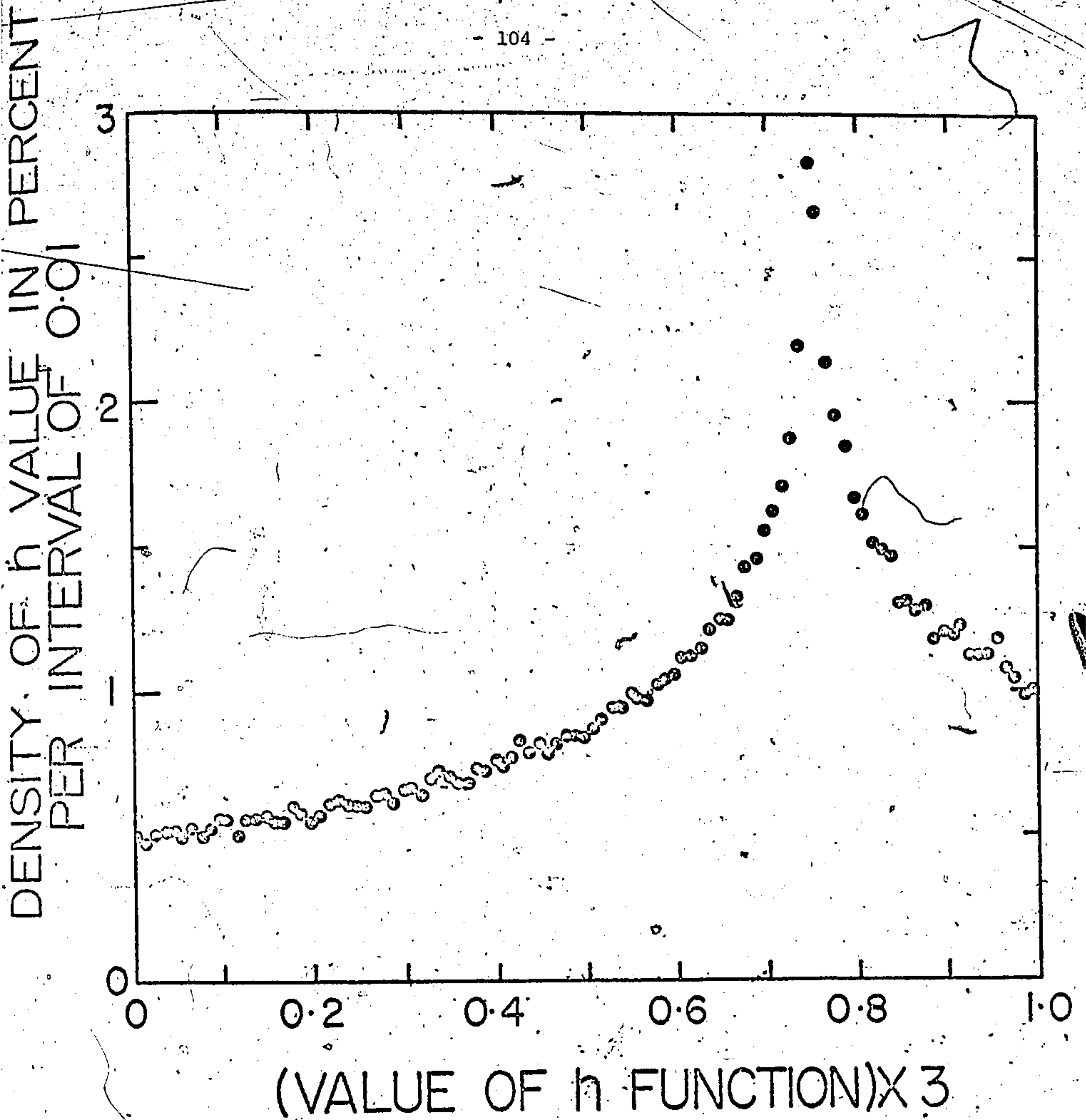

Figure 13. Density of values of 3h on a spherical surface in k-space.

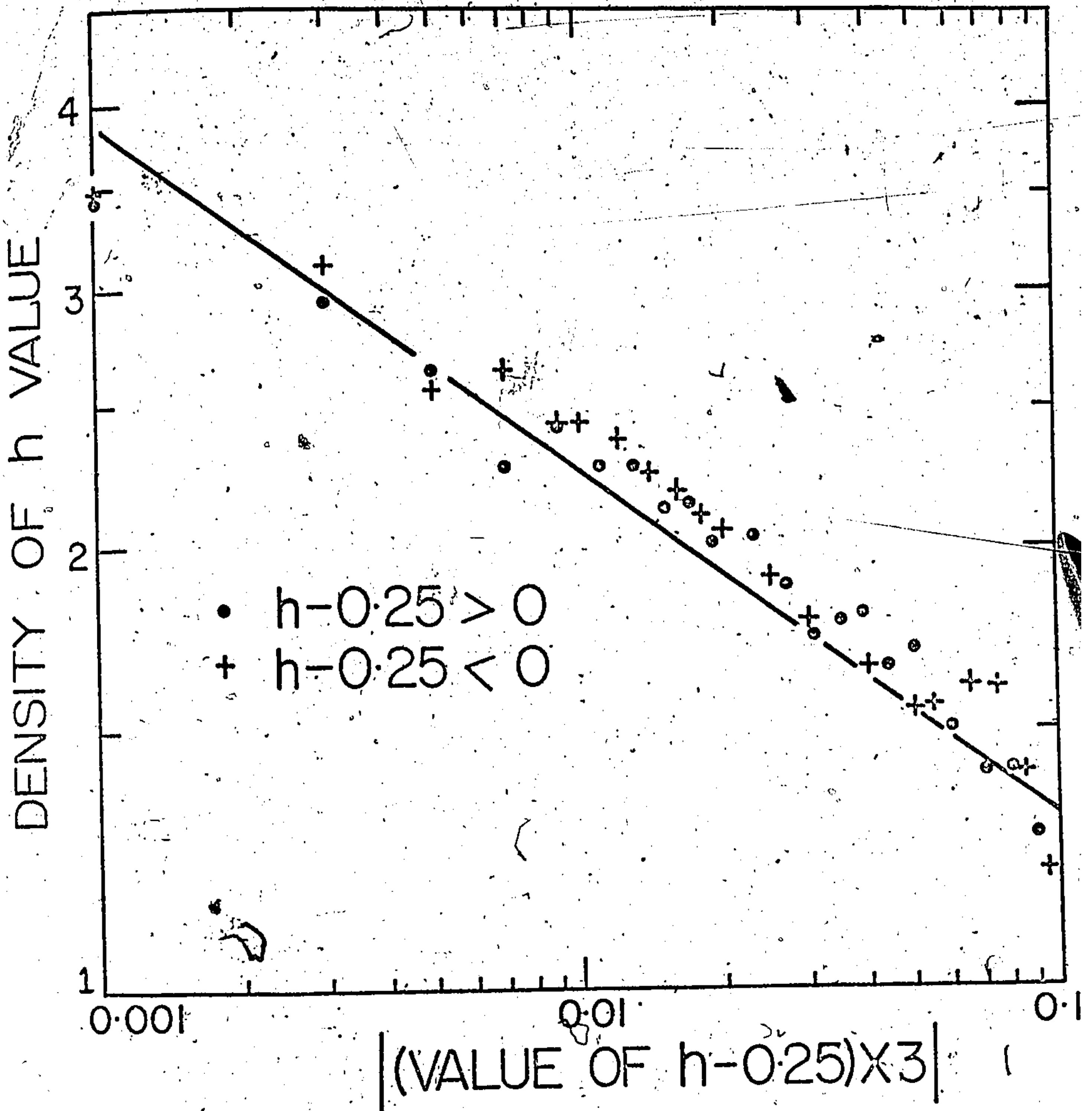

Figure 14. Density of values of 3h in the neighbourhood of the peak in the distribution. The diagnal line has a slope equal to -1/4.

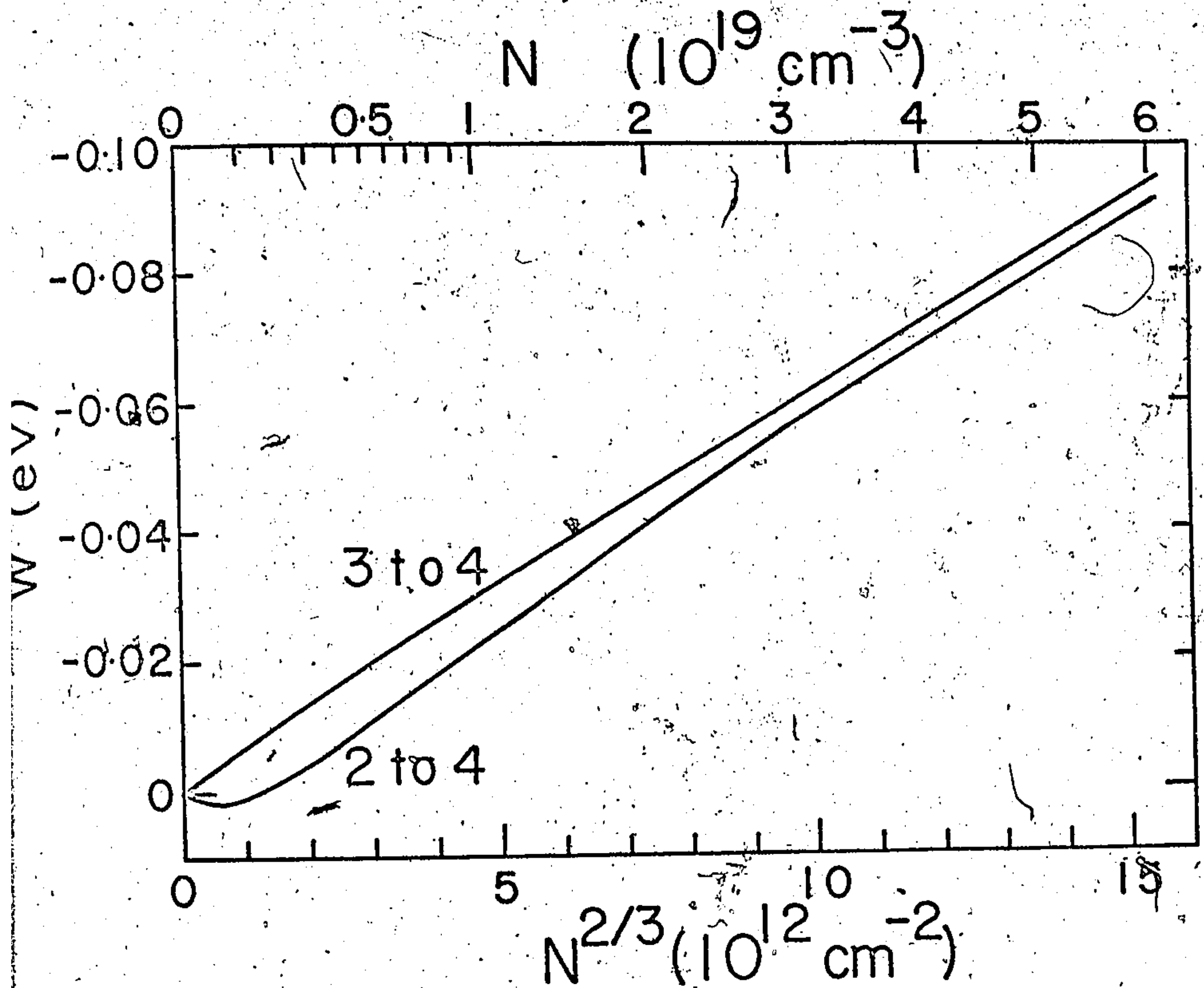

Figure 15. Width of the energy distribution with respect to E'<100>at k_F for 2 to 4 and 3 to 4 transitions, as a function of doping level.

In order to evaluate $(dN/dE''(\langle 100\rangle)_{E'}$, graphs were plotted of $(dN/dE''\langle 100\rangle)_{E'}$ vs $E'\langle 100\rangle$, and linear relations were found according to

$$(dN/dE''(\langle 100\rangle))_{E'} = g(E_F') + g' \cdot (E'\langle 100\rangle - E_F') \qquad 5-(12)$$

where $g' = (dg/dE'(\langle 100\rangle))$ evaluated at E_F', and where E_F' is the energy difference between E_F and the energy of a valence band at $k_F\langle 100\rangle$. The values for g and g' for $N = 0.3$, 1, and $6 \times 10^{19} cm^{-3}$ for $3 \rightarrow 4$ transitions, and $N = 0.3 \times 10^{19} cm^{-3}$ for $2 \rightarrow 4$ transitions are (2.6, 10.5), (5.2, 14.8), (14.9, 19.5) and (1.7, 7.4) in units of $10^{19} cm^{-3} eV^{-1}$ and $10^{19} cm^{-3} eV^{-2}$, respectively.

The values of β required for the modified Fermi-Dirac factor described in Section 5.3.3a were determined as 1.13, 1.18, 1.32, and 1.57 for $N = 0.3$, 1, $6 \times 10^{19} cm^{-3}$ for $3 \rightarrow 4$ and $N = 0.3 \times 10^{19} cm^{-3}$ for $2 \rightarrow 4$ transitions, respectively. The effective temperatures, that is, the values for βT, would be much higher for measurements in p-type material. This has been discussed in detail by Gobeli and Fan.[18]

Thus, including the temperature, anisotropy, and band curvature effects $\rho(E')$ is determined by

$$\rho(E') = [g(E_F') + g' \cdot (E' - E_F')] \cdot \int_0^{-W} \{1 - [1 + \exp(\frac{E' + E'' - E_F'}{\beta k_o T})]^{-1}\} q(E_F', E'')dE'' \qquad 5-(13)$$

where $q(E_F', E'')$ is the distribution function of the type of Figure 13, normalized according to

$$\int_0^{-W} q(E_F', E'')dE'' = 1$$

5.3.4 Modulation of the dielectric constant

Modulated reflectance is related to the modulation of the real and imaginary parts of the dielectric constant, ε_1 and ε_2 respectively, by[94,89,91] (see Section 4.2.1)

$$(\Delta R/R) = \alpha_1 \Delta\varepsilon_1 + \alpha_2 \Delta\varepsilon_2 \qquad 5 - (14)$$

where α_1 and α_2 are expressible as functions of n_1 and n_2 the refractive index and the extinction coefficient, respectively. α_1 and α_2 were calculated using existing data,[71] with n_1 set to 3.51 for the range above 1.7 microns where data is missing. The result, over the relevant range, is shown in Fig. 16. The discontinuity results from the disagreement between two sets of data;[71] however, it is accepted here that, as shown in the figure, $\alpha_1\alpha_2^{-1}$ is greater than 5 over the range 0.6 to 1.5 eV. The contributions of free carriers to n_1 and n_2 were calculated using the

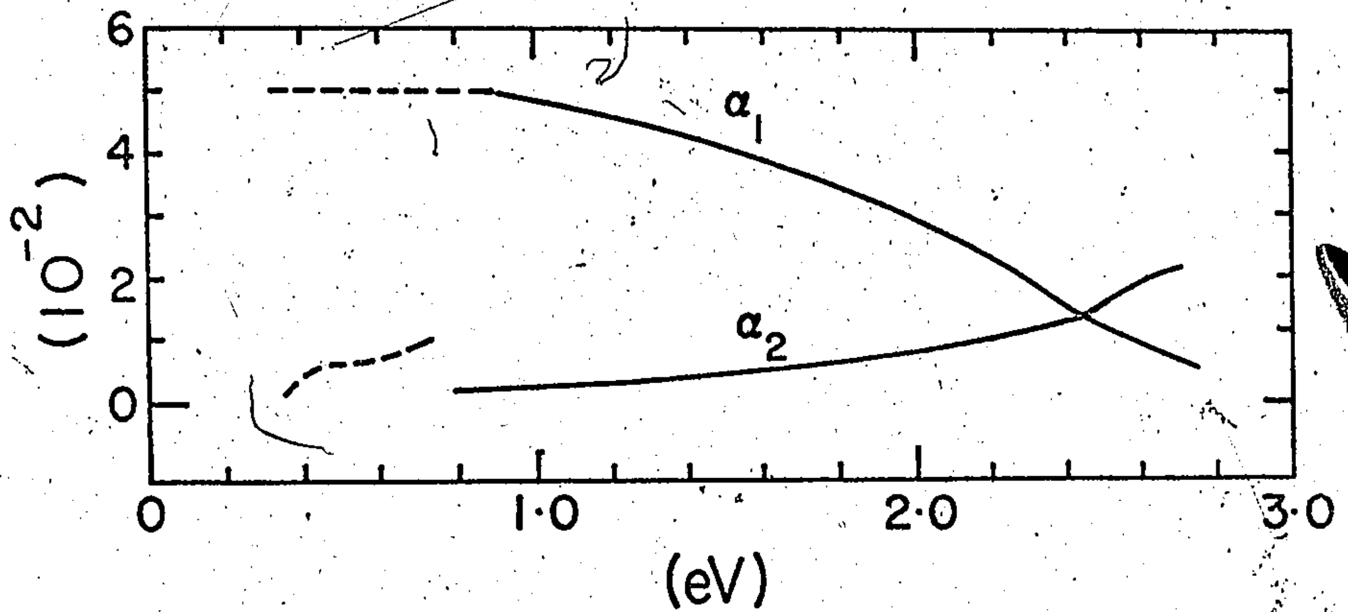

Figure 16. The modulated reflectance coefficients α_1, α_2 for InAs. The dashed portions of the curves were calculated using $n_1 = 3.51$, and n_2 as published (Ref. 71).

expressions of Spitzer and Fan,[9] and found to be negligible. Also, the modulation of such terms is not calculated because they give no structure in the measured region. Because the magnitude of the variation in $\Delta\varepsilon_2$ from band-to-band transitions is within twenty per-cent of that in $\Delta\varepsilon_1$, as calculated by methods similar to those below, the description here considers only $\Delta\varepsilon_1$.

Four possible temperature modulation effects have been considered: a) the variation of E_F' resulting from the change of E_G with temperature; b) the change of the Fermi distribution with temperature; c) the modulation of the broadening parameter; and d) the change in $\rho(E')$ due to changes in band curvatures (i.e., the modulation of g in Eq. 5-(11)). This latter effect was calculated to be a hundred times smaller than a) and b), and is not discussed further.

Factors a) and b) affect $\rho(E')$ according to

$$\frac{d\rho(E')}{dT} = -\frac{g(E_F')+g'\cdot(E'-E_F')}{\beta k_o T}\int_o^{-W}\frac{\left[\left(\frac{\partial E_F'}{\partial E_G}\right)\left(\frac{\partial E_G}{\partial T}\right)+\frac{(E'+E''-E_F')}{T}\right]\exp\left(\frac{E''+E'-E_F'}{\beta k_o T}\right)qdE''}{\left[1+\exp\{(E'+E''-E_F')/\beta k_o T\}\right]^2}$$

5 - (15)

where the first and second terms in the numerator correspond to modulation effects a) and b), respectively. The temperature modulation

of Γ modifies the real part of the integral of Eq. 5-(8) simply by changing the part of the integrand which contains terms in Γ to

$$-(2\Gamma/P)\{1 + 2[E^4 - E'^2 + \Gamma^2]^2/P\}(\partial\Gamma/\partial T)$$

where

$$P = [(E - E')^2 + \Gamma^2][(E + E')^2 + \Gamma^2]$$

It is to be noted that although Γ is taken as constant in the analysis, small changes in Γ over an energy variation of $\beta k_o T$ would have little effect on the evaluation of $\Delta\varepsilon_1$ for the a) and b) factors. Furthermore, the effect on the modulation through the terms in $(\partial\Gamma/\partial E')(\partial E'/\partial T)$ would change the magnitude of factor c), but have little effect on the shape.

5.3.5 Line shape calculations

In the calculations, $(\partial E_G/\partial T)$ has been put equal to the temperature dependence given by Adachi[85] for the optically-measured variation of the gap. Since there is no data available on $(\partial\Gamma/\partial T)$, it was abritrarily set equal to $0.5|\partial E_G/\partial T|$, which puts the contribution from factor 3) at the same level as those from factors a) and b). In order to determine the numerical values for $(d\varepsilon_1/dT)$, in units of K^{-1}, from the curves in Figs. 17-19, the plotted numbers would be multiplied by $(2.1 \times 10^{16} C)\,cm^{-3}\ eV^{-3}\ K^{-1}$, where C is given in Eq. 5-(8).

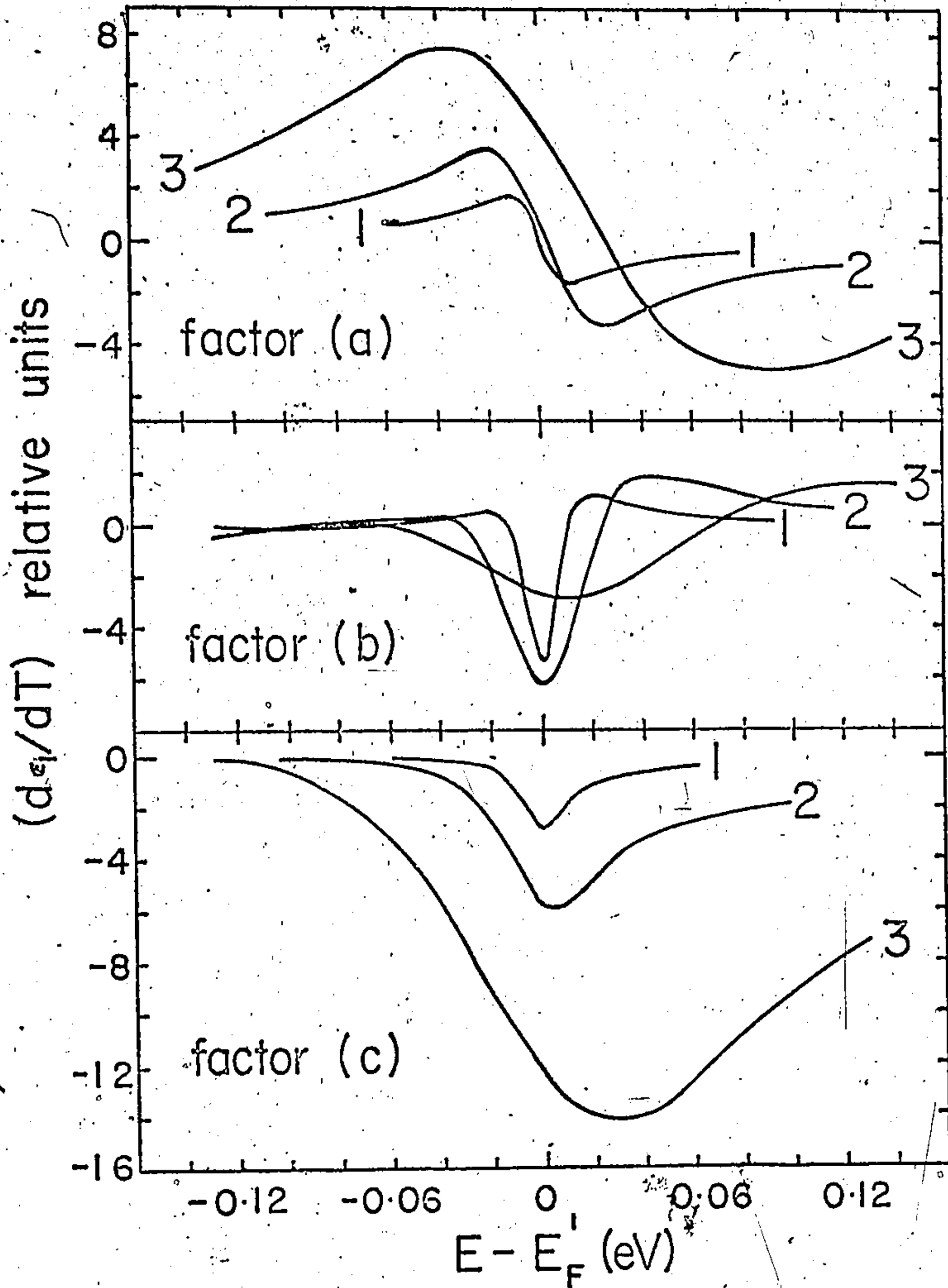

Figure 17. Contributions to ($d\epsilon_1/dT$) from factors a), b), and c) (see text), with β =1.18, and Γ = 0.01 eV, at three temperatures: 1, 20K; 2, 85K; 3, 300K.

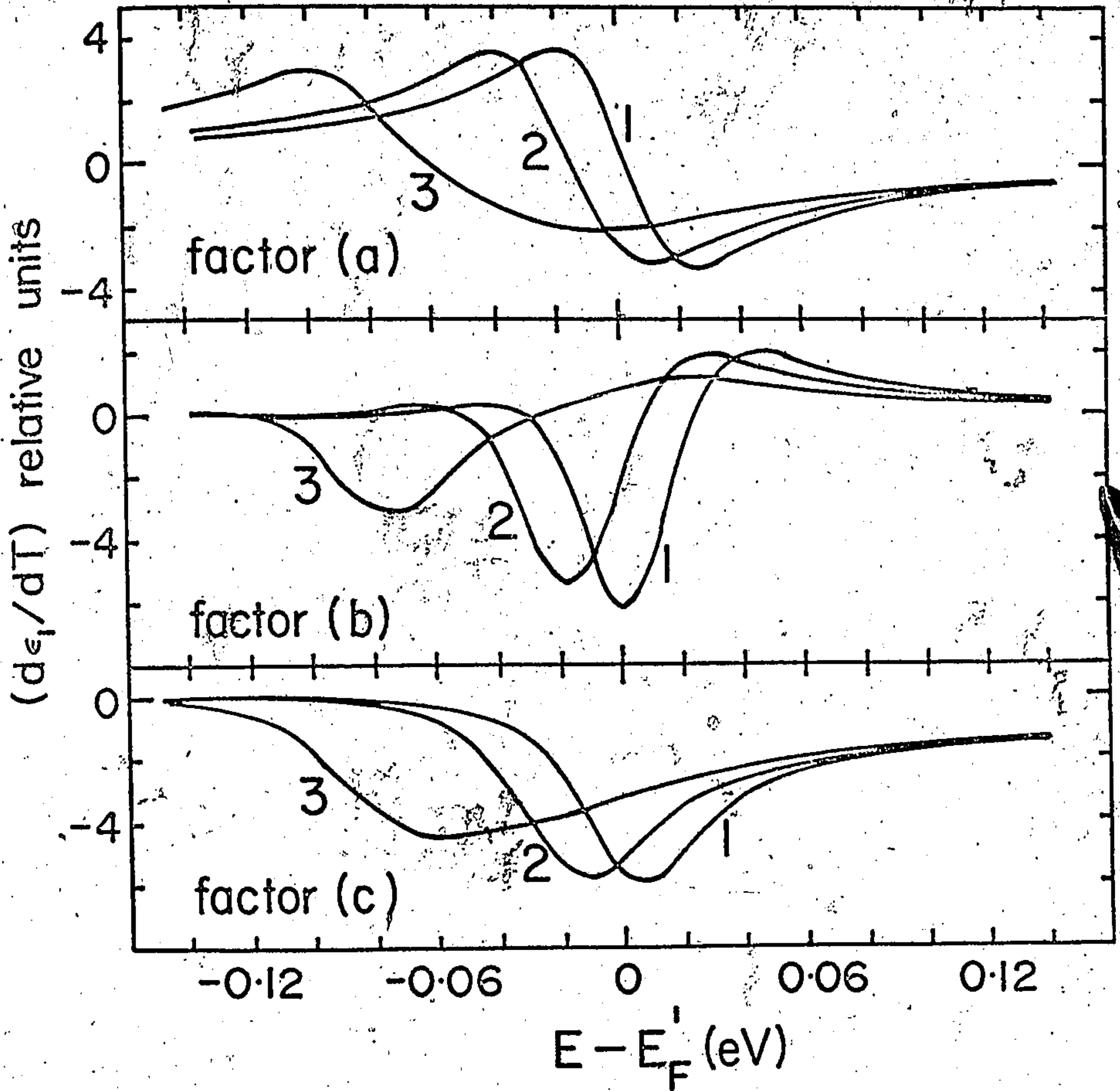

Figure 18. Contributions to $(d\epsilon_1/dT)$ from factors a), b), and c) (see text), with $\beta = 1.18$, and $\Gamma = 0.01$ eV, at 85K, for three values of W: 1, -0.0001eV; 2, -0.03eV; 3, -0.10eV.

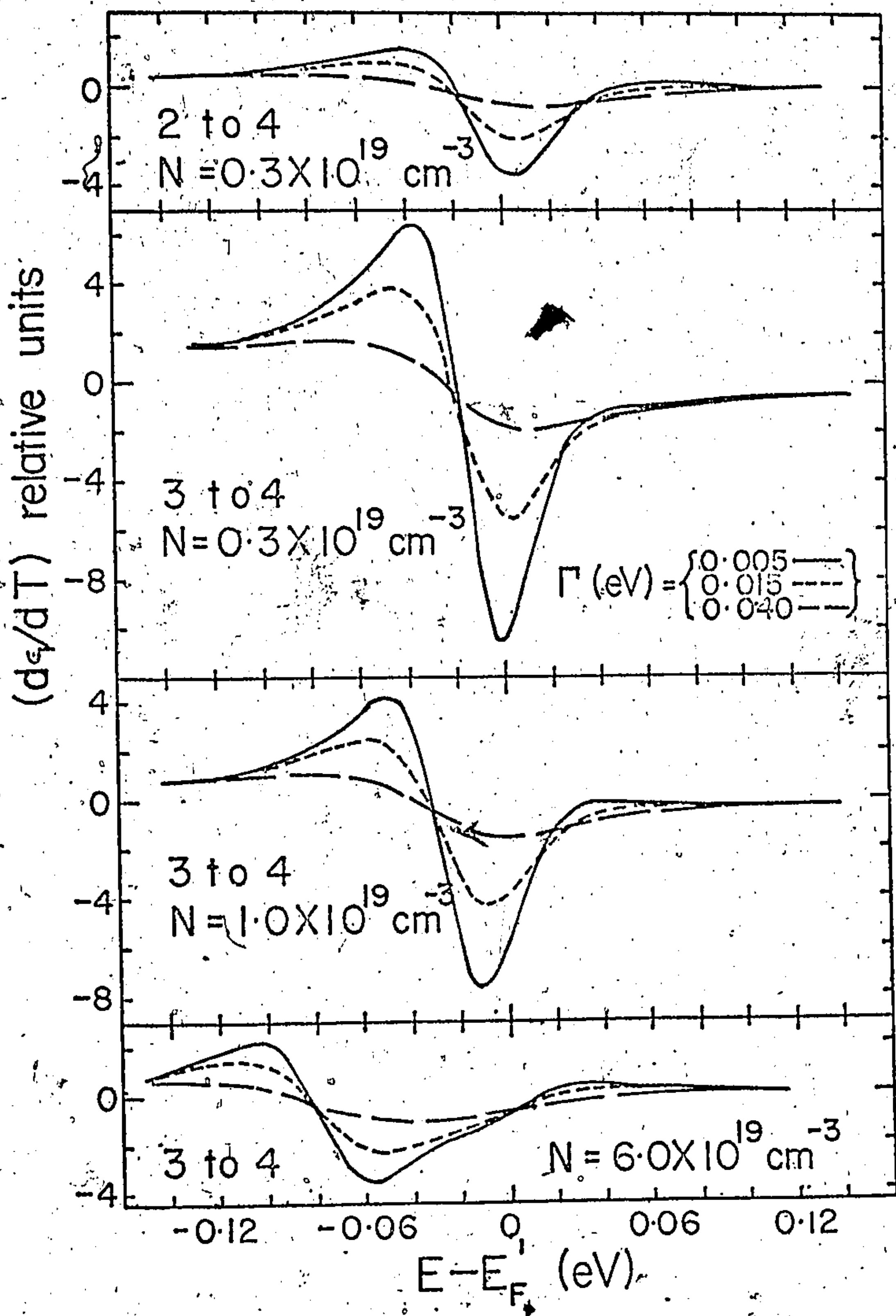

Figure 19. The combined contributions of factors a) and b) (see text) to $(d\varepsilon_1/dT)$ for three values of Γ, for four representative spectral regions.

Fig. 17 shows the contributions of factors a), b), and c) to $(d\varepsilon_1/dT)$ at 20, 85 and 300K, for $\Gamma = 0.01$ eV which were made using the g, β, M^2, E_F' and q-function values corresponding to transitions between the heavy hole band and the conduction band for $N = 1 \times 10^{19} cm^{-3}$; however, for the purpose of seeing only the temperature effect, W was set to 10^{-4} eV. Figure 18 is a study of the effect of the anisotropy of the bands on the magnitude and shape of $(d\varepsilon_1/dT)$ at 85K. The same parameters for the integral were used as for Fig. 17, except that W was set to -0.0001, -0.03 and -0.1 eV.

In the comparison of Figs. 17 and 18 with Figs. 8 and 9, it was concluded that $(d\Gamma/dT)$ is not the dominant factor in the modulation, because while there are large positive swings in $(\Delta R/R)$ relative to the steady high energy values, the calculated contribution for the $(d\Gamma/dT)$ term is a negative peak. Therefore, as an approximation to the anticipated modulation, $(d\varepsilon_1/dT)$ was calculated by summing the effects of factors a) and b). The results are shown in Fig. 19 for three Γ values, for N-values of 0.3, 1 and $6 \times 10^{19} cm^{-3}$ for band 3→ band 4 transitions, and for $N = 0.3 \times 10^{19} cm^{-3}$ for band 2→ band 4 transitions. There are many similarities between the measured and predicted shapes; however, a common disagreement is that the measured structures are almost twice as broad as the calculated shapes.

For a quantitative check on the levels of $(\Delta R/R)$, it was first noted that the maximum variation in $(\Delta R/R)$ in the InAs E_1 peak for a sample with $N \cong 1 \times 10^{16} cm^{-3}$ was 7×10^{-4}. This is the same level that was obtained by Matatagui et al.[112] who estimated that $\Delta T \sim 2K$. Assuming this ΔT, the maximum variation in the band 3→ band 4 structure for $N = 1 \times 10^{19} cm^{-3}$ was calculated as 1.4×10^{-4}, assuming $\Gamma = 0.01$ eV and only contributions from factors a) and b), whereas the measured level was about 2.5×10^{-4}. On the other hand, the magnitude of the non-excitonic component (see Chapter 6) of the Ge peak was calculated to be 1.6×10^{-4}, using $E_p = 26.3$ eV, two joint-density-of-states masses, 0.020m and 0.034m, calculated from Lawaetz's values,[34] $\Gamma = 1.65$ meV (See Chapter 6), and $(dE_G/dT) = -$[illegible]9×10^{-4} eV K^{-1},[15] whereas it was measured at 0.4×10^{-4}. This discrepancy is not understood. A possibility is that the ΔT estimate in Ref. 112 is too high. Using the results of Fig. 7 in section 4.3.2c, the temperature modulation in the present experiment is estimated at 0.6K. A loop hole to then bring the InAs results into place would be through the uncertainty in the momentum matrix elements. An alternative approach in the Ge calculation would have been to obtain a value for the reduced mass in the joint density of states from the experimentally determined value obtained for the exciton binding-energy, R_o^* (see section 6.2). According to that, one obtains 0.037m, which, when a factor of two is added to account for the valence band degeneracy, would make the discrepancy larger. One can only say at this point that the theoretical and experimental results for the amplitudes of $(\Delta R/R)$ are of the same order in the InAs case as well as in the Ge case.

Fig. 20 compares the locations of the negative peaks in $(\Delta R/R)$ with the calculated values of E_F', as a function of doping. The experimental points are about 0.15 eV below the calculated curves for the most heavily-doped samples. From the curves in the lowest section of Fig. 19, one sees that only about 0.06 eV of this can be accounted for. On the other hand, the difference in energy between the negative peaks approaches the value $(2/3)\Delta_o$ in the predicted way.

5.3.6 The possibility of the broadening of the line shape by sample inhomogeneity

In Sections 2.5.1 and 2.5.2, mention was made of the manifestation of inhomogeneity effects both in the transport data and in the infrared reflectivity data. The calculation of line shapes in this chapter has ignored the possible influence of inhomogeneity. On the basis of the data of Table I, Section 2.5.1, an upper limit on the inhomogeneity over a 5 mm extension along the long dimension of an ingot is considered to be 10 percent. Using the values following Eq. 5-(12) for (dN/dE_F'), one calculates that the changes in the values of E_F' for $3 \rightarrow 4$ transitions for a 10 percent change in N for N-values of 0.3, 1, and 6×10^{19} cm^{-3} are 0.01, 0.02, and 0.04 eV, respectively.

These values are approximately the same as the widths of the theoretical lines presented in Figure 19. Thus, although 10 percent is an upper limit for the inhomogeneity, it is reasonable to say that some of the discrepancy between the measured line widths and the calculated line widths can be accounted for by inhomogeneity broadening.

5.4 Discussion and Conclusions

The difference between theory and experiment in Fig. 20 could be accounted for by slight variations in the parameters used in the analysis. If the Luttinger parameters γ_2 and γ_3 were each increased by 0.3, the two upper theoretical curves would be lowered by 0.09 eV without affecting W. However, other reasons for the difference could be that the upper band corrections are inadequate at such large k-values and that there is a contribution to the energy lowering from the tailing of the bands near the gap.[113]

The disagreement in the widths of the structures seems to indicate that a type of anisotropy different from that which has been considered is present. The inclusion of the spin-splitting terms would broaden the structures, although no information is available on

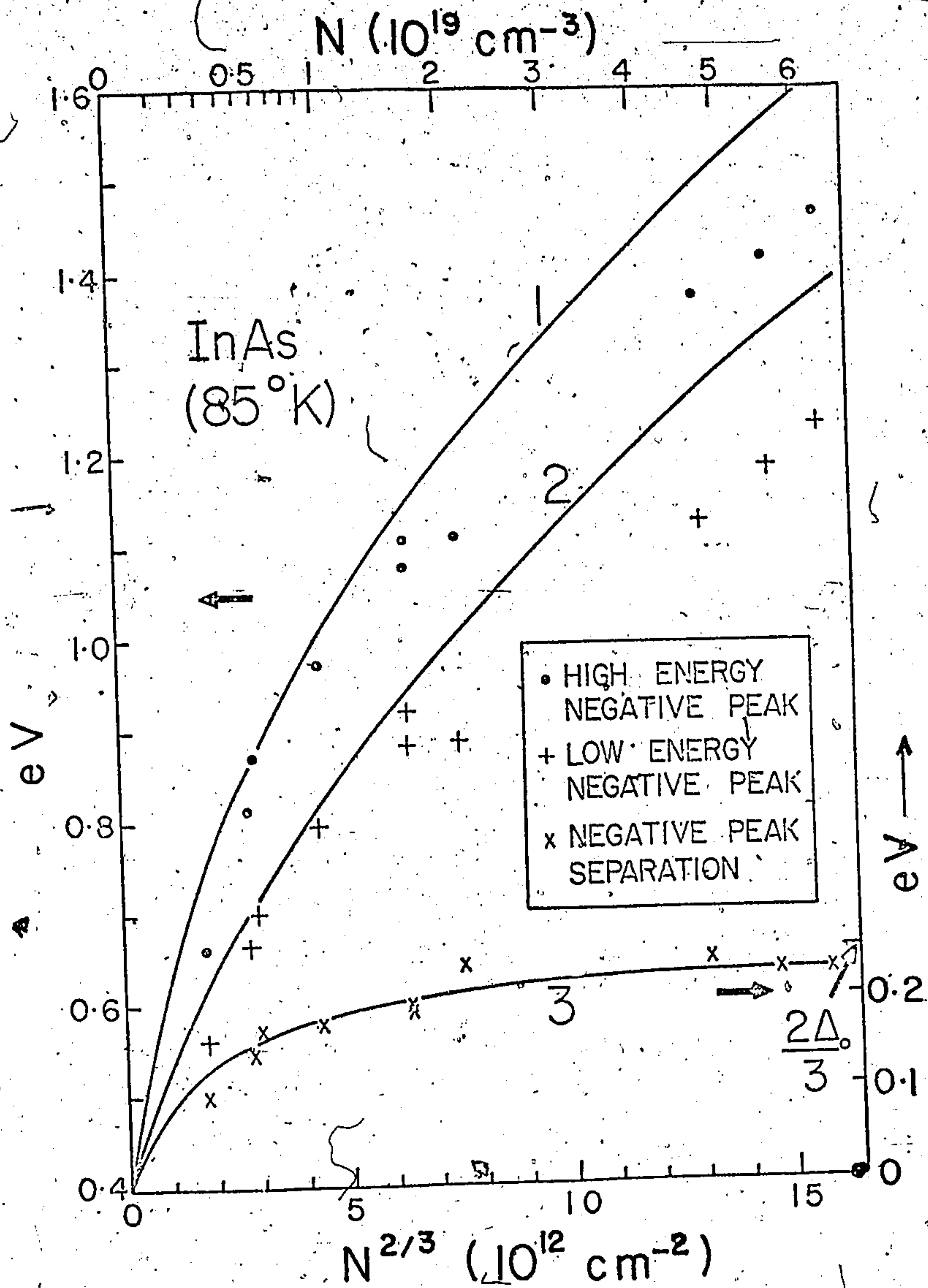

Figure 20. Curves 1 and 2 are the calculated values of E_F' for band 2 to band 4, and band 3 to band 4, respectively, as a function of $N^{2/3}$. Curve 3 is the difference between curves 1 and 2. Also plotted are the energies of the negative peaks in $(\Delta R/R)$ as well as the difference in energy between the negative peaks in each spectra.

Kane's B parameter. It is considered better to await a theoretical estimate of B, or further experimental results before extending the present simple analysis to some fitting procedure.

In conclusion, it seems that thermoreflectance can be a useful tool in locating the energies where there are rapid changes in absorption due to the onset of direct band-to-band transitions in heavily-doped n-type III-V semiconductors. A particularly satisfying aspect of these results is that, with some further refinement in the measurement of the amplitude of the first harmonic of the temperature modulation, the amplitudes as well as the shape and location of this type of spectrum can be used to make a close quantitative check with theoretical predictions. Referring specifically to the present results, a simple analysis based on Kane's model has been able to account for many of the features in the $(\Delta R/R)$ spectra of InAs. The dominant modulation mechanisms as determined from the analysis have been found to be the temperature shift of the energies of the direct transition to the Fermi level and the temperature change of the Fermi distribution function. All the features of the structures can be accounted for, except that each structure is about twice as broad as predicted, and the energies of the negative peaks are about 0.1 eV lower than predicted for the most heavily-doped samples.

CHAPTER 6

THERMOREFLECTANCE OF PURE GERMANIUM AT ITS LOWEST DIRECT GAP

6.1	Introduction	122
6.2	Theory of Excitons at the Direct Gap	123
6.3	The Dielectric Constant and Its Temperature Modulation	131
6.4	Experiment	133
6.4.1	Specific details including strain effects	133
6.4.2	Data	135
6.4.2a	time constant and slit broadening effects	136
6.4.2b	thermoreflectance data	139
6.4.2c	data on temperature variation of E_g	139
6.5	Analysis of the Thermoreflectance Data	143
6.6	Discussion and Conclusions.	147

6.1 Introduction

This chapter presents data and analyses of the thermoreflectance of pure germanium at several temperatures. Before the present work, no correct data for thermoreflectance at E_o for a group IV or III-V semiconductor had been published. Furthermore, there were no published expressions which predicted the shape of $(\Delta R/R)$ at E_o. The literature contained Elliott's theory[3, 114] for the absorption coefficient associated with excitonic states created by the Coulomb interaction between holes and electrons of two non-degenerate parabolic bands. This had been applied to the absorption data of several semiconductors in an unbroadened form (e.g., Refs. 5 and 6), and in a Lorentzian broadened form to absorption data of GaP by Sell and Lawaetz.[4] Thus, all that remained in order to try that interpretation on $(\Delta R/R)$ was to convert the absorption expression into a complex dielectric constant, find the temperature derivative of ε_1, put it in a simple form, and then try to fit the data and determine the variable parameters in $\Delta\varepsilon_1$. This has been done.

However, although everyone uses Elliott's theory, they know that it does not correctly apply to the E_o gap because the valence band is doubly degenerate at $k = 0$. Elliott's theory fits the data well, although the theory has not been theoretically justified. Some recent works[115, 116] have taken the degeneracy into account and have determined

the energies of the ground and excited states. To the author's knowledge, the treatment of the degenerate case has not yet yielded an expression for the absorption coefficient in the gap region.

The degeneracy of the valence bands has been ignored in the present work. Undoubtedly, it will be included when an analysis is made of the line shapes in the thermoreflectance data of Ge in a magnetic field.

6.2 Theory of Excitons at the Direct Gap

The following is a summary of the treatment in the literature of the eigenstates which are excited by light between two non-degenerate bands, one conduction and one valence, with their extrema at $\underline{k} = 0$, when the Coulombic interaction of the excited state is taken into account. The original complete results were obtained by Elliott, following preliminary work by Dresselhaus.[117] Since then, more comprehensive review articles, which extend the treatment to degenerate bands, consider further interactions such as exciton-impurity complexes, and evaluate the approximations made in these developments, have been prepared by Dimmock,[118] Johnson,[110] and Knox.[119] The effective mass approximation, basic to all of this work, was initially formulated by Luttinger and Kohn,[120] and applied by them in the treatment of the perturbation due to a shallow impurity in a semiconductor, and has been presented in perhaps a more palatable form by Smith[121] and Dimmock,[118] and has been

summarized by Aspnes and Bottka.[122]

In Chapter 4, the states excited by light were assumed to be eigenstates of the pure crystal; this is, it was assumed that the ground state

$$\Psi_o = (N!)^{-\frac{1}{2}} P\, b_v(\underline{k}_1, \underline{r}_1)\, b_v(\underline{k}_2, \underline{r}_2) \ldots b_v(\underline{k}_N, \underline{r}_N) \qquad 6 - (1)$$

and that the excited state

$$\Psi(\underline{k}_e, \underline{k}_h) = (N!)^{-\frac{1}{2}} P\, b_v(\underline{k}_1, \underline{r}_1)\, b_v(\underline{k}_2, \underline{r}_2) \ldots b_c(\underline{k}_e, \underline{r}_i) \ldots \ldots b_v(\underline{k}_N, \underline{r}_N) \qquad 6 - (2)$$

where P is the antisymmetric operator giving the same combinations of Bloch states $b(\underline{k}, \underline{r})$ as the Slater determinant, and N is the number of unit cells. If however, there is an interaction in the excited state which is not present in the pure crystal states, simple time-dependent perturbation theory cannot be used immediately to find the rate of transition to the final states, as was done in Chapter 4, because we do not know the wave functions for the excited states. As a start, an excited state, Φ_ℓ, can be expanded in basis functions of the form 6 - (2). It is assumed that one need consider excitations to the first band only; that is,

$$\Phi_\ell = \sum_{\underline{k}_e, \underline{k}_h} C(\underline{k}_e, \underline{k}_h)\, \Psi(\underline{k}_e, \underline{k}_h) \qquad 6 - (3)$$

This can be simplified when the only interaction which creates the excited state is light, that is the transition is not phonon assisted. In such a case Φ will contain only wave functions which have a non-vanishing matrix element of $\underline{A}.\underline{p}$ with respect to the ground state, where $\underline{A} = \underline{A}_o\, e^{-i\underline{k}_\lambda \cdot \underline{r}}$ is the vector potential and $\underline{k}_\lambda$ is the light's wave vector. These matrix elements reduce to evaluations of the type $\langle b_c(\underline{k}_i) | \underline{A}.\underline{p} | b_v(\underline{k}_j) \rangle$, where the integral is taken over unit volume of the crystal. By transforming such an integral to integrations over unit cells using the lattice periodicity of the atomic-type part of the Bloch functions, one finds non-zero elements only when $\underline{k}_i - \underline{k}_j - \underline{k}_\lambda = 0$. Since $\underline{k}_\lambda$ is very small compared to the electron $\underline{k}$-values at the zone edge, this condition is essentially $\underline{k}_i = \underline{k}_j$, or $\underline{k}_e = -\underline{k}_h$, where $\underline{k}_h$ is the wave vector of the positive hole represented by the total wave function in 6-(2) excluding $b_c(\underline{k}_e)$. Thus, eq. 6-(3) reduces to

$$\Phi_\ell = \sum_{\underline{k}_e} C(\underline{k}_e)\, \Psi(\underline{k}_e, \underline{k}_h = -\underline{k}_e) \qquad 6 - (4)$$

Consider now the expansion of 6-(4) in terms of Wannier functions, treating $\Psi(\underline{k}_e, \underline{k}_h)$ as the product of two Bloch functions $b_c(\underline{k}_e, \underline{r}_e)\, b_v(\underline{k}_h, \underline{r}_h)$, although the more elaborate definition of 6-(2) is meant, and is not approximated. A Wannier function is defined by[121]

$$a_n(\underline{r} - \underline{R}_j) = N^{-\frac{1}{2}} \sum_{\underline{k}} b_n(\underline{k})\, e^{-i\underline{k}\cdot\underline{R}_j} \qquad 6 - (5)$$

and it is easy to see that this sum constructively adds the Bloch functions around the lattice site $\underline{R}_j$, and destructively interferes elsewhere in the crystal. The inverse transformation gives the Bloch functions in terms of the Wannier functions as

$$b_n(\underline{k}) = N^{-\frac{1}{2}} \sum_j e^{i\underline{k}\cdot\underline{R}_j} a_n(\underline{r} - \underline{R}_j) \qquad 6 - (6)$$

Thus

$$\Phi = N^{-\frac{1}{2}} \sum_{j,j'} F(\underline{R}_j, \underline{R}_{j'}) a_c(\underline{r}_e - \underline{R}_j) a_v(\underline{r}_h - \underline{R}_{j'}) \qquad 6 - (7)$$

where

$$F(\underline{R}_j, \underline{R}_{j'}) = N^{-\frac{1}{2}} \sum_{\underline{k}} C(\underline{k}) e^{i\underline{k}\cdot(\underline{R}_j - \underline{R}_{j'})} \qquad 6 - (8)$$

It can be shown that $|F(\underline{R}_j, \underline{R}_{j'})|^2 dV_e dV_h$ is the probability of finding the electron in the volume dV_e around $\underline{R}_j$, and the hole in the volume dV_h around $\underline{R}_{j'}$. It does not give the probability at points, but the average of a probability over a small volume, like a unit cell, thus averaging over the rapid variations which would occur due to the rapidly varying atomic potentials. This is suggestive of the hydrogen atom problem, but where $|\psi|^2$ has been replaced by F^2. It can be shown that the $F_{jj'}$'s are the roots of a set of N^2 simultaneous equations, which include matrix elements of the perturbation potential, for which one

would have to know all the Bloch functions. Here the effective mass approximation comes in and states that if the perturbation potential varies slowly over a unit cell, then $F_{jj'}$ can be considered to be a continuous function of $\underline{r}_e$ and $\underline{r}_h$, and the energies of the crystal with respect to the unperturbed state can be determined from a solution of the equation

$$[E_c(-i\underline{\nabla}_e) + E_v(-i\underline{\nabla}_h) + V(\underline{r}_e, \underline{r}_h) - E] F(\underline{r}_e, \underline{r}_h) = 0 \qquad 6-(9)$$

where $E_c(\underline{k})$ and $E_v(\underline{k})$ are the dispersion relations in the pure crystal for the conduction and valence bands, and V is the potential. With conduction and valence bands with constant effective masses m_e and m_h, respectively, Eq. 6-(9) becomes

$$[\frac{-h^2}{2m_e} \nabla_e^2 - \frac{h^2}{2m_h} \nabla_h^2 - \frac{1}{4\pi\varepsilon_1} \frac{e^2}{|\underline{r}_e - \underline{r}_h|} - E] F = 0 \qquad 6-(10)$$

where the Coulomb potential between hole and electron is reduced by ε_1, the dielectric constant of the crystal. It can be shown that the effective mass approximation is equivalent[118,121] to stating that Φ can be expanded using Bloch functions near $\underline{k} = 0$, that is, $C(\underline{k})$ is large only near $\underline{k} = 0$.

Making the change of co-ordinates $\underline{r} = \underline{r}_e - \underline{r}_h$, and $\underline{R} = \frac{1}{2}(\underline{r}_e + \underline{r}_h)$, (with conjugate momenta $\underline{k} = \frac{1}{2}(\underline{k}_e - \underline{k}_h)$, and $K = (\underline{k}_e + \underline{k}_h)$, and separating the wave equation into two equations, Eq. 6-(10) becomes

$$\left(\nabla^2_{\underline{r}} + \frac{2\mu e^2}{4\pi\varepsilon_1 \hbar^2 |\underline{r}|} + E_1 \right) F_1(\underline{r}) = 0 \qquad 6 - (11)$$

$$\left(\nabla^2_{\underline{R}} + \frac{2M}{\hbar^2} E_2 \right) F_2(\underline{R}) = 0 \qquad 6 - (12)$$

where $E = E_1 + E_2$, $F = F_1 F_2$, $\mu = (m_e^{-1} + m_h^{-1})^{-1}$, and $M = (m_e + m_h)$. $E_2 = \hbar^2 K^2/(2m)$, equals zero in this case, since as we have seen above $K = 0$. Eq. 6-(11) is the hydrogen atom problem with bound energies $E_1 = -R_o^*/n^2$, where n is an integer, and where R_o^* = Rydberg x $(\mu/m)(\varepsilon_o/\varepsilon_1)^2$. The matrix element required in order to evaluate the absorption coefficient is, as in Chapter 4,

$$M = A_o \langle \Phi_\ell | \underline{a}.\underline{p} | \Psi_o \rangle \qquad 6 - (13)$$

which, with the aid of Eq. 6-(4) reduces to

$$M_\ell = A_o \sum_{\underline{k}} C(\underline{k}) \langle b_c(\underline{k}) | \underline{a}.\underline{p} | b_v(\underline{k}) \rangle \qquad 6 - (14)$$

Now since, as stated above, the effective mass approximation implies that $\underline{k}$ in this expansion varies over a small range, the bracketed term

in 6-(14) is assumed constant, and

$$M_\ell = A_o <b_c(0) \ |\underline{a}.\underline{p}|\ b_v(0)> \sum_{\underline{k}} C(\underline{k}) \qquad 6-(15)$$

Looking at Eq. 6-(8) and letting $\underline{R}_{j'} = \underline{R}_j$

$$\sum_{\underline{k}} C(\underline{k}) = N^{\frac{1}{2}} F(\underline{R}_j, \underline{R}_{j'} = \underline{R}_j) \qquad 6-(16)$$

Now $|F_1(0)|^2$ from Eq. 6-(11) gives the probability that the electron and hole are at the same place; that is, it is N times larger than the square of F in Eq. 6-(16), since there are N $\underline{R}_j$'s where one could have $\underline{R}_{j'} = \underline{R}_j$. Thus, the square of the matrix element in 6-(15), becomes

$$|M_\ell|^2 = |A_o|^2 \ |<b_c(0)|\ \underline{a}.\underline{p}|\ b_v(0)>|^2 |F_1(0)|^2 \qquad 6-(17)$$

$F_1(0)$ is non-zero only for s-states, at which

$$|F_1(0)|^2 = (\pi a_o^{*3} n_c^3)^{-1} \qquad 6-(18)$$

where $a_o^* = 4\pi\varepsilon_1 \hbar^2 (\mu e^2)^{-1}$ is the effective Bohr radius. For the unbound states

$$|F_1(0)|^2 = \pi z e^{\pi z} (\sinh(\pi z))^{-1} \qquad 6-(19)$$

where $z^2 = (R_o^*/E_1)^{\frac{1}{2}}$. From Section 4.2.2., it is easily found that

$$K(\omega) = T\ \delta(\omega - \omega_n) \qquad 6-(20)$$

for discrete states of energy $E_G - \hbar\omega_n$, where $T = \pi e^2 |M|^2 (n_1 c m^2 \varepsilon_o \omega)^{-1}$, while, for the unbound states

$$K(\omega) = T\,\rho(\omega) \qquad 6-(21)$$

$\hbar\omega > E_G$, where

$$\rho(\omega) = \frac{1}{2\pi^2}\left(\frac{2\mu}{\hbar^2}\right)^{3/2}(\hbar\omega - E_g)^{\frac{1}{2}} \qquad 6-(22)$$

is the usual energy density of states for a parabolic $(E - E_G)$ vs. k relationship, which applies here since the eigenvalues for the hyper-geometric functions which are the eigenfunctions of Eq. 6-(11) for $E_1 > 0$ are $\hbar^2 k^2 (2\mu)^{-1}$. Eqs. 6-(20) and 6-(21) can be joined together in a neater form as

$$K(E) = \frac{2^{\frac{1}{2}}(\mu)^{3/2} e^2 f_{cv} R_o^{*\frac{1}{2}}}{n_1 \varepsilon_o c \hbar^2 m}\left[\frac{2R_o^* \delta(E - E_n)}{n^3} + \frac{\rho(E')\,\delta(E - E')}{1 - e^{-2\pi z}}\right] \qquad 6-(23)$$

where f_{cv}, the conduction to valence band oscillator strength $= 2(mE)^{-1} |\langle b_c(0) | a.p | b_v(0)\rangle|^2$. This is Elliott's result[3] and has been put in the convenient form presented by Sell and Lawaetz.[4]

6.3 The Dielectric Constant and Its Temperature Modulation

All the analysis and techniques and measurements described from this point to the end of this chapter are the original work of the author.

ε_2 is related to K by $\varepsilon_2 = n_1 c\hbar\kappa E^{-1}$. Thus using ε_2 to obtain the Lorentzian-broadened form of the complex dielectric constant as in Chapter 4, and, anticipating the calculation of the modulation, retaining only the rapidly varying energy term, the contribution of the direct gap, including electron-hole interaction, is

$$\varepsilon(E) \propto - 2\pi R_o^{*\frac{1}{2}} \left[\sum_{n=1}^{\infty} 2R_o^{*} n^{-3} (E - E_n + i\Gamma)^{-1} + \int_{E_G}^{\infty} \{1 + [\exp(2\pi z) - 1]^{-1}\} (E - E' + i\Gamma)^{-1} dE' \right] \qquad 6-(24)$$

where $E_n = E_g - R_o^{*} n^{-2}$.

One may notice the difference in the form of the terms with exp $(2\pi z)$ between Eqs. 6-(23) and 6-(24). It has been so presented as to permit the evaluation of integrals below.

For Ge and E_o, the direct gap, a modulated reflectance signal $(\Delta R/R)$ is proportional to $\Delta\varepsilon_1$,[94] where $\varepsilon = \varepsilon_1 + i\varepsilon_2$. By observation of Eq. 6-(24), one has

$$(\partial\varepsilon/\partial E_g) = - (\partial\varepsilon/\partial E), \quad (\partial\varepsilon/\partial\Gamma) = i(\partial\varepsilon/\partial E)$$

from which, for thermal modulation at temperature T,

$$(\Delta R/R) \propto -\{Re(\partial\varepsilon/\partial E)\ (\partial E_g/\partial T) + Im(\partial\varepsilon/\partial E)(\partial\Gamma/\partial T)\}\Delta T \qquad 6-(25)$$

Making the substitution $E'' = E' - E_g$, one gets

$$(\partial\varepsilon/\partial E) \propto 2\pi R_o^{*\frac{1}{2}} \left[\sum_{n=1}^{\infty} 2R_o^{*} (E_{Dn})^{-2} n^{-3} + \int_0^{\infty} 1 + [\exp(2\pi z) - 1]^{-1} (E'' - E_c)^{-2} dE'' \right] \qquad 6-(26)$$

where $E_{Dn} = E - E_n + i\Gamma$ and $E_c = E - E_g + i\Gamma$. Letting $x = (R_o^*/E'')^{\frac{1}{2}}$, the part of the integral containing the term $[\exp(2\pi z) - 1]$ goes into a standard form:[123,124]

$$\int_0^{\infty} [\exp(2\pi x) - 1]^{-1} (x^2 + q^2)^{-2} x dx = -(2q)^{-3} - (2q)^{-2} + (4q)^{-1} \sum_{m=0}^{\infty} (m + q)^{-2} \qquad 6-(27)$$

with $q = (-R_o^*/E_c)^{\frac{1}{2}} = (R_o^*/2\Gamma)^{\frac{1}{2}} [F(-X) + iF(X)]$ where[23]

$F(X) = [(X^2 + 1)^{\frac{1}{2}} + X]^{\frac{1}{2}} (X^2 + 1)^{-\frac{1}{2}}$ and $X = (E - E_g)\Gamma^{-1}$.

The final result is then

$$(\partial\varepsilon/\partial E) \propto \pi\Gamma^{-\frac{1}{2}} \{4X_R^{3/2} \sum_{n=1}^{\infty} X_{Dn}^{-2} n^{-3} + 8^{-\frac{1}{2}} [F(-X) + iF(X)] - X_R^{\frac{1}{2}} X_c^{-1} + X_R^{3/2} X_c^{-2} q^{-1} \sum_{m=1}^{\infty} (m + q)^{-2}\} \qquad 6-(28)$$

where $X_{Dn} = E_{Dn}\Gamma^{-1}$, $X_R = R_o^*\Gamma^{-1}$, $X_c = E_c\Gamma^{-1}$. As $X_R \to 0$, Eq. 6-(28)

reduces to Batz's result[23] for an M_o discontinuity without excitons.

It is noted that the real part of $(d\varepsilon/dE)$ gives the curve predicted at E_o in a wavelength modulation experiment. Also should the modulation of $\Delta\varepsilon_2$ be measured, as in a modulated absorption experiment, an equation similar to 6-(25) could easily be written down.

6.4 Experiment

6.4.1 Specific details including strain effects

Thermoreflectance measurements were made on undoped germanium* with a carrier concentration of less than $5 \times 10^{12} cm^{-3}$ at 200K. The general experimental details have been described in Section 4.3. Four runs were made at 17 and 85K, and two runs at 204 and 291K, using two samples. Particular care was taken to eliminate strain and back reflection effects. (The previously published thermoreflectance data[22] for Ge at E_o contained a large component due to light reflected from the region of the back surface of the sample). To demonstrate strain effects, Figure 21 was prepared. Curve 2 shows the results for $(\Delta R/R)$ at 85K using a tantalum film heater on an alumina substrate. Curve 1 is a result which was obtained when the sample was mounted on the GaAs heater with the thick white silicone grease, and the germanium pedestal was attached to the copper cold finger with the white grease rather

* The germanium was kindly supplied by Dr. H. Pullan of the Ontario Research Foundation.

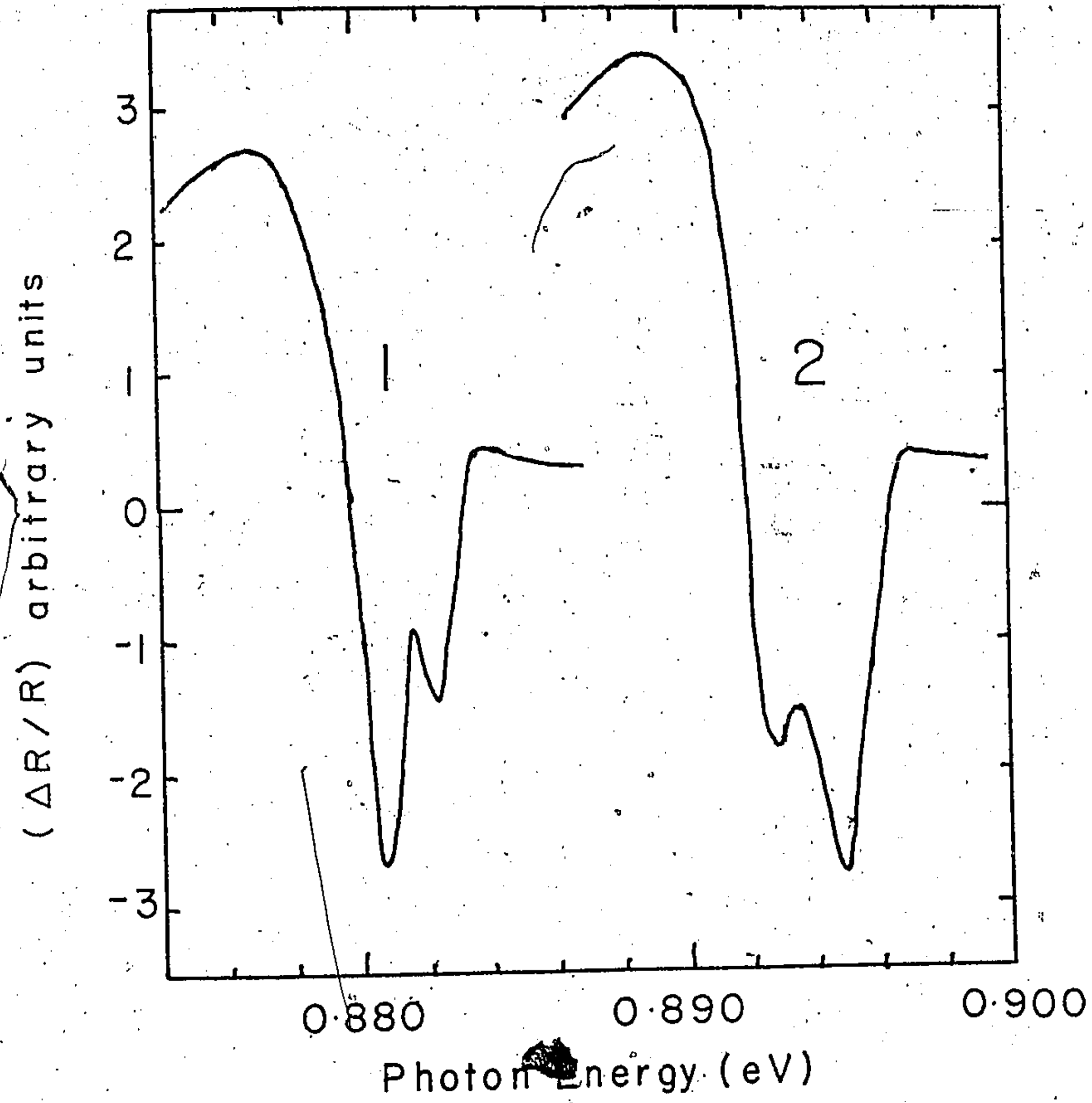

Figure 21. ($\Delta R/R$) as a function of photon energy for Ge samples under two different strain conditions at 85K. (The grating may not have been calibrated for curve 2.)

than via a layer of indium. In both cases the sample was evidently under strain, and the degenerate valence bands at $k = 0$ are split. This is reminiscent of Sturge's absorption result[6] on a strained thin film of GaAs. The useful information from Fig. 21 is that, since the two peaks are apparently much the same, the so-called light- and heavy-hole bands have the same excitonic behaviour. This will perhaps contribute something to an exciton theory which includes degenerate valence bands.

As a subsidiary experiment, the location of the negative peak in $(\Delta R/R)$ was determined for a number of temperatures near 77K, by varying the power level in the heater, to see if this technique would be a quick way to get accurate values of the temperature coefficient of E_g.

6.4.2 Data

The values of $(\Delta R/R)$ were determined ~~by measur~~ing ΔRI and RI separately, where I is the intensity of the light on the sample, and then dividing afterwards. In some of the runs either the time constant of the lock-in or the slit widths were such as to add broadening to the peaks in the raw data. However, all the data in its final form represents the structures with the time constant eliminated and with an effective slit width of 0.2 mm, that is, a window of 4Å or about 0.2 meV. The techniques of achieving this is described in the following section.

6.4.2a broadening due to experimental procedures

(i) time constant broadening

The problem can be stated as follows: given the form of a signal which has gone through a circuit with a known time constant τ, can one find what the shape of the signal was at the input to the circuit? One can, however, there may be practical limitations due to noise in the data.

Let $f(t)$ and $F(t)$ be the signals at the input and the output, respectively. One wishes to obtain $f(t)$ from $F(t)$. Let us look at $f(t)$ as two signals, $f_1(t)$ which is $f(t)$ for $t < 0$, and $f_2(t)$ which is $f(t)$ for $t > 0$. Thus $f_1(t)$, $f_2(t)$ are zero for $t > 0$, and $t < 0$, respectively. The response F_1 to f_1 will drop off, in a time interval Δt, according

$$F_1(\Delta t) = F(0) \exp(-\Delta t/\tau) \qquad 6 - (29)$$

For the response to the second component, note first that the response $R(t, t')$, at t to a δ-function at t' is

$$R(t, t') = \tau^{-1} \exp[-(t - t')/\tau] \qquad 6 - (30)$$

This can be verified by noting that the response must drop exponentially, and that the normalization can be found with a step function. Now we

make the restriction that Δt be small enough such that f(t) can be treated as linear in the interval; that is, between t = 0 and t = Δt,

$$f_2(t) = f_2(\frac{\Delta t}{2}) + m(t - \frac{\Delta t}{2}) \qquad 6 - (31)$$

Thus

$$F_2(\Delta t) = \int_0^{\Delta t} f_2\,(t')\; R(\Delta t,\, t')\; dt' \qquad 6 - (32)$$

Since

$$\int e^{ax}\, x dx = a^{-1} e^{ax} \; (x - a^{-1})$$

Eq. 6-(32) reduces to

$$F_2(\Delta t) = f(\frac{\Delta t}{2})\; (1 - e^{-\Delta t/\tau}) - \frac{m\Delta t}{2}\, (1 - e^{-\Delta t/\tau}) + m\, [\Delta t - \tau(1 - e^{-\Delta t/\tau})] \qquad 6 - (33)$$

If one expands the expressions with m in powers of $(\Delta t/\tau)$, the first non-vanishing term is $(m\Delta t/12)(\Delta t/\tau)^2$, which, for $(\Delta t/\tau) < 1/3$, is less than one-hundredth of the change in f in the Δt interval. Denote this term δF_2. Combining Eqs. 6-(29) and 6-(33)

$$f(\frac{\Delta t}{2}) = \frac{F(\Delta t) - \delta F_2 - F(0)e^{-\Delta t/\tau}}{(1 - e^{-\ t/\tau})} \qquad 6 - (34)$$

If δF_2 is dropped, the error in $f(\frac{\Delta t}{2})$ is $\frac{m\Delta t}{12}\; (\frac{\Delta t}{\tau})$. One chooses Δt

such that this is negligible. With the present data, a choice of $(\Delta t/\tau) = 0.3$ gave very accurate results. With δF_2 dropped, Eq. 6-(34) becomes

$$f(\frac{\Delta t}{2}) = F(0) + \frac{F(\Delta t) - F(0)}{(1 - e^{-\Delta t/\tau})} \qquad 6 - (35)$$

which is a very simple calculation.

In order to check the method experimentally before applying it, the time constants of the lock-ins were measured from appropriate logarithmic plots of signals from both stepped-on and stepped-off light beams incident on the detector. Then, with both slits at the same setting, an equal-sided triangular pulse was produced by scanning the grating through the specular reflection point, to produce a peak of 3 seconds half-width. When this was subjected to a 10 second time constant, the peak was reproduced within minutes using Eq. 6-(31), giving a height 4 percent less than the original, although the time constant had reduced the height by more than a factor of 5.

(ii) slit broadening

The problem can be stated as follows; given the form of a signal which results from slits of window α angstroms, can one predict the form the signal would have had for slits of window β angstroms. The case of $\alpha > \beta$ will be treated.

For convenience choose β such that $(\alpha/\beta) = 2n + 1$, where n is integral. Divide the relevant wavelength range into sections of length β such that the wavelength of the beginning of each such section is labeled by β_i, $i = 1, 2, \ldots N$. Consider sections of length α such that the section beginning at β_i is labeled α_i. The problem is to find the signal $S'(\beta_i)$ from section β_i, knowing the signals $S(\alpha_i)$ from sections α_i. One first finds an interval, $S(\alpha_j)$ to $S(\alpha_{j'})$ where S is linear over a wavelength range of at least length α. One can convince oneself that $S(\alpha_j) = (2n + 1) S'(\beta_{j+n})$. Also,

$S(\alpha_{j+1}) - S(\alpha_j) = S'(\beta_{j+2n+1}) - S'(\beta_j) = (2n+1) [S'(\beta_{k+1}) - S'(\beta_k)]$

where $k = j, j+1, \ldots, j+2n$. Thus one can find $S'(\beta_k)$ for $k = j, \ldots, j+2n$. From this, one can go through the whole signal since

$S'(\beta_{j+2n+1}) = S(\alpha_{j+1}) - S(\alpha_j) + S'(\beta_j)$, and so on. If, as a starting point, one chooses a wavelength interval of length α where S is constant, the initial calculations are slightly simpler. This transformation must be done twice to the data in order to close down both slits.

6.4.2b thermoreflectance data

Typical examples of the reduced thermoreflectance data are given by the solid curves in Figures 22 and 23. The zero levels for the experimental results were taken as the unvarying signal levels around 0.95 eV.

6.4.2c data on the temperature variation of E_g

Figure 24 is a plot of the location of the negative peak in

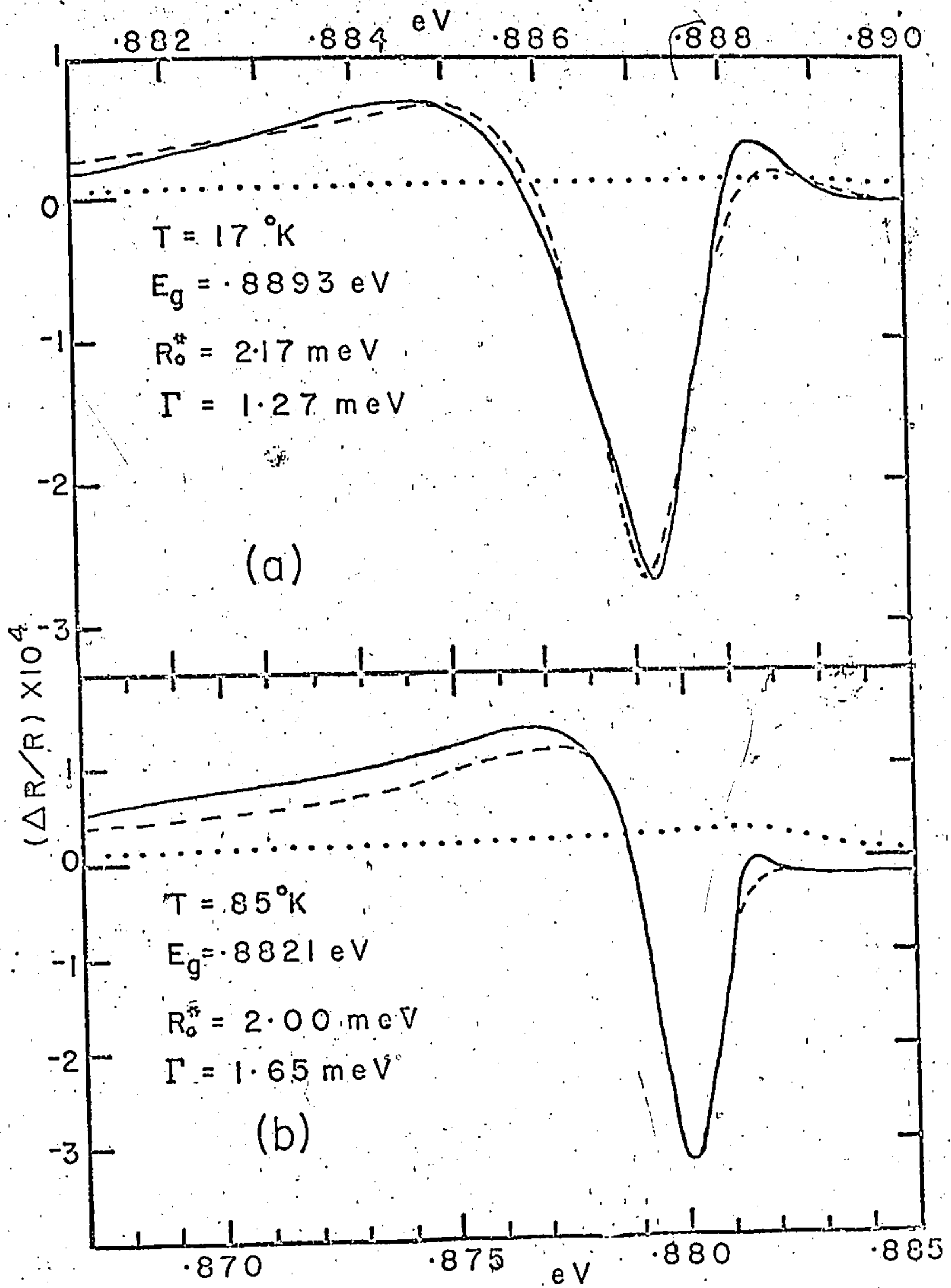

Figure 22. Thermoreflectance data, solid line, and fit using Eq. 6-25, dashed line, for Ge around E_o near 17 and 85K. The dotted lines give the contribution to Eq. 6-25 from the terms in Eq. 6-28 which do not contain X_R.

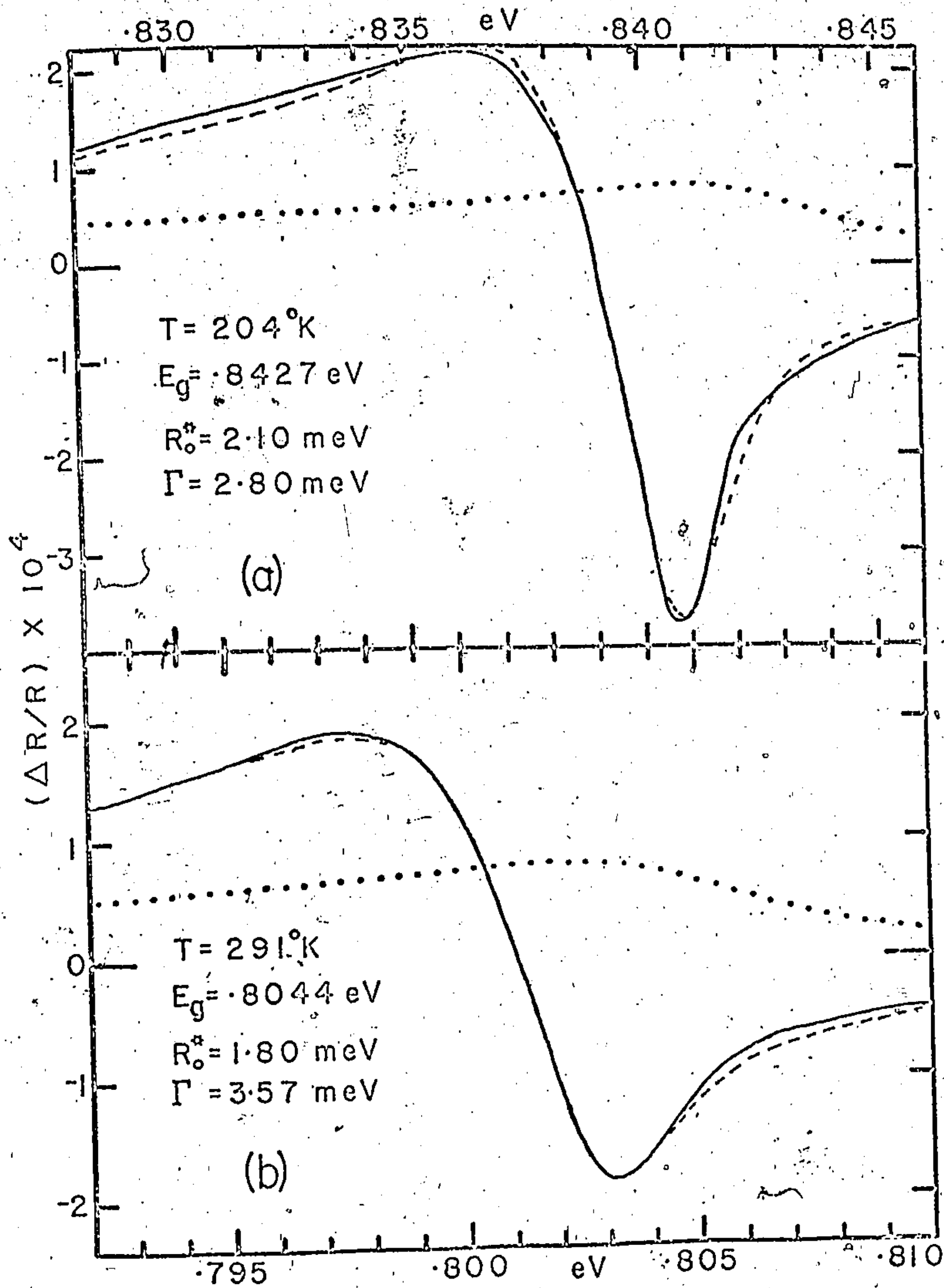

Figure 23. Thermoreflectance data, solid line, and fit using Eq. 6-25, dashed line, for Ge around E_0 near 204 and 291K. The dotted lines give the contribution to Eq. 6-25 from the terms in Eq. 6-28 which do not contain X_R.

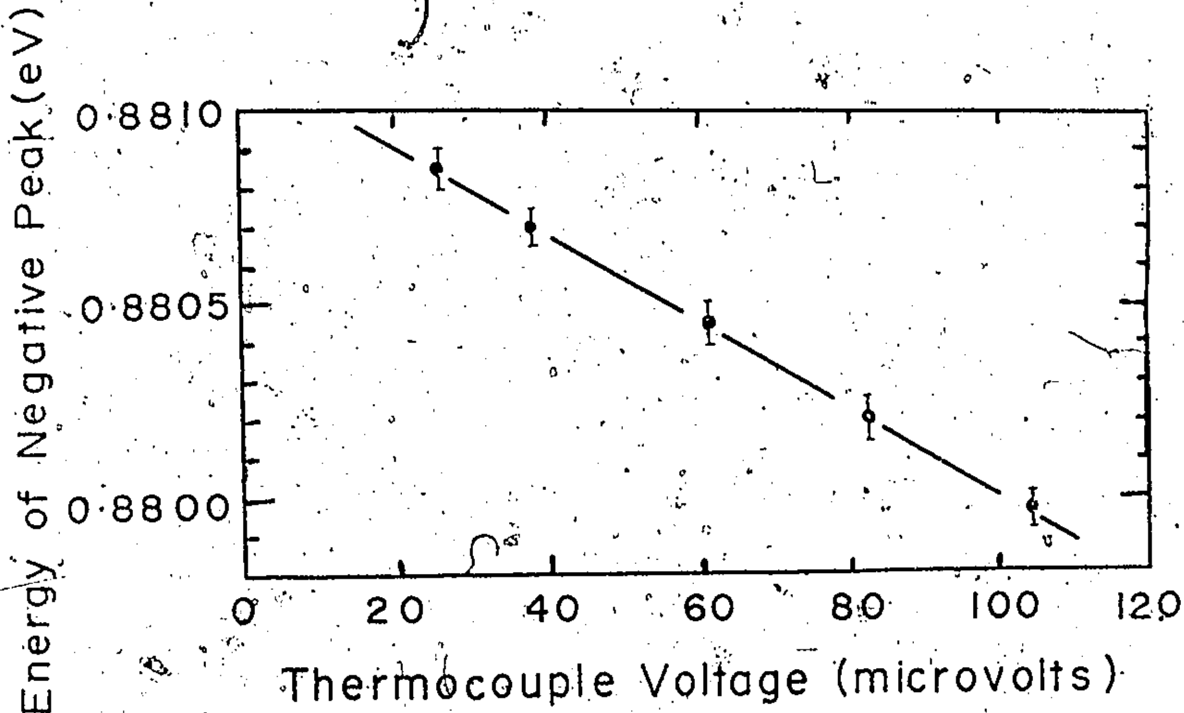

Figure 24. Photon energy of the negative peak in (ΔR/R) vs the thermocouple voltage generated by two copper-constantan junctions, one on the heater, the other in liquid nitrogen.

$(\Delta R/R)$ as a function of the voltage difference between a thermocouple junction on the heater and one at liquid nitrogen. Using the copper-constantan calibration data,[107] a linear approximation gives the sensitivity as 17.0 microvolts/K at 82K. This gives a value for (dE_g/dT) of -2.04×10^{-4} eV/K. This compares well with a value of 1.9×10^{-4} eV/K calculated by taking E_g values of MacFarlane et al.[5] obtained from absorption measurements at 77 and 90K. Thus one can conclude that the thermoreflectance technique offers a quick way for obtaining such information.

6.5 Analysis of the Thermoreflectance Data

Eq. 6-(25) was fitted to the data in the following way: Eq. 6-(28) was mathematically simplified by combining the terms from the discrete lines for $n > 4$ with the continuum terms. The series with the sum over m was carried out to $m = 50$; it can be shown that any further contribution from that series is negligible in the present fitting. A preferable method would be to convert the series to an integral once beyond a particular value of m. It can be noted that Eq. 6-(28) is a function of X, X_R, E_g and Γ. Thus a procedure is to give values to X_R, E_g and Γ, and calculate the values of $(\partial\varepsilon/\partial E)$ to compare with the data whose energy scale is converted to X by putting it in units of Γ. A variation of an amplitude factor is required to bring the amplitudes into line. One aspect of Eq. 6-(28) which simplifies the fitting is that the negative peak is always within

one or two angstroms of the energy $E_g - R_o^*$. Thus the fit is made with $E_g - R_o^*$ pinned to vary only within the range ±5Å of the experimental negative peak in $(\Delta R/R)$. In order to reduce the computer time for a fit by a factor of about 10, the following approximation was made in the fit. Since, from Eq. 6-(28), the continuum contribution is a function of X and X_R, a matrix of two (100 x 100) blocks was put on a magnetic disc to store the real and imaginary parts of $(\partial\varepsilon/\partial E)$ for 10,000 sets of (X, X_R). Then when the contribution from the continuum was required for a particular (X, X_R) set, a linear interpolation was made between the four enclosing sets in the matrices. This technique was checked for several computer-generated sets of data for $(\partial\varepsilon/\partial E)$ and the known parameters were extracted to ±0.05 meV.

The fit was made by letting E_g, R_o^*, and Γ vary independently with R_o^* and Γ varying over a range from one-third to twice the values which gave the best fit. The criterion for the best fit was the minimum in the sum of squares of the deviations. From extended use, it is believed that the fitting procedure was satisfactory from the point of view of what was expected of it. The ratio $(\partial\Gamma/\partial T)/(\partial E_g/\partial T)$ was determined in a self-consistent way from the temperature dependences of $E_g(T)$, $\Gamma(T)$. Specifically, one starts with values of Γ found at the 4 temperatures with $(\partial\Gamma/\partial T)$ set to zero. Then, by plotting $E_g(T)$ and $\Gamma(T)$ and estimating the slopes at the 4 temperatures, one finds a ratio $(\partial\Gamma/\partial T)/(\partial E_g/\partial T)$. Using these values in the fit, one finds new

values of Γ, and so on. During the initial runs of the program, Γ_D for the discrete lines was allowed to vary independently from Γ_C for the continuum. Representative results for the fit of Γ_D and Γ_C are shown below in Table II.

Table II

T(K)	17	85	204	291
Γ_D (meV)	0.12, 0.13	0.16	0.27	0.35
	0.11, 0.11	0.17	0.27	
Γ_C (meV)	0.10, 0.11	0.15	0.27	0.35
	0.10, 0.10	0.14	0.27	

It is doubtful that such small differences are significant and the final fits were made using the same Γ for the lines and the continuum.

The fits to the data in Figures 22 and 23 are shown as dashed lines. The fit is not as good at the lower temperatures; in particular, the positive peak at high energies is not reproduced well in the fit.

This peak was also the first thing to go in the data if the sample temperature was not uniform. This is understandable because it is narrower than the other structure. The values obtained for R_o^*, Γ, and the modulation ratio is given in Table III.

Table III

Range of fitting parameters determined at various temperatures by fitting Eq. 6-(25) to the thermoreflectance data of Ge at E_o

T(K)	17	85	204	291
R_o^* (meV)	2.06±0.12	1.95±0.3	2.05±0.05	1.95±0.15
Γ (meV)	1.18±0.08	1.67±0.08	2.72±0.08	3.65±0.08
$(\partial\Gamma/\partial T)/(\partial E_g/\partial T)$	-0.08	-0.05	-0.02	-0.01

6.6 Discussion and Conclusions

The fit is considered good. It is suspected that Gaussian broadening of the form[125] $\exp(-\frac{1}{2}((E - E')/\sigma)^2)$ in an absorption line would have given a better fit of the positive high energy peaks in the spectra at 17 and 85K. The problem here is that the author does not know how to put Gaussian form broadening in the expression for the complex dielectric constant. One must instead make Kramers-Kronig a transform of $\Delta\varepsilon_2$ to get $\Delta\varepsilon_1$, as has been done by Pake and Purcell[126] in another context. To show the difference in the sharpness, the real part of $(\partial\varepsilon_1/\partial E)$ has been calculated in this way for a Gaussian shape of $(\partial\varepsilon_2/\partial E)$. This is shown and compared with a Lorentz shape for $(\partial\varepsilon_1/\partial E)$ in Figure 25. One sees that the positive peaks are sharper for the Gaussian form. Although a fit would be too expensive it would not require much computer time to generate the Gaussian form of $(\Delta R/R)$ using the parameters given in Table III.

The value for R_o^* of 2.0 ± 0.2 meV is to be compared with 1.1 ± 0.1 and 1.8 ± 0.4 meV which were obtained from the interpretation of absorption,[5] and magnetoabsorption[127] data, respectively. The lower value of 1.1 meV may have resulted from the omission of broadening in the fit. Sell and Lawaetz[4] found that an analysis, including broadening, of absorption data for GaP gave a value for R_o^* double that of an earlier analysis which did not include broadening. Theoretical calculations[115] have given 1.4 meV for R_o^* in Ge. The values of Γ in

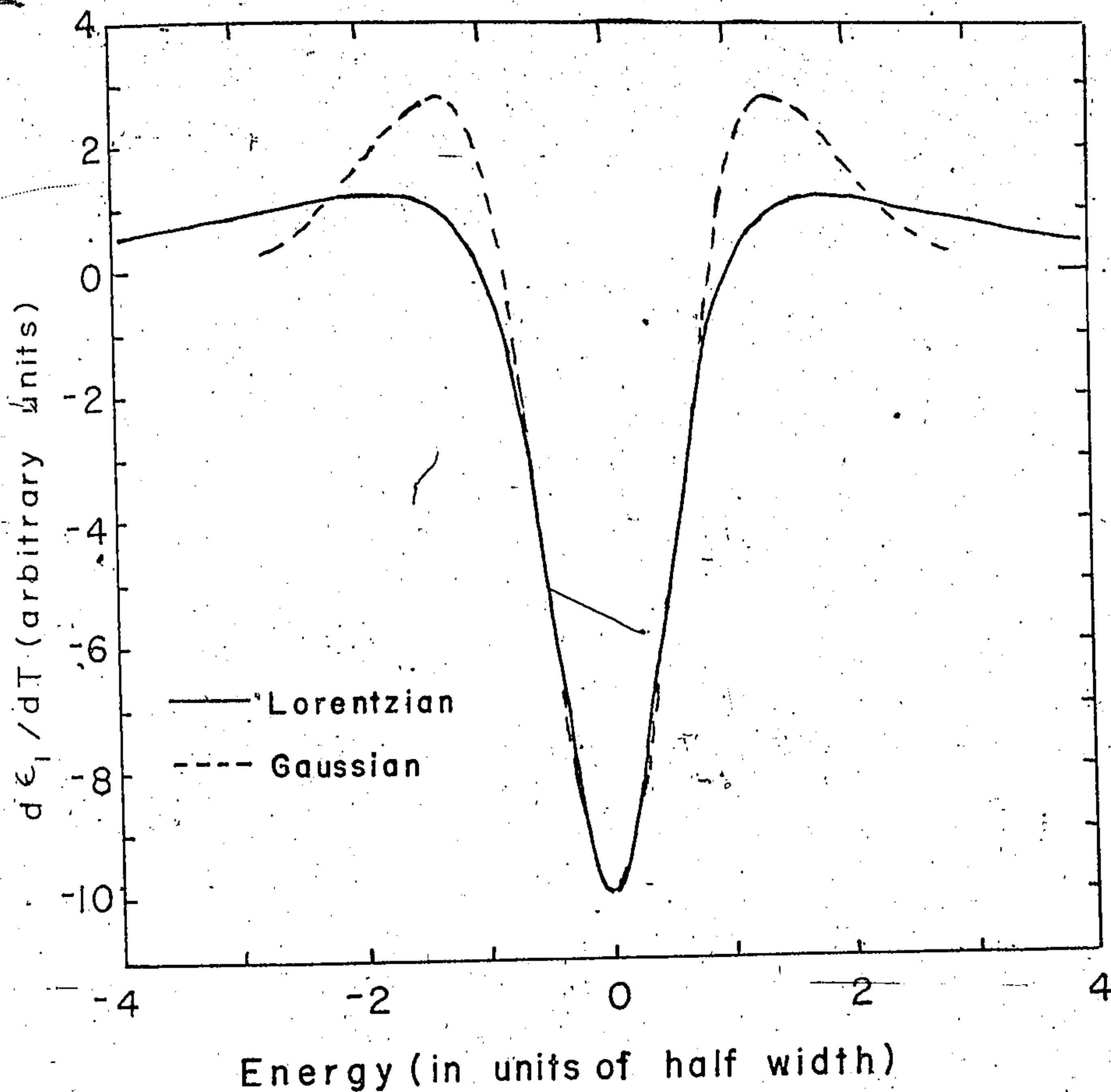

Figure 25. Comparison of $(d\epsilon_1/dT)$ of a broadened Gaussian line (dashed curve) and that of a broadened Lorentzian line (solid curve). Note that they both have the same half-width.

Table III compare well with values of σ, the parameter in Gaussian broadening mentioned in the last paragraph, of 1.0, 1.1 and 2.7 meV at 20, 77 and 290K, respectively, obtained by Hobden[128] from a Gaussian broadening analysis of the edge in absorption data.

It should be mentioned that the electron-hole interaction has been taken into account in previous work[129,130] in the interpretation of modulation spectra. They were studies of E_1 structure, and are not applicable to the present problem. For example, Rowe and Aspnes[130] fitted the E_1 electroreflectance structure of Ge using the Slater-Koster interaction as an approximation to the Coulomb interaction. Also, there are many instances where the E_o peak in modulation spectra has been identified as the n = 1 hydrogenic line (e.g. Ref. 112); however, there has been no previous fit which includes Elliott's continuum terms.

It is concluded that Elliott's formulation, in derivative expressions, can describe the thermal modulation spectra of pure Ge over a large temperature range. The fit has yielded a value for the exciton's binding energy somewhat higher than the predicted value.

CHAPTER 7

INTERIM REPORT ON THE WORK WITH GERMANIUM ON THERMALLY-MODULATED ABSORPTION, AND THERMOREFLECTANCE IN A MAGNETIC FIELD.

7.1 Thermoabsorption in Ge 151

7.1.1 Introduction 151

7.1.2 Methods of thinning samples 152

7.1.2a mechanical 152

7.1.2b chemical 153

7.1.2c ion beam 154

7.1.2d tests for damage in samples 155

7.2 Thermoreflectance of Ge at E_o in a Magnetic Field 158

7.2.1 Introduction 158

7.2.2 Experiment 159

7.2.2a a feedthrough design for helium temperatures 163

7.2.3 Representative data and some observations 164

7.1 Thermoabsorption in Ge

All the techniques and measurements described in this chapter are the original work of the author. Although no analysis of data is given, the author believes that the experimental successes of this chapter represent an advancement in the state of the art.

7.1.1 Introduction

As mentioned in Chapter 1, it is considered important to develop the thermoabsorption technique in order to confirm the modulation theory, which would be done by checking the parameters obtained with the thermoreflectance method. In addition, it is possible that some of the broadening in the thermoreflectance results is due to surface fields; if so, one may get narrower structure in absorption, and perhaps the n = 2 exciton line would give a discernible peak. Some calculations could easily be made to find out what the value of Γ would have to be for this to be observed. One can show (e.g. Ref. 20, p. 154) that the thermoabsorption result would be given mainly by

$$\frac{\Delta I}{I} \doteq - \frac{1 + R^2 e^{-2Kd}}{1 - R^2 e^{-2Kd}} \, d\Delta K \qquad 7 - (1)$$

where I is the transmitted intensity, R, the reflectivity, and d, the sample thickness. When Kd > 1, this is essentially $-d\Delta K$. Thus one can calculate the modulation from $\Delta\varepsilon_2$ as given in Chapter 6.

The substrate on which the sample is placed must be transparent in the spectral region to be studied. Trial runs were made on samples prepared by chemical polishing. The samples can be mounted on a heater by means of a thin film of Kodak photoresist preparation,[131] diluted with xylene. The sample is placed on the substrate, and a

small drop at one corner spreads out evenly under the sample. However, the samples used were not of uniform thickness, and it was decided that the project would be worthless without damage-free samples with usable regions of uniform thickness. That program is described below.

7.1.2 Methods of thinning samples

7.1.2a mechanical

Three quarter-inch glass discs, of 9-inch diameter, mounted on aluminum discs, served as the lapping plates. They were made flat in the usual way by grinding against each other, and checked for flatness with "mechanics blue" grease.[132] The initial flatness was achieved quickly using #150, and #240 silicon carbide powders. The roughness then comes off with 10-15 micron aluminum oxide powder. A short nap synthetic mechanical polishing cloth mounted on a fourth disc served as the 1 micron aluminum oxide powder lap.

With the sample mounted on the sliding center piece of a hardened-steel block, the sample was reduced in thickness to about 80 microns using 12 and 5 micron aluminum oxide powders. Then one side was mechanically polished on the 1 micron lap. Although smoother surfaces can be obtained by using a 1 micron glass lap before the mechanical polish, there is a high probability that the surface will be destroyed by scratches from small pieces which break off from the sample's edge. The sample is then transferred to another block with

an adjustable leading edge. Using this, the sample can be thinned without caution to 20-25 microns, with 5 micron powder on glass followed by the 1 micron treatment. It is essential that there be no dust under the sample. The dust creates tiny star-shaped cracks above it in the crystal. To avoid this, one can apply a small chip of filtered paraffin wax to an edge region of the sample when it is lying on the heated block. The wax spreads evenly under the sample. It is unwise, the author believes, to attempt to make the sample thinner than 20 microns by this method. The results were not improved over those with aluminum oxide when diamond powder was used.

7.1.2b chemical

Considerable effort was made to obtain thinned samples by chemical etching. The solution used is described in Section 4.3.1. The main obstacle is that the etch removes preferentially, presumably at dislocations. There is also a slight "orange peel" texture, perhaps due to strain introduced during crystal growth. Also the edge region is removed more quickly than the central region. This is not due to solution flow rates, since flow patterns were used which, it is believed, gave uniform flow across the full sample surface. There is instead a catalytic effect, presumably due to surface fields, between the masking material (black wax) and germanium such that the etch rate is accelerated (perhaps threefold) along the wax-germanium-solution contact line. Thus, one ends up with samples of about 0.5 cm^2, of thickness

ranging from 1 to 10 microns, pocked up several small holes. Some improvement over these results could be obtained perhaps with the iodine replaced by bromine (which is known to be less preferential in silicon polishing), and with dislocation-free cyrstals. On the other hand, from a knowledge of the difference in the polished surfaces, the author is confident that good thermoabsorption samples of GaAs of thickness about 5 microns could be prepared by chemical polishing.

An attempt at electropolishing was discontinued when it was appreciated that the sample resistance of pure material caused a very non-uniform potential across the sample between the electrical contact and the sample-solution interface.

7.1.2c ion beam*

As a non-preferential method of reducing the material beyond 20 microns, low-angle ion beam etching was attempted. Some details are: 6KV, 100 microamperes, argon gas, 15 degree striking angle. The removal rate was about 1 micron/hr. This equipment is normally used for the preparation of electron microscope transmission samples, where only very small-area, thin regions are required. However, it was found ideal for thinning large area 2 cm^2 samples. The samples were rotated in the ion beam (which consisted of about 25 small beams)

* This work was done on equipment at Bell-Northern Research Labs., Ottawa. I am grateful to Mssrs. L. Brosselard, S. Entwistle, and B. Piwczyk for their generosity in instructing me in the use of the equipment, and in permitting me to use it. The successful method of mounting the sample was developed by the author.

on brass discs. Although the brass becomes hot, around 100°C, during etching, a film of molten paraffin wax kept the sample well positioned. The samples' thicknesses were determined from mass and area measurements. It is estimated that the almost shiny surface finish had a uniform roughness of the order of 0.1 to 0.3 microns. Presumably that could be improved by lower angle beam incidence. Samples of thicknesses around 7 microns and areas 0.5 cm^2 were obtained, the reduced areas resulting from inexperience in handling. This method is recommended; however, it is cautioned that some damage remains in the surface (see below) and should be removed by a short etch.

7.1.2d tests for damage in samples.

Emperical methods for determining whether or not damage remained in the surface were developed. These can be divided into two types: (i) chemical, and (ii) optical.

(i) chemical

Two methods were investigated here, surface appearance, and etch rate.

For the appearance test, 4 Ge surfaces were prepared with the following Al_2O_3 lap treatments: (1) 5μ on glass; (2) 5μ, 1μ on glass; (3) 5μ, 1μ, 0.3μ on glass; (4) 5μ on glass, 1 micron on cloth. These surfaces, in the order given, were progressively shinier (flatter), the 0.3μ on glass, however, was considerably scratched. Each surface

was then put in the Ge etch for 1 min. 40 sec. The thickness reduction was the same ±10% for all, and the surfaces, except for scratch marks, looked identical. One can conclude that the surface shininess before etch is indistinguishable by the chemicals, and all are equally damaged. The same result was obtained using 1-5μ diamond grit on pitch lap, and with Ge of different growth procedures (i.e., zone-refined, and Czochralski). As the etching continues, the appearance changes as follows: very high density of small pits, reduction in density of pits, flattening of pits, and increase in reflectance. It appears that most of the damage is introduced at the 5μ lapping stage, and traces of these defects remain for tens of microns of chemical removal. On the other hand, it has been found that etching of a surface which had previously been given an ion beam treatment results in a immediate improvement in reflectance.

Because of the apparent requirement (see optical method below) to etch an ion-beamed surface before making optical measurements, a test was made on ~~the etch rate at such a surface~~. Three successive etches of 15 seconds removed 2.3, 0.8, and 0.8 microns respectively. It is concluded that there is damage in the upper 2 micron layers.

(ii) optical

The thermoreflectance result near E_o at room temperature for two ion-beamed samples is shown in Fig. 26(a) and (b), as well as $(\Delta R/R)$

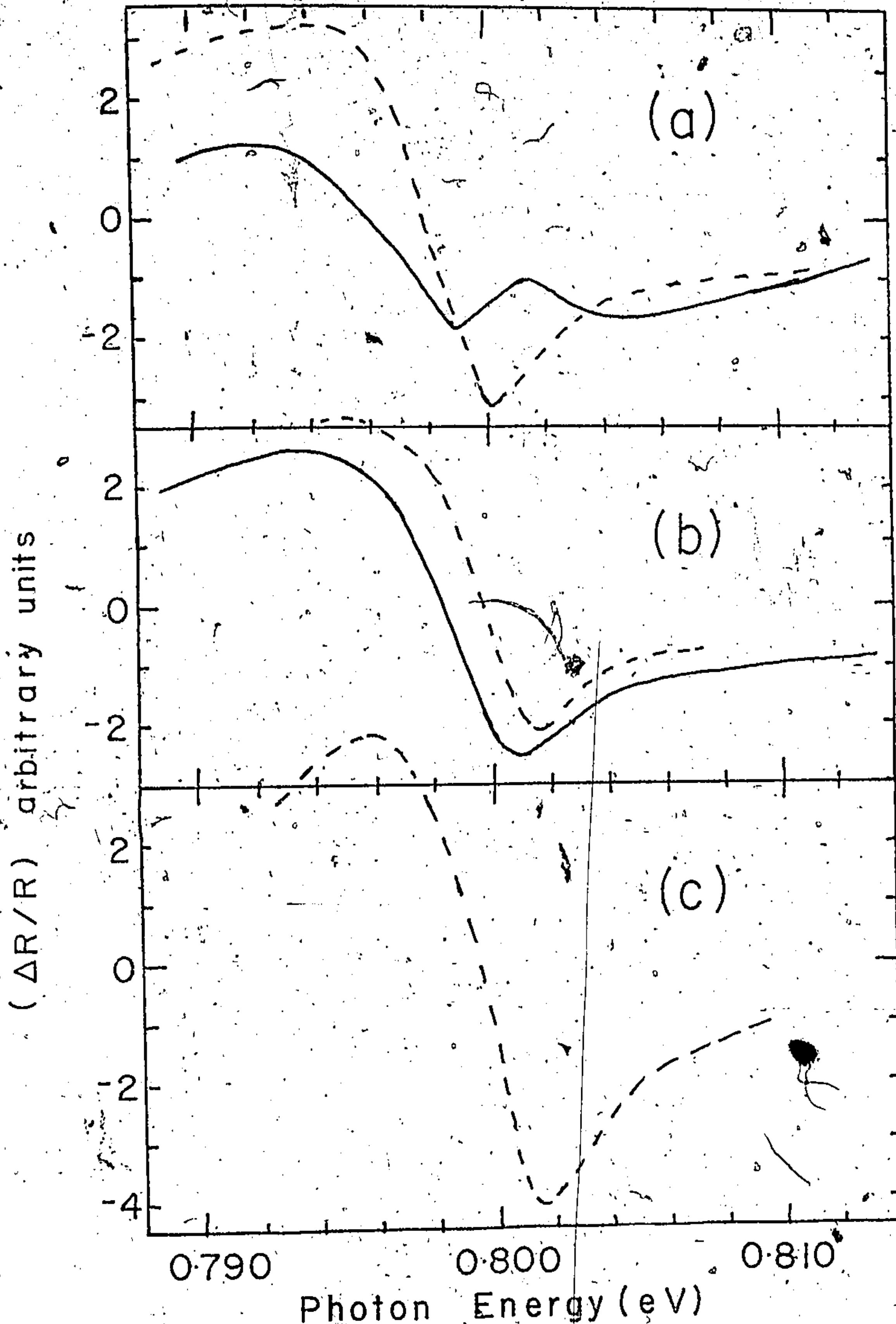

Figure 26. (a),(b): (ΔR/R) near room temperature for two Ge samples just following ion beam treatment (solid lines), and after the ion-beamed surfaces were chemically etched for 15 seconds (dotted lines). c) (ΔR/R) at room temperature of a Ge sample, the surface of which was chemically polished for four minutes.

after the same surfaces were given a 15 sec. etch. Fig. 26(c) shows (ΔR/R) for a sample from the same slice which had been chemically polished for 4 minutes. The negative peaks of the ion-beamed surfaces were broadened, and even split in one case. This was the only time that valence band splitting was observed at room temperature. It would be difficult to understand as well, except that at some unknown time during the 23 hour period during the ion beam treatment, the sample rotator stopped. That explains why one might expect a directional effect. It is concluded that the surface should be etched for 15 seconds before measurement, and that thermoreflectance may be a good tool for identifying shallow strain in some surfaces.

7.2 Thermoreflectance of Ge at E_o in a Magnetic Field

7.2.1 Introduction

There have been statements made in the literature[133] to the effect that the measurement of thermoreflectance at low temperatures in a magnetic field would be of dubious value because of the heating of the sample and the resultant line broadening. After finding the sharp structure near 20 degrees Kelvin in zero field, the author decided to test that prejudice. In addition it was believed that the experience in line shape analysis at zero field would help in the interpretation of line shapes in a magnetic field. The experiment was fruitful, yielding data of a higher quality than the best existing data for Ge from a modulation experiment, namely, Aggarwal's piezoreflectance

experiment.[39] The quality of the data has been judged from two points of view, line width, and the number of easily identifiable lines in the spectra. From the broad shape of Aggarwal's ($\Delta R/R$) structure at $H = 0$, it appears that the sample was subject to a non-uniform strain. However, there was no easily observable spectra in the $E_o + \Delta_o$ region in the present experiment for fields up to 30 kG. Aggarwal obtained most of his data for $E_o + \Delta_o$ above 30 kG, so one cannot conclude that the thermoreflectance technique failed in this respect. Only a vague account of the experiment and data will be presented here, since it is considered unwise to be explicit about work which is still going on.

7.2.2 Experiment

A Ferranti-Packard superconducting solenoid magnet, with a 1½ inch bore, was used. The sample was mounted, in a way similar to that described in Section 4.3, on a relatively massive cylindrical copper heat sink, designed so that the temperature rise of the sink would be minimal. The heat conductivity between the sink and the solenoid was optimized by a pressure of He gas in the chamber of about 10 cm of Hg.[134]

There are some difficulties with the optics in this experiment. It is a difficult alignment job to get the light beam in and out of the magnet hole without reflecting off the sides, and without obstructing the beam by required mirrors. Also, considerable light

intensity is lost in the two-way passage through the double windows of the cryostat, and in the passage through the polarizers. Perhaps the major drawback is that, because of the small magnet hole, one must use a long distance to image the slit on the sample with the result that, to get sufficient signal, one is required to illuminate a considerable length along the sample. Thus, a non-uniform temperature will increase the broadening in the spectra. This was slightly present in this case, since an analysis of the zero-field spectrum gave R_o^* and Γ as 2.3 and 1.3 meV, respectively, which are higher than the values reported in Chapter 6.

Thermoreflectance was measured for right- and left-circularly polarized light for nine magnetic field values up to 60 kG. The light was circularly polarized by passing linearly polarized light[135] through a quarter-wave plate.[136] The quarter-wave plate used had a retardation value of 315 mμ, but used at an angle, the plate had a value of 350 mμ. Figure 27 shows the effectiveness of such an arrangement as a function of photon energy. The percentage of the light intensity which was circularly polarized in one sense was determined from a measurement of I_{min}/I_{max}, the ratio of the minimum to the maximum intensities of the light which passes through an analyzer placed in the beam after the quarter-wave plate. The percentage of the intensity in one sense of circular polarization was calculated from

$$\% = \left(1 - \frac{1 - \alpha}{2(1 + \alpha)}\right) \times 100 \qquad 7 - (2)$$

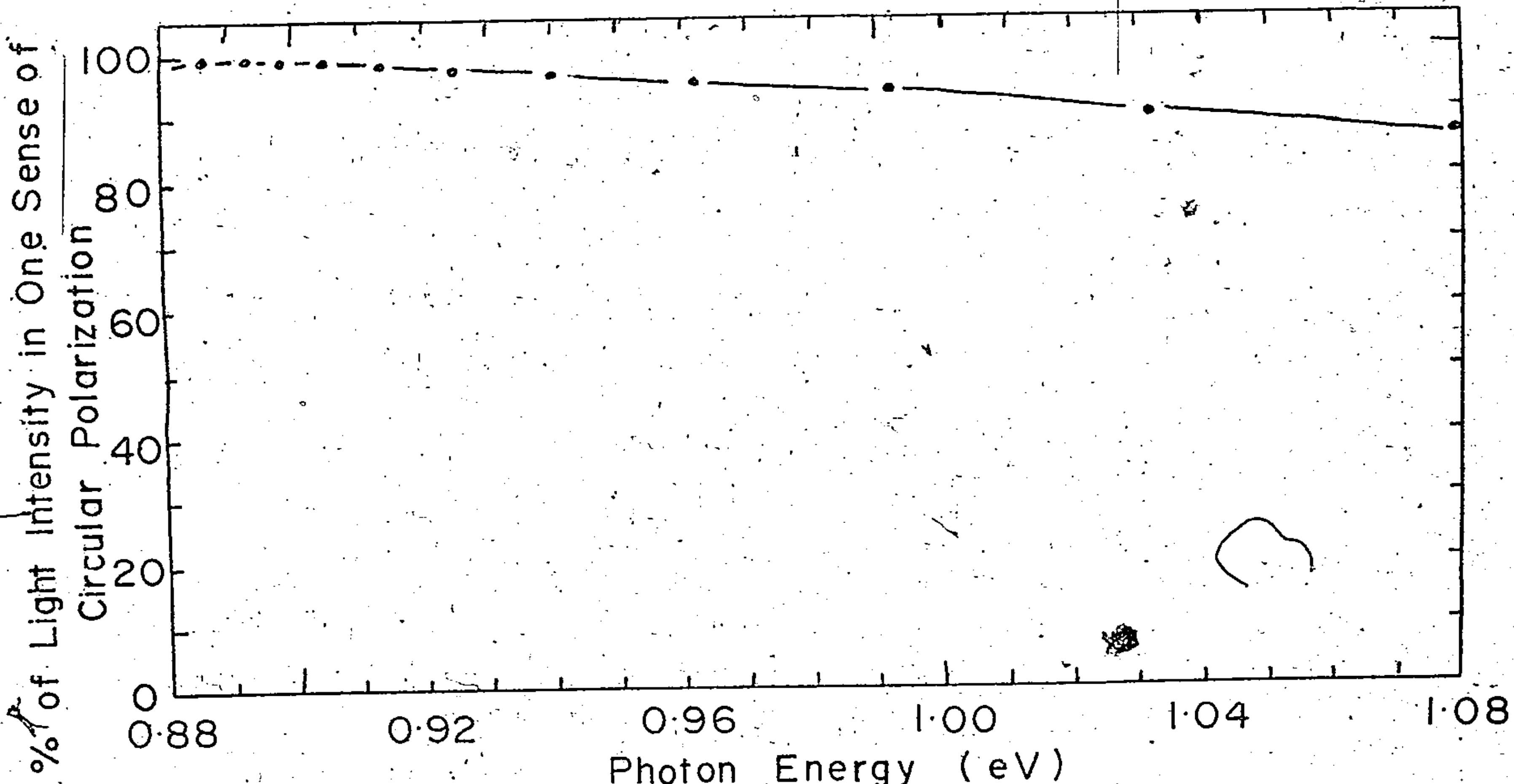

Figure 27. Percentage of total light intensity circularly polarized in one direction as a function of photon energy by a quarter-wave plate arrangement as described in the text.

where $\alpha = I_{min}/I_{max}$. That this is a good indicator can be seen as follows. The light after passing through the quarter-wave plate is elliptically polarized. Choosing an orthogonal co-ordinate system with unit vectors $\underline{i}$ and $\underline{j}$, the electric vector (to within a constant factor) at a particular point in space varies as

$$\underline{\mathcal{E}} = \underline{i} \cos \omega t + \underline{j} \sin (\omega t + \delta) \qquad 7 - (3)$$

which can be rewritten as

$$\underline{\mathcal{E}} = \cos \delta(\underline{i} \cos \omega t + \underline{j} \sin \omega t) + \cos\omega t \left[(1 - \cos \delta)\underline{i} + (\sin \delta)\underline{j} \right] \qquad 7 - (4)$$

Thus the elliptical polarization can be expressed in one circularly and one linearly polarized component. Between 1.4 and 1.2 microns, δ varies between 0 and $(\pi/12)$ radians, so to shorten the expressions, the $(1 - \cos \delta)$ term is dropped. Now the difference between I_{max} and I_{min} is $(\sin^2 \delta)/2$, whereas I_{min} equals one-half the intensity of the circularly polarized component, or $(\cos^2 \delta)/2$. Since the linearly polarized light can itself be decomposed into right- and left-circularly polarized light, the total intensity of the light in one sense of polarization can be seen to be $\cos^2 \delta + (\sin^2 \delta)/4$, with $(\sin^2 \delta)/4$ in the other sense. Thus the percentage of the total intensity in one sense of circular polarization is

$$\% = \left(1 - \frac{(\sin^2 \delta)/4}{\cos^2\delta + (\sin^2\delta)/2} \right) \times 100 \qquad 7 - (5)$$

which reduces to 7-(2).

7.2.2a a feedthrough design for helium temperatures.

Because of the requirement for several electrical feedthroughs at He temperatures, and because of the frequent failure of such units, tests were made on a new design. The constituent parts were: a hole in a stainless steel plate, an indium collar in the hole, and a wire in the hole, with epoxy between the wire and the indium. Twelve holes of 1/4 and 3/16 inch diameters were drilled in 3/16 inch stainless steel plates. The holes were filled with indium using Duzall flux,[137] the plate being supported on graphite. Holes of 7/64 inch diameters were drilled in the indium, washing with water during drilling. Copper wires, AWG 28 and 40 were supported at the hole centers, with masking tape across the holes on the undersides. The places where the wires passed through the tape were sealed with fingernail polish. A mixture of 1:10 by weight of Shell Epon Curing Agent "D" and Epon Resin 408 was put in the holes around the wires. (It is important to degas this mixture in a vacuum system before application.) Two heat treatments were tried: (1) 7 hrs at 60°C + 3/4 hrs. at 140-150°C; (2) 20 hrs at 60°C + 3/4 hrs at 140-150°C. They were tested by 10 cycles of the following: immersion in liquid nitrogen followed by air blasting (3½ min. to room temperature). There were no leaks in any of them as measured by the He leak detector. However, AWG 28 wire is considered too large because movement of such wire displaces the epoxy with eventual opening of the joint. It is suggested that only smaller wires, about AWG 35 and smaller, be tried in such a feedthrough.

7.2.3 Representative data and some observations

Figure 28 shows the modulation signal at 30 kG for right-circularly polarized (RCP) light. It was verified that none of the observed structure, except for the small ripple at 0.888 eV, corresponds to structure in the incident beam. If one compares with previous modulated reflectance data on Ge, the magnetoelectroreflectance[138] and magnetopiezoreflectance[39] data, one sees that the structures continue to much higher energies with the present thermoreflectance technique. Thus the Pidgeon and Brown theory[40] for the locations of the Landau levels would be subjected to a stiffer test with the present data. However, such a fit will not be the main effort of the eventual analysis. Figure 29 shows the shapes and magnitude of ($\Delta R/R$) associated with the first transition (in RCP) for several magnetic fields. This data is considered more valuable than that of Fig. 28. Until recently, little work[139,140] has been done on the interpretation of exciton peaks in a magnetic field. This has been summarized by Johnson.[14] The spectra of Fig. 29 are being investigated from the points of view of shape, magnitude and energy location. That such data is fruitful can be seen from a recent photluminescence study[141] of GaAs in a magnetic field: just the location of the free exciton peak was able to establish that the heavy hole mass gives the total contribution from the valence bands in the reduced mass used to calculate the exciton binding energy. This is in disagreement with theory,[115,116] and if valid for Ge would put R_o^* for Ge at 1.8 meV, in agreement with the results of Chapter 6.

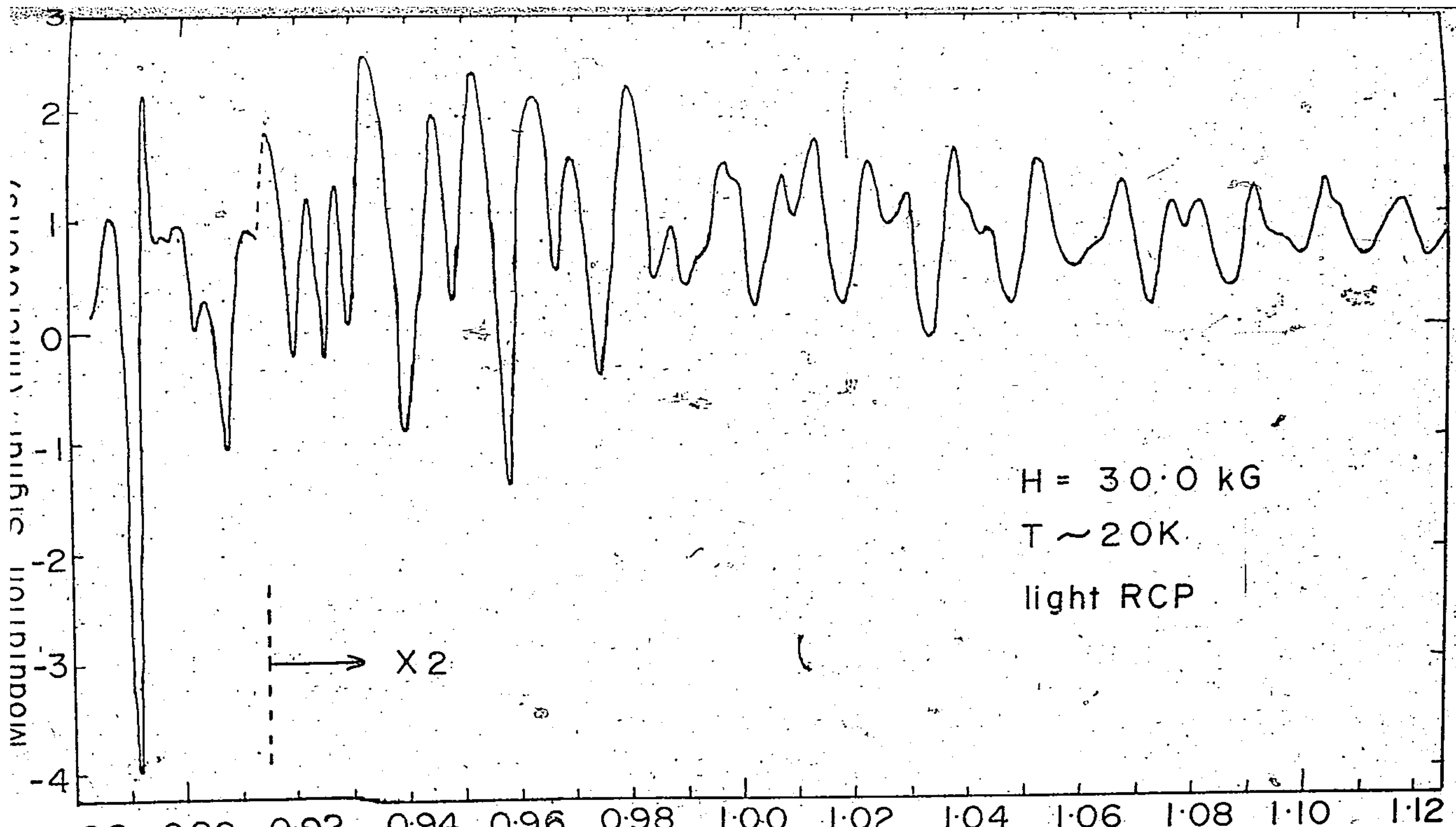

Figure 28. Modulation signal at 30kG near 20K with right-circularly polarized light for a Ge sample.

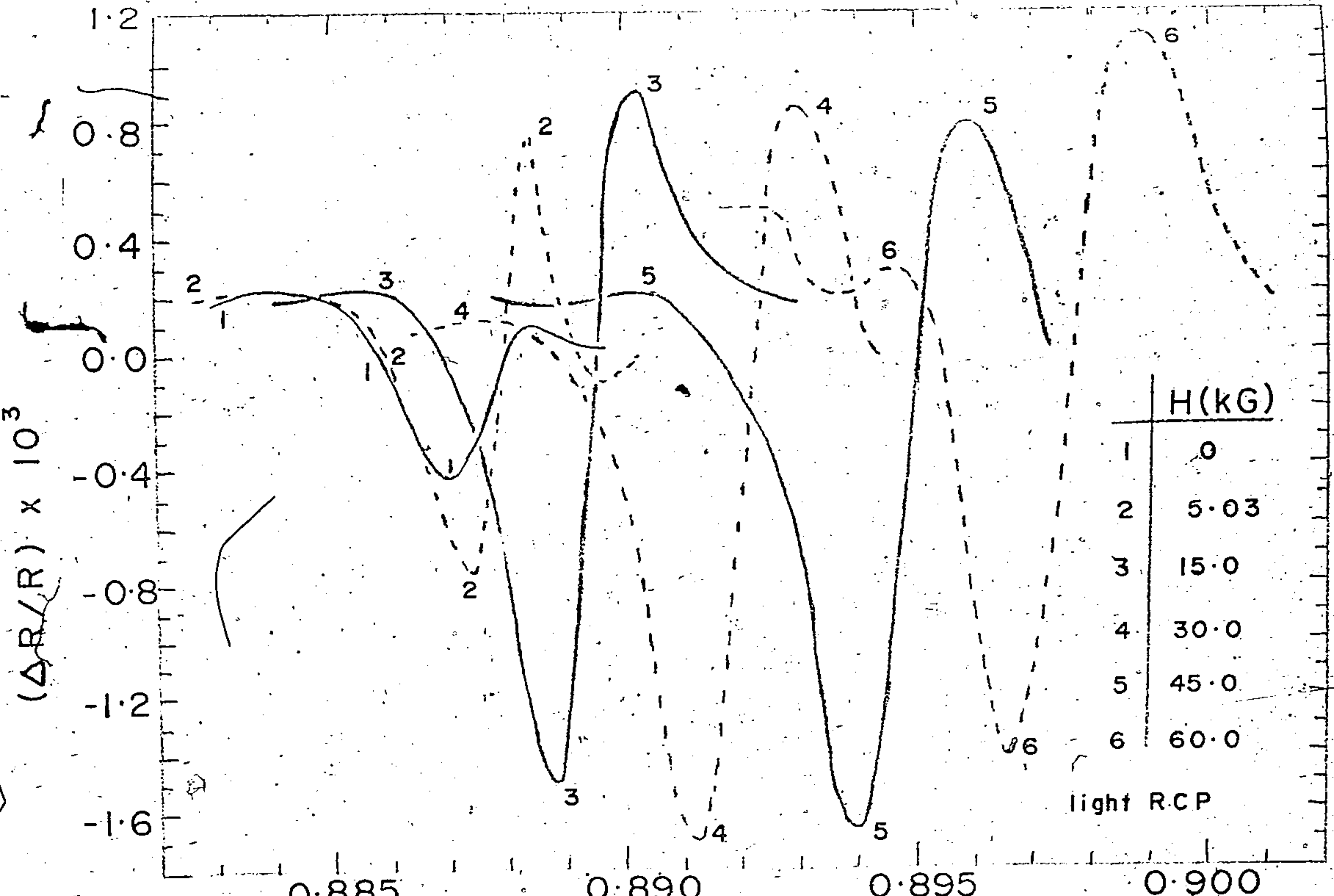

Figure 29. The first structure at the low energy end in $(\Delta R/R)$ near 20K with right-circularly polarised light for a Ge sample at several magnetic field strengths.

To conclude this chapter, the titles of relevant articles published during the past year in only one journal, Physical Review B, are listed as Ref. 142, to indicate how active the exciton field has become, as well, by omission, to indicate how much of the field has not yet been treated.

CHAPTER 8

SUMMARY AND POSSIBLE DIRECTIONS OF FUTURE WORK

The main contribution of this work is believed to be that it has helped establish thermoreflectance more firmly as a tool with which to study optical transitions in solids. Generally speaking, the author believes it to be the best of the modulation techniques. It is often claimed of some of the other techniques that they have the advantage of being able to vary a directional parameter, such as stress or electric field. However, in fact, they are seldom used to profit from that feature. Furthermore, it is believed the thermoreflectance of a sample subjected to a uniform dc directional stress of some sort would yield better results in some cases.

Data obtained here has supported Elliott's theory for the excitonic absorption edge in germanium. Other data has revealed structure in the reflection spectra of heavily-doped n-type InAs, which could be related to transitions between the light- and heavy-hole valence bands and the conduction band, following a Kane model. The conduction band has also been studied by more conventional techniques.

The most promising area of work opened up seems to be the

interpretation of magnetothermoreflectance data. There is little hope of making a real contribution before a careful theoretical study of the excitonic behaviour of the degenerate valence bands - conduction band combination in a magnetic field is made.

Another useful area would be the tracing of conduction bands in k-space from thermoreflectance data of heavily-doped n- and p-type materials. This, presumably, would be able to identify closely the energies at which populations of higher bands begin.

A more critical treatment could be made of the theory of infrared reflectivity in the plasma resonance spectral region of semi-conductors.

APPENDIX A

A DERIVATION OF THE FARADAY ROTATION RESULT WITHOUT DECOMPOSITION INTO CIRCULARLY POLARIZED COMPONENTS

All derivations of the Faraday rotation of which we are aware (e.g., Ref. 143, for an elementary treatment, and Refs. 144, 145 for an advanced treatment) begin with the decomposition of a linearly polarized wave into two oppositely rotating circularly polarized components. The derivations then look for $\sigma+$ and $\sigma-$ which relate $J_x \pm iJ_y$ to $\mathcal{E}_x \pm i\mathcal{E}_y$. For the free carrier case, where the conditions $\mu B << 1$, $\omega\tau >> 1$ apply, where ω is the optical angular frequency and τ, μ the carrier scattering time and mobility, the result is that the light which leaves the sample is linearly polarized, with the plane of polarization rotated by an angle θ with respect to the incident polarization. This is suggestive of the idea that one need not use circularly polarized components in the analysis, but instead follow the linearly polarized wave through the sample and see what rotation, if any, is required by Maxwell's equations. Perhaps the main service of such a derivation would be to give more "feel" to the treatment of wave solutions of Maxwell's equations.

Consider the equation for the average motion of charges q (q is positive for holes and negative for electrons), of effective mass m*,

in an electric field $\mathcal{E}$ exp($i\omega t$), and in a magnetic field B_o

$$\dot{\underline{v}} = \frac{q}{m^*}\underline{\mathcal{E}}e^{i\omega t} + \frac{q}{m^*}(v \times B_o) - \frac{\underline{v}}{\tau} \qquad A - (1)$$

For low magnetic fields, where $\mu B << 1$, and for $\omega\tau >> 1$, this reduces in the first approximation to

$$\dot{\underline{v}} = \frac{q}{m^*}\underline{\mathcal{E}}\, e^{i\omega t} \qquad A - (2)$$

from which

$$\underline{v} = \frac{q}{i\omega m^*}\underline{\mathcal{E}}\, e^{i\omega t} \qquad A - (3)$$

Substituting this into A-(1), still neglecting the damping force term, we find, if $\underline{B_o}$ is in the z-direction and $\underline{\mathcal{E}}$ is in the x-direction, that

$$v_y = \frac{q^2|\mathcal{E}|B_o}{m^{*2}\omega^3}\cos\,\omega t \qquad A - (4)$$

Also, at any point within the sample, with x chosen as the direction of the electric field, assuming a plane wave solution with the possibility of rotation, the current density in the y-direction, J_y, will be given by

$$J_y = \frac{Nq^3|\mathcal{E}|B_o}{m^{*2}\,\omega^3}\cos\,(\omega t + \phi) \qquad A - (5)$$

where N is the number of carriers per cc and ϕ is just a phase angle.

Now consider Maxwell's fourth equation:

$$\underline{\nabla} \times \underline{H} = \underline{J} + \varepsilon_b \frac{\partial \mathcal{E}}{\partial t} \qquad \text{A - (6)}$$

where J takes into account the charge movement of free charges and $\varepsilon_b \frac{\partial \mathcal{E}}{\partial t}$ takes into account the movement of the bound charges as well as $\varepsilon_o \frac{\partial \mathcal{E}}{\partial t}$, the vacuum component of the displacement current. Choosing the x-axis along $\mathcal{E}$ the y-component of Eq. A-(6) is

$$\frac{\partial H_x}{\partial z} = J_y + \varepsilon_b \left(\frac{\partial \mathcal{E}}{\partial t}\right)_y \qquad \text{A - (7)}$$

One sees that H_x does not remain zero; that is, the current perpendicular to $\mathcal{E}$ has required a **rotation** in the plane of polarization. The component on the left hand side of Eq. A-(7) becomes $H_y \frac{d\theta}{dz}$, where θ is the rotation of the plane of polarization. For the right hand side, which gives the total current density in the y-direction, one component is given by Eq. A-(5). There is also a component due to the fact that the current which is in the direction of $\mathcal{E}$ rotates in going a distance dz.

This can be easily visualized by considering a small surface element of height h and length dz which is in a plane in the z-direction and through which $\mathcal{E}$ passes. For convenience we lump the total current due to this in the form $\varepsilon_1 \frac{\partial \mathcal{E}_y}{\partial t}$, where $\varepsilon_1 = \varepsilon_{free} + \varepsilon_b$. Then the

charge density through such a loop is $\varepsilon_1 \frac{\partial \mathcal{E}_y}{\partial z}\frac{dz}{dt}$. Now $\frac{\partial \mathcal{E}_y}{\partial z} = \mathcal{E}_x \frac{d\theta}{dz}$, and $\frac{dz}{dt} = \frac{c}{n_1}$, where c is the velocity of light in a vacuum. Therefore Eq. A-(7) becomes

$$-H_y \frac{d\theta}{dz} = \frac{Nq^3 B_o \mathcal{E}_x}{m^{*2}\omega^2} + \varepsilon_1 \mathcal{E}_x \frac{c}{n_1} \left(\frac{d\theta}{dz}\right) \qquad \text{A - (8)}$$

Remembering that $H_y = \varepsilon_1 \frac{c}{n_1} \mathcal{E}_x$, and $\varepsilon_1 = \varepsilon_o n_1^2$ Eq. A-(8) can be rewritten as

$$\frac{d\theta}{dz} = -\frac{Nq^3 B_o}{2c\,\varepsilon_o n_1 m^{*2}\omega^2} \qquad \text{A - (9)}$$

Which is the standard result for the free carrier Faraday rotation effect.

We are confident that, if the damping force term of Eq. A-(1) were included, a few more observations would yield the result for Faraday ellipticity. Although the present development has been undesirably lengthy, it represents only the beginning of the author's understanding of the Faraday effect; one imagaines that this could be abbreviated such that a single vector (time- and space-dependent) could be written down as the complete solution.

APPENDIX B

AN ATTEMPT AT A DIFFERENT APPLICATION OF THE KRAMERS-KRONIG RELATIONSHIPS

The Kramers-Kronig expressions for the relationships between ε_1 and ε_2, the real and imaginary parts of the dielectric constant are[97]

$$\varepsilon_1(\omega) - 1 = \frac{2}{\pi} P \int_0^\infty \frac{\omega' \varepsilon_2(\omega') d\omega'}{\omega'^2 - \omega^2} \qquad B-(1)$$

$$\varepsilon_2(\omega) = \frac{2\omega}{\pi} P \int_0^\infty \frac{\varepsilon_1(\omega') d\omega'}{\omega^2 - \omega'^2} \qquad B-(2)$$

where P indicates the principal value[147] of the integral. These are often used locally.[148] For example, given ε_2 (particularly changes in ε_2) over a region $\Delta\omega$, what is the behaviour of ε_2 over $\Delta\omega$? This is established by performing the integral in B-(1) above, noting that the contribution to $\varepsilon_1(\omega)$, for ω in the central part of $\Delta\omega$, from $\varepsilon_2(\omega)$ outside $\Delta\omega$ will be fairly constant. However, it would be more ambitious to try to obtain ε_1 everywhere using Eq. B-(2). Suppose ε_2 is known in the region ω_o to $\omega_o + \Delta\omega$. Divide this interval into N parts, and denote the center frequencies of each interval by ω_i, $i = 1, N$. Also divide the whole domain into N parts, centered at ω_j, $j = 1, N$. Since the denominators in B-(2) are smallest when ω_i' is within the region ω_o to $\omega_o + \Delta\omega$, the density of the ω_j' values selected should be greater around that region. A reasonable choice was thought to be (N/3) parts evenly distributed over the interval $\Delta\omega$, with increasingly larger parts chosen in a

fairly symmetrical way outside the $\Delta\omega$ interval. The centre frequencies of the $N/3$ intervals in the range ω_o to $\omega_o + \Delta\omega$ are chosen to be at positions half-way between the centre frequencies chosen for ε_2 so as to avoid zero denominators in the evaluation of Eq. B-(2). Now one can set up a set of N simultaneous equations in $\varepsilon_1(\omega_j)$.

$$\varepsilon_2(\omega_i) = \frac{2\omega_i}{\pi} \sum_{j=1}^{N} \frac{\varepsilon_1(\omega_j)\Delta\omega_j}{\omega_i^2 - \omega_j^2} \qquad \text{— B - (3)}$$

If one assumes that ε_1 is linear in the region ω_j to ω_{j+1}, one can divide $\Delta\omega_j$ into many smaller parts so as to eliminate the improper weighting of the factor $(\omega_i^2 - \omega_j^2)^{-1}$ in the sum B-(3). This was done using for ε_2 the imaginary part of $[(\omega - \omega_o) + i\Gamma]^{-1}$ in the range $|\omega - \omega_o| < \Gamma$, with the frequency interval divided into 51 parts. All the subroutines in the computer for the solutions of simultaneous equations were tried. The results for ε_1 were fairly good in the region of $\Delta\omega$ provided double precision was used. Since this is unrealistic from an experimental point of view, three figures being considered very good, the result was considered academic. Beyond this interval the results were very unrealistic, presumably due to round-off errors in the solution.

It is concluded that Eq. B-(3) cannot be solved in standard ways. Perhaps a closer look at the solution methods as applied to this type of data would yield more information.

APPENDIX C

MAGNETORESISTIVITY AND HALL EFFECT: TWO DERIVATIONS

Two derivations of magnetoresistivity will be developed here: both are in the charged ball model as labelled in Section 2.2.1. The first of these derivations using the damping force approach of Section 2.2.2. The second describes the electron orbits. Although it is understood that these derivations are not the proper quantum mechanical ones, the author believes that juggling of concepts from various points of view eventually leads to deeper understanding. Since the charged ball model is already widely used in introducing the student to magnetoresistivity these derivations contribute to that approach.

(a) the damping force approach

The average acceleration, $\dot{\vec{v}}$, of electrons of mass, m, in a medium with scattering time τ, is given by

$$\dot{\vec{v}} = -\frac{e\vec{\mathcal{E}}}{m} - \frac{e}{m}\vec{v} \times \vec{B} - \frac{\vec{v}}{\tau} \qquad \text{C-(1)}$$

---

where $\vec{v}$ is the average velocity of electrons of mass m. With $\vec{B}$ in the z-direction and the external component of $\vec{\mathcal{E}}$ in the x-direction, any additional electric field can only occur in the y-direction, and since there is no z-directed force, there is no acceleration in the

z-direction. Thus writing $\vec{v}$ as $v_x + iv_y$ and $\vec{\mathcal{E}}$ as $\mathcal{E}_x + i\mathcal{E}_y$, in the steady state Eq. C-(1) becomes

$$\frac{v_x + iv_y}{\tau} = -\frac{e}{m}(\mathcal{E}_x + i\mathcal{E}_y) + \frac{ieB}{m}(v_x + iv_y) \qquad \text{C - (2)}$$

from which

$$v_x + iv_y = -\frac{1}{(\tau^{-1} - i\omega_c)}\frac{e}{m}(\mathcal{E}_x + i\mathcal{E}_y) \qquad \text{C - (3)}$$

where $\omega_c = eB/m$.

If there is no net current in the y-direction, $v_y = 0$. This implies two results from C-(3):

$$\frac{\mathcal{E}_y}{\mathcal{E}_x} = -\omega\tau \qquad \text{C - (4)}$$

and

$$v_x = -\frac{e\tau\mathcal{E}_x}{m} \qquad \text{C - (5)}$$

the usual result for the Hall effect and conductivity of a single type of carrier.

Suppose there are ℓ different types of carriers, of concentrations, n_j, mass, m_j, and scattering times, τ_j. Then Eqs. C-(2) and C-(3) are valid for each type of carrier; however, when the total y-current is set to zero, one has

$$\frac{\mathcal{E}_y}{\mathcal{E}_x} = \frac{\displaystyle\sum_{j=1}^{\ell} \frac{n_j \omega_{cj}}{m_j(\omega_{cj}^2 + \tau_j^{-2})}}{\displaystyle\sum_{j=1}^{\ell} \frac{n_j \tau_j^{-1}}{m_j(\omega_{cj}^2 + \tau_j^{-2})}} \qquad C - (6)$$

and

$$\sigma = \rho^{-1} = \frac{\left(\displaystyle\sum_{j=1}^{\ell} \frac{\sigma_j}{1 + \omega_{cj}^2 \omega_j^2}\right)^2 + \left(\displaystyle\sum^{\ell} \frac{\sigma_j \omega_{cj} \tau_j}{1 + \omega_{cj}^2 \tau_j^2}\right)^2}{\displaystyle\sum_{j=1}^{\ell} \frac{\sigma_j}{1 + \omega_{cj}^2 \tau_j^2}} \qquad C - (7)$$

where $|\omega_{cj}| = eB/m_j$ and $\sigma_j = n_j e^2 \tau_j / m_j$. This is the usual result[149] for the Hall effect and magnetoconductivity for more than one type of carrier. It is to be noted that ω_j is positive for electrons and negative for holes in the convention used above.

(b) the orbit approach

Consider the equation relating the instantaneous velocity $\underline{v}$ and acceleration $\dot{\underline{v}}$ in the x-y plane of an electron with an electric field $\mathcal{E}$ in the x-y plane, and a magnetic field along the positive z-direction.

$$\dot{\underline{v}} = -\frac{e\mathcal{E}}{m_e} - \frac{e}{m_e}(\underline{v} \times \underline{B}) \qquad C - (8)$$

The solution is

$$v_x + i v_y = \frac{e}{i m_e \omega_{ce}} (\mathcal{E}_x + i\mathcal{E}_y)(1 - e^{i\omega_{ce} t}) + (v_{xo} + i v_{yo})\, e^{i\omega_{ce} t} \qquad \text{C - (9)}$$

where v_{xo}, v_{yo} give the instantaneous velocity in the x-y plane right after a collision. It is assumed to be zero on the average, and is not carried in the analysis. Eq. C-(9) can be written in two parts:

$$v_x = -\frac{e}{m\omega_{ce}} (\mathcal{E}_x^2 + \mathcal{E}_y^2)^{\frac{1}{2}} [\sin (\omega_{ce} + \delta) - \sin \delta] \qquad \text{C - (10)}$$

$$v_y = \frac{e}{m\omega_{ce}} (\mathcal{E}_x^2 + \mathcal{E}_y^2)^{\frac{1}{2}} [\cos (\omega_{ce} t + \delta) - \cos \delta] \qquad \text{C - (11)}$$

The analagous result for holes is

$$v_x = \frac{e}{m\omega_{ch}} (\mathcal{E}_x^2 + \mathcal{E}_y^2)^{\frac{1}{2}} [\sin (\omega_{ch} t + \delta) - \sin \delta] \qquad \text{C - (12)}$$

$$v_y = -\frac{e}{m\omega_{ch}} (\mathcal{E}_x^2 + \mathcal{E}_y^2)^{\frac{1}{2}} [\cos (\omega_{ch} + \delta) - \cos \delta] \qquad \text{C - (13)}$$

where we are still adhering to the convention of part (a) regarding the ω's. $\delta = \tan^{-1}(\mathcal{E}_y/\mathcal{E}_x)$. For definiteness, consider $\mathcal{E}_x$ as the applied external field in the positive x-direction. Then δ is positive or negative when the Hall field, $\mathcal{E}_y$, is positive or negative. Eqs. C-(10), C-(11), describe the motion of a point on a wheel of radius

$e(m_e\omega_{ce}^2)^{-1}(\mathcal{E}_x^2 + \mathcal{E}_y^2)^{\frac{1}{2}}$ which rolls downwards on the left side of an inclined plane, tilted at an angle δ with respect to the positive y-axis, with angular frequency ω_{ce}. Eqs. C-(12), C-(13) describe the motion of a point on a wheel of radius $e(m_h\omega_{ch}^2)^{-1}(\mathcal{E}_x^2 + \mathcal{E}_y^2)^{\frac{1}{2}}$ which rolls downward on the right side of the same plane with angular frequency ω_{ch}. These orbits are called cycloids.

Consider, for the moment, Eqs. C-(10), C-(11), subject to the physical restriction that the average $v_y = 0$

$$\int_0^\infty \frac{e^{-t/\tau_e}}{\tau_e} \left(\cos(\omega_{ce}t + \delta) - \cos\delta\right)dt = 0 \qquad C - (14)$$

One finds $\tan\delta = -\omega_{ce}\tau_e$, and $(v_x)_{av} = -(e\tau_e/m_e)\mathcal{E}_x$. This result can be interpreted in a more general way. Consider the carriers in any cycloid characterized by (m_j, τ_j). Consider new axes x', y', such that the average $v_{y'}$ is zero. Then one would find that $(\mathcal{E}_{y'}/\mathcal{E}_{x'})$ equals $-\omega_j\tau_j$. [illegible] the net velocity of the carriers in this cycloid is directed at an angle $-\theta_j$ with respect to $\mathcal{E}$, where $\tan\theta_j = -\omega_j\tau_j$, with $0 < \theta_j < \pi/2$, for holes, and $\frac{\pi}{2} < \theta_j < \pi$, for electrons.

As an example of an application of the above consider two types of carriers, n_e electrons characterized by τ_e, m_e, and n_h holes characterized by τ_h, m_h. See Fig. 30 for the disposition of the cycloids. Although δ is shown as a negative angle it is treated generally in the

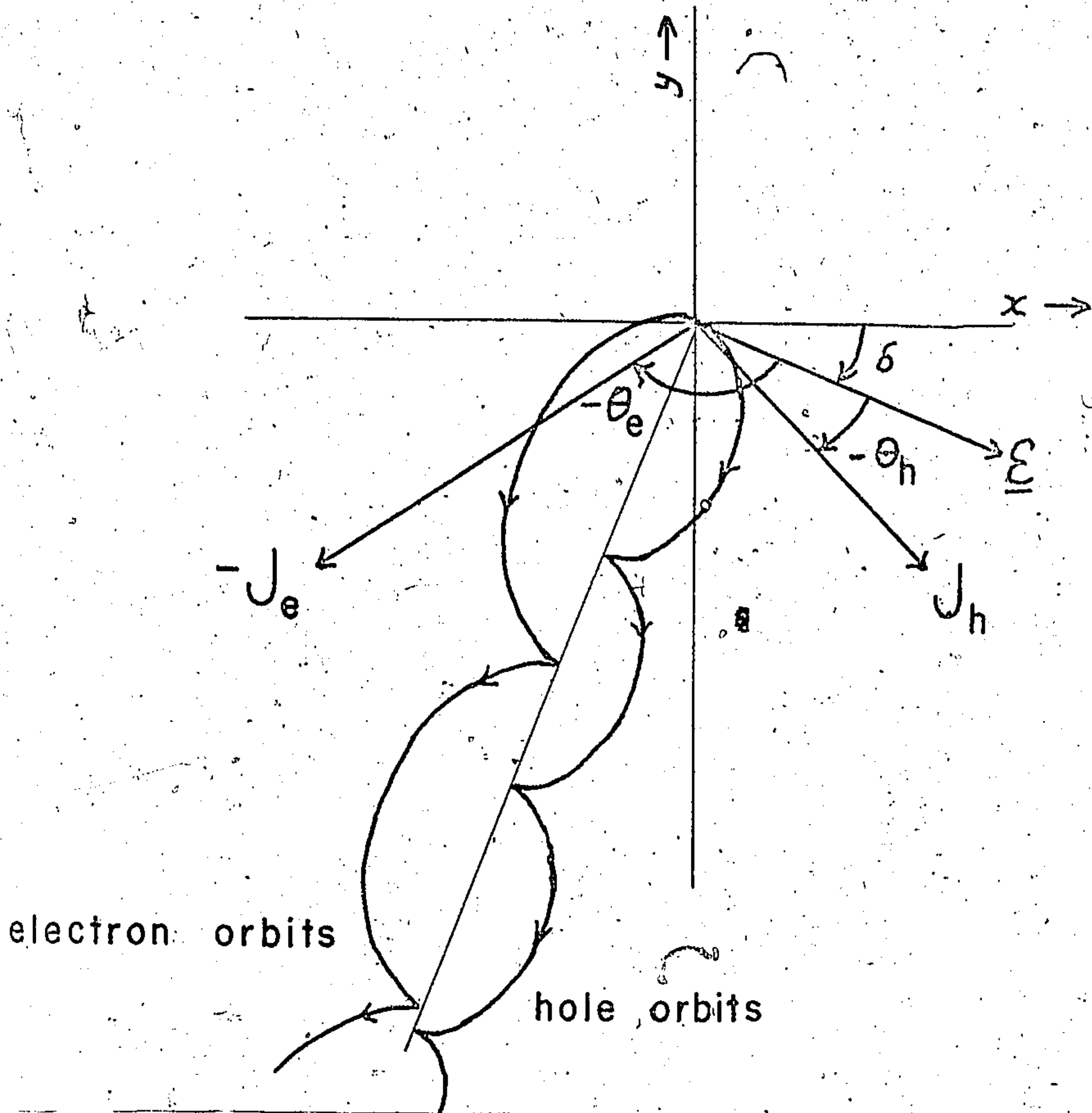

Figure 30. Electron and hole orbits in mutually perpendicular electric and magnetic fields.

algebra below. One requires for a Hall measurement that the y-current is zero; that is

$$|\mathcal{E}| \cos\theta_h \sigma_h \sin(\theta_h - \delta) = -|\mathcal{E}| \cos\theta_e \sigma_e \sin(\theta_e - \delta) \qquad C-(15)$$

Solving for tan δ, one finds

$$\tan\delta = \frac{\sigma_e \sin\theta_e \cos\theta_e + \sigma_h \sin\theta_h \cos\theta_h}{\sigma_e \cos^2\theta_e + \sigma_h \cos^2\theta_h} \qquad C-(16)$$

Remembering that $\sin\theta_e = \omega_{ce}\tau_e (1 + \omega_{ce}^2 \tau_e^2)^{-1}$, $\cos\theta_e = -(1 + \omega_{ce}^2 \tau^2)$, and so on, one arrives at the same result as Eq. C-(6) for such carriers.

In order to understand the magnetoresistance effect a little, let us see what has happened. Consider a given magnetic field, and the problem with the electron cycloid alone. The cycloid would have a base line with a positive slope with $\underline{\mathcal{E}}$ directed at an angle $\phi = \tan^{-1}\omega_{ce}\tau_e$ below the positive x-axis. Considering holes with no electrons, the cycloid base line would have negative slope. When these holes and electrons are both present, the common base line must be somewhere between the individual base lines. It is easy to show that this base line shift results in a reduction in the x-current due to holes as well as that due to electrons. It is possible, however, that there be more total current in one cycloid than there would be were the other carrier not present. The case of two carriers of the

same sign is different. Because the cycloid bases rotate in opposite directions toward a common base line, one of the carriers shows an increase in x-current, while the other shows a decrease. This suggests the result, which can be proven, that given two carrier types characterized by n_j, m_j, τ_j, the magnetoresistance is greater when the types are of opposite sign than when they are of the same sign. The extreme case of this is for $n_1 = n_2$, $m_1 = m_2$, $\tau_1 = \tau_2$: the magnetoresistance $\to \infty$, as $B \to \infty$ for types of opposite sign, whereas it is zero for just a single type.

As a further application, consider the result of Chambers[150] that if one knows $\sigma(B)$, $R_H(B)$ (Hall coefficient) for two groups of ~~carriers, in each of~~ which there may be various values of m and τ, then the result for R_H for the combination is formally that for two carrier types. Note first that R_H is proportional to $\mathcal{E}_y/I_x$, and that $\sigma = I_x/\mathcal{E}_x$. Thus one can obtain $\mathcal{E}_y/\mathcal{E}_x$, and thence δ, for each group of carriers as a function of magnetic field. When they are put together in a given magnetic field, the net current vector for each group is in its same relative position relative to $\mathcal{E}$; hence one obtains the result for $\sigma_{combined}$ and $(\tan \delta)_{combined}$ in the same form as for the two-carrier types case.

As a final picture, one can look at what happens when $\omega\tau \gg 1$ for one carrier in a holes-electrons two carrier case. If the current

in that carrier is sufficient, the other carrier will not only have a negative magnetoresistance, it will have a negative resistance; that is, the x-current will be oppositely directed from what it was in the absence of a magnetic field.

APPENDIX D

AN ALTERNATIVE DERIVATION OF THE QUANTUM MECHANICAL EXPRESSION FOR THE DIELECTRIC CONSTANT

The following is a derivation for the dielectric which is somewhat different than that which has been presented by Ehrenreich and Cohen,[96] and by Cardona[20]. In particular, the method of introducing the lifetime broadening parameter is believed to be original.

Consider an electric field $\underline{\mathcal{E}}(t) = \underline{\mathcal{E}}_o \delta(t)$. Let f(t) be the response to the field such that the current, $\underline{J}(t)$, equals $f(t)\underline{\mathcal{E}}_o$. Similarly, $f(t - \tau)$ is the response function to a δ-function, $\delta(t - \tau)$, applied at $t = \tau$. Thus

$$\underline{J}(t) = \int_{-\infty}^{t} f(t - \tau)\, \underline{\mathcal{E}}(\tau)\, d\tau \qquad \text{D - (1)}$$

One could similarly define a response function between $\underline{J}$ and $\underline{A}$. Anticipating that $\underline{\mathcal{E}} = -i\omega\underline{A}$ in the present case one sees that there is just a constant factor difference between the two response functions.

Consider now the effect of a δ-function perturbation $\underline{A} = \underline{A}_o\, \delta(t - \tau)$ on the wave function. For definiteness we shall consider transitions in

which one Bloch state $|vk\rangle$ is affected, with the excited state containing a Bloch function from higher bands, ℓ. Performing the time integral in the usual time dependent perturbation theory result,[151] one gets

$$\Psi_o \rightarrow \Psi_o + \sum_\ell c_\ell(t) \; \Psi_\ell \; e^{-E_\ell t\hbar^{-1}} \qquad D-(2)$$

and,

$$c_\ell(t) = \frac{e}{i\hbar m} A_o \langle \ell | \underline{a} \cdot \underline{p} | \; v\underline{k} \rangle e^{iE_\ell \tau \hbar^{-1}} \qquad D-(3)$$

where the ground state has energy equal to zero. However, rather than accept the time dependence of Eq. D-(2), we state that, due to collisions, the effect of an impulse at $t = \tau$ dies out as $e^{-\Gamma(t-\tau)\hbar^{-1}}$ that is

$$\Psi = \Psi_o + e^{-\Gamma(t-\tau)\hbar^{-1}} \sum_\ell c_\ell(t) \; \Psi_\ell \; e^{-E_\ell t/\hbar} \qquad D-(4)$$

Let us now calculate[99] the current associated with the wave function D-(4). Consider the new Ψ normalized:

$$\underline{J} = \tfrac{1}{2}\frac{e}{m}\left[\Psi^*(t) \; \underline{p} \; \Psi(t) - \Psi(t) \; \underline{p} \; \Psi^*\right] - \frac{e^2}{m} \Psi^* \Psi \underline{A} \qquad D-(5)$$

If one averages the current over a unit volume, it is straightforward to show, to first order in A, that

$$J = -\frac{2e^2}{\hbar m^2} A \cdot \sum_{\ell} |\langle \ell | p_x | k \rangle|^2 \cdot \mathrm{Re}\left[\frac{e^{-i(E_\ell - i\Gamma)(t-\tau)\hbar^{-1}}}{i}\right] - \frac{e^2}{m} A \qquad D-(6)$$

where, for convenience, A has been taken in the x-direction, and J and A are written as scalars. Therefore, the response function $f_A(t - \tau)$ of J for a δ-function of A at t = τ is just the coefficient of A in Eq. D-(6).

Now setting up the integral of Eq. D-(1) using $\mathcal{E}(\tau)$ equals $-i\omega A(\tau)$, and making the change of variables $u = t - \tau$, and anticipating that the major contribution will come only from the state where $E_\ell = \hbar\omega$

$$J = \frac{e^2}{i\hbar m^2 \omega} \mathcal{E} |\langle \ell | p_x | k \rangle|^2 e^{-i\omega t} \int_0^\infty \left[\frac{e^{-i(\omega_\ell - i\eta)u}}{i} + c.c.\right] e^{i\omega u} du$$

$$- \frac{e^2}{i\omega m} \mathcal{E} e^{-i\omega t} \qquad D-(7)$$

where $\eta = \Gamma\hbar^{-1}$

Evaluating the integral, and remembering $\tilde{\sigma} = -i\omega\tilde{\varepsilon}$, the contribution from the transition at k to band ℓ to $\tilde{\varepsilon}$ becomes

$$\tilde{\varepsilon}(\omega) = -\frac{e^2}{\hbar m\omega^2} |\langle \ell | p_x | k \rangle|^2 \frac{2\omega_\ell}{(\omega - \omega_\ell + i\eta)(\omega + \omega_\ell + i\eta)} - \frac{e^2}{\omega^2 m} \qquad D-(8)$$

Eq. D-(8) agrees with Eq. 2.8 in Cardona's book,[20] except for the first negative sign which, I believe, is wrong in the book, and with this agreement the author believes a credible method has been presented for the introduction of Γ. One may suspect that the response function approach could have been bypassed. The value of this approach in the author's view is that one identifies an exponential time decay of any effect due to radiation at any time.

In order to convert Eq. D-(8) into the result of Eq. 4-(19), one does a little algebra and then applies a sum rule, as has been done, e.g., by Cardona. Noting that,

$$\frac{\omega_\ell}{(\omega_\ell^2 + (\omega + i\eta)^2)} = \frac{(\omega + i\eta)^2}{\omega_\ell(\omega_\ell^2 - (\omega + i\eta)^2)} + \frac{1}{\omega_\ell} \qquad D-(9)$$

and summing over all occupied $\underline{k}$ values in the valence band, neglecting (η/ω) in the numerator, Eq. D-(8) becomes,

$$\tilde{\varepsilon}(\omega) = - \frac{e^2}{m^2} \sum_\ell \frac{2|\langle \ell|p_x|v\underline{k}\rangle|^2}{\hbar\omega_\ell(\omega - \omega_\ell + i\eta)(\omega + \omega_\ell + i\eta)}$$

$$- \frac{e^2}{m\omega^2} \sum_{\underline{k}} \left(1 - \frac{2|\langle \ell|p_x|v\underline{k}\rangle|^2}{m\hbar\omega_\ell}\right) \qquad D-(10)$$

The f-sum rule[100] states that

$$\sum_{\ell \neq n} f^x_{\ell n} = 1 - \frac{m}{\hbar^2} \frac{\partial^2 E_n}{\partial k_x^2} \qquad D-(11)$$

where the band from which transitions are taking place has been labeled by n, and where the f's are the oscillator strengths previously defined. Although the sum over ℓ was dropped at Eq. D-(7), it could have been retained, so that Eq. D-(10) becomes

$$\varepsilon(\omega) = \frac{e^2}{m} \sum_{\ell, \underline{k} \text{ occupied}} \frac{f^x_{\ell n}}{(\omega_\ell^2 - (\omega + i\eta)^2)}$$

$$- \frac{e^2}{\hbar^2 \omega^2} \sum_{\underline{k} \text{ occupied}} \frac{\partial^2 E_n}{\partial k_x^2} \qquad D-(12)$$

The last term is the free carrier term, in that if all the bands are full it would sum to zero. It is actually the same contribution to the dielectric constant as was discussed in Chapter 2 in the classical and Boltzmann equation treatment of infrared reflectivity. In order to see this easily, consider, for the moment, that we are treating a spherical conduction band with Fermi level at E_F. Then

$$\Sigma \frac{\partial^2 E}{\partial k_x^2} = \Sigma \frac{\partial^2 E}{\partial k_y^2} = \Sigma \frac{\partial^2 E}{\partial k_z^2} = \frac{1}{3} \Sigma \nabla_k^2 E \qquad D-(13)$$

Now the radial part of ∇^2 in spherical co-ordinates is $k^{-2}\,\partial/\partial k(k^2\partial/\partial k)$.

Thus converting the sum to an integral, and remembering that the density of states in k-space (including spin) is $(4\pi^3)^{-1}$, one has

$$\Sigma = \frac{1}{12\pi^3}\int \left(\frac{1}{k^2}\left[\frac{d}{dk}\left(k^2\frac{dE}{dk}\right)\right]\right) f \quad 4\pi k^2 dk \qquad D - (14)$$

where f is the Fermi-Dirac distribution. Integrating by parts, and then changing the variable from k to E, one has

$$\Sigma = -\frac{1}{3\pi^2}\int \left(k^2\frac{dE}{dk}\right)\frac{\partial f}{\partial E}\frac{dE}{dk}\,dE \qquad D - (15)$$

Since $(\partial f/\partial E)$ is effectively $-\delta(E - E_F)$, this becomes

$$\Sigma = \frac{1}{3\pi^2}\left(k^2\frac{dE}{dk}\right)_{E_F} \qquad D - (16)$$

However, the total number of occupied states N equals $k_F^3(3\pi^2)^{-1}$. Thus the free carrier term in D-(12) becomes

$$\tilde{\varepsilon}_{\text{free carrier}} = -\frac{Ne^2}{m_F^*\,\omega^2} \qquad D - (17)$$

where, as before, m_F^{*-1} has been defined as $\hbar^{-2}[\,k^{-1}(dE/dk)\,]_F$. The broadening of this term has been discussed by Ehrenreich,[101] and is done by changing ω^2 to $\omega(\omega + i\tau^{-1})$. Thus one has exactly the same result as is given in Chapter 2. However, whereas there, one considered, in the Boltzmann treatment, the change of the k values of states under the influence of a field $\mathcal{E}_o \exp(i\omega t)$, here one has treated the change by transitions out of the band into other bands. There is something revealing about this coincidence that the author does not appreciate.

References

1. E. O. Kane, J. Phys. Chem. Solids 1, 249 (1957).
2. E. O. Kane, Semiconductors and Semimetals, Vol. 1, edited by R. K. Willardson and A. C. Beer (Academic Press, New York, 1966), p. 75.
3. R. J. Elliott, Phys. Rev. 108, 1384 (1957).
4. D. D. Sell and P. Lawaetz, Phys. Rev. Lett. 26, 311 (1971).
5. G. G. MacFarlane, T. P. McLean, J. E. Quarrington, and V. Roberts, Proc. Phys. Soc., London 71, 863 (1958).
6. M. D. Sturge, Phys. Rev. 127, 768 (1962).
7. W. J. Turner, W. E. Reese, and G. D. Pettit, Phys. Rev. 136, A1467 (1964).
8. P. J. Dean, G. Kaminsky, and R. B. Zetterstrom, J. Appl. Phys. 38, 3551 (1967).
9. W. G. Spitzer and H. Y. Fan, Phys. Rev. 106, 882 (1957).
10. J. R. Dixon and J. M. Ellis, Phys. Rev. 123, 1560 (1961).
11. G. W. Gobeli and H. Y. Fan, Semiconductor Research, Second Quarterly Report, Purdue Univ., 1956.
12. I. G. Austin and D. R. McClymont, Physica 20, 1077 (1954).
13. F. Oswald and R. Schade, Z. Naturforsch. 9a, 611 (1954).
14. E. J. Johnson, Semiconductors and Semimetals, Vol. 3, edited by R. K. Willardson and A. C. Beer (Academic Press, New York, 1967), p. 154.
15. V. L. Bonch-Bruevich, see Reference 2, p. 101.
16. E. Burstein, Phys. Rev. 93, 632 (1954).

17. T. S. Moss, Proc. Phys. Soc. (London) B 67, 775 (1954).

18. G. W. Gobeli and H. Y. Fan, Phys. Rev. 119, 613 (1960).

19. N. V. Zotova, D. N. Nasledov, and L. D. Neuimina, Sov. Phys. - Semicond. 5, 1837 (1972).

20. M. Cardona, Solid State Physics, Suppl. 11, edited by H. Ehrenreich, F. Seitz, and D. Turnbull, (Academic Press, New York, 1969).

21. Semiconductors and Semimetals, Vol. 9, edited by R. K. Willardson and A. C. Beer (Academic Press, New York, 1972).

22. B. Batz, Solid State Commun. 4, 241 (1966).

23. B. Batz, Solid State Commun. 5, 985 (1967).

24. R. A. Smith, Semiconductors, (University Press, Cambridge, 1959).

25. W. G. Spitzer and J. M. Whelan, Phys. Rev. 114, 59 (1959).

26. M. Cardona, Phys. Rev. 121, 752 (1961).

27. L. L. Korenblit, D. V. Mashovets, and S. S. Shalyt, Sov. Phys. - Solid State 6, 438 (1964).

28. F. P. Kesamanly, Yu. V. Mal'tsev, D. N. Nasledov, L. A. Nikolaeva, M. N. Pivovarov, V. A. Skripkin, and Yu. I. Ukhanov, Sov. Phys. Semicond. 3, 993 (1970).

29. S. S. Shalyt, Sov. Phys. - Solid State 4, 1403 (1962).

30. M. Rodot, Solid State Phys. Electr. Telecom. 2, 689 (1960).

31. L. A. Kazakova, V. V. Kostsova, R. K. Karymshakov, Yu. I. Ukhanov, and V. P. Yagup'ev, Sov. Phys. - Semicond. 5, 1495 (1972).

32. C. R. Pidgeon, D. L. Mitchell, and R. N. Brown, Phys. Rev. 154, 737 (1967).

33. C. R. Pidgeon, S. H. Groves and J. Feinleib, Solid State Commun. 5, 677 (1967).

34. P. Lawaetz, Phys. Rev. B4, 3460 (1971).

35. D. E. Aspnes and A. Frova, Phys. Rev. B2, 1037 (1970).

36. W. A. Albers, Jr., Phys. Rev. Lett. 23, 410 (1969).

37. B. Ayrault, Thèse de Doctorat d'Etat à la Faculté des Sciences de Paris, 1970.

38. I. Balslev, Solid State Commun. 3, 213 (1965).

39. R. L. Aggarwal, Phys. Rev. B2, 446 (1970).

40. C. R. Pidgeon and R. N. Brown, Phys. Rev. 146, 575 (1966).

41. A. Baldereschi and N. O. Lipari, Phys. Rev. Lett. 25, 373 (1970).

42. O. Madelung, Physics of III-V Compounds (John Wiley and Sons, Inc., New York, 1964), Chapter 1.

43. E. Schillmann, Compound Semiconductors, Vol. I, Preparation of III-V Compounds, Eds. R. K. Willardson and H. L. Goering, (Reinhold Publishing Corp., New York, 1962), p. 390.

44. J. M. Ziman, Principles of the Theory of Solids (Cambridge University Press, 1965), Chapter 7.

45. J. Kolodziejczak and L. Sosnowski, Acta phys. Polon. 21, 399 (1962).

46. J. Kolodziejczak, Acta phys. Polon. 20, 379 (1961).

47. J. W. McClure, Phys. Rev. 101, 1642 (1956).

48. J. M. Ziman, Electrons and Phonons (Clarendon Press, Oxford, 1960), p. 501.

49. R. S. Allgaier, Phys. Rev. 165, 775 (1968).

50. R. S. Allgaier, Phys. Rev. B2, 3869 (1970).

51. W. K. H. Panofsky and M. Phillips, Classical Electricity and Magnetism, second edition (Addison-Wesley, Reading, Mass., 1962) p. 186.

52. M. Born and E. Wolf, Principles of Optics (Pergamon Press, New York, 1959), Chapter 1.

53. C. Kittel, Introduction to Solid State Physics (John Wiley and Sons, New York, 1956), second edition, pp. 236, 372.

54. R. P. Feynman, R. B. Leighton, and M. Sands, The Feynman Lectures on Physics, Vol. 2 (Addison-Wesley, Reading, Mass., 1964), Chapter 32.

55. S. Wang, Solid State Electronics (McGraw-Hill Book Co., New York, 1966), p. 130.

56. T. S. Moss, Optical Properties of Semiconductors, (Butterworths Scientific Publications, London, 1959), Chapter 2.

57. O. G. Lorimor and W. G. Spitzer, J. Appl. Phys. 36, 1841 (1965).

58. H. Y. Fan, Solid State Physics, edited by F. Seitz and D. Turnbull (Academic Press, New York, 1955), Vol. 1, p. 352.

59. H. J. Lippmann and F. Kuhrt, Zeitschrift fur Naturforschung 13 A, 474 (1958).

60. R. F. Wick, J. Appl. Phys., 25, 741 (1954).

61. H. J. Lippmann and F. Kuhrt, Zeitschrift fur Naturforschung 13 A, 462 (1958).

62. J. R. Drabble and R. Wolfe, J. Electronics and Control 3, 25[illegible] (1957).

63. T. M. Rodgers, Handbook of Practical Electroplating, (Macmillan New York, 1959), p. 196.

64. L. J. van der Pauw, Phillips Research Reports 13, 1; (1958).

65. G. Dionne, Ph.D. Thesis, University of Ottawa, 1971, p. 177.

66. R. R. Senechal and J. Basinski, J. Appl. Phys. 39, 4581 (1968).

67. E. Fortin, Rev. Sci. Instrum. 41, 1252 (1970).

68. C. C. Y. Kwan and J. C. Woolley, Can. J. Phys. 46, 1669 (1968).

69. T. S. Moss, T. D. F. Hawkins, and G. J. Burrell, J. Phys. C 1, 1435 (1968).

70. U. Zhumakulov, Sov. Phys. - Solid State 8, 2476 (1967).

71. B. O. Seraphin and H. E. Bennett, Semiconductors and Semimetals, Vol. 3, Eds. R. K. Willardson and A. C. Beer (Academic Press, New York, 1967). p. 499.

72. Yu. L. Ukhanov, Yu. V. Mal'tsev, Sov. Phys. - Solid State 5, 1124, (1963).

73. I. M. Nesmelova, L. L. Kremp and N. S. Baryshev, Sov. Phys. - Semicon. 2, 894 (1969).

74. G. Dionne and J. C. Woolley, Phys. Rev. B 6, 3898 (1972).

75. J. R. Dixon and H. R. Riedl, Phys. Rev. 138, A873 (1964).

76. H. R. Riedl, J. R. Dixon, and R. B. Schoolar, Phys. Rev. 162, 692 (1967).

77. R. F. Bis and J. R. Dixon, Phys. Rev. B 2, 1004 (1970).

78. W. Zawadzki, phys. stat. sol. 2, 385 (1962).

79. H. Ehreneich, J. Phys. Chem. Solids 2, 131 (1957).

80. S. Zukotynski and J. Kolodziejczak, phys. stat. sol. 3, 990 (1963).

81. M. J. Stephen and A. B. Lidiard, J. Phys. Chem. Solids 9, 43 (1959).

82. B. Lax and J. G. Mavroides, Phys. Rev. 100, 1650 (1955).

83. J. Kolodziejczak and S. Zukotynski, phys. stat. sol. 16, K55 (1966).

84. L. M. Roth, B. Lax, and S. Zwerdling, Phys. Rev. 114, 90 (1959).

85. E. Adachi, J. Phys. Soc. Japan 24, 1178 (1968).

86. C. W. Litton, R. B. Dennis, and S. D. Smith, J. Phys. C 2, 2146 (1969).

87. M. Cardona, Semiconductors and Semimetals, Vol. 3, Eds. R. K. Willardson and A. C. Beer (Academic Press, New York, 1967), Chapter 5.

88. D. D. Sell, Appl. Op. 9, 1926 (1970); D. E. Aspnes, Phys. Rev. Lett. 28, 168 (1972); D. E. Aspnes and A. A. Studna, Appl. Op. 10, 1024 (1971).

89. Y. Hamakawa, F. A. Germano and P. Handler, Phys. Rev. 167, 709 (1968).

90. M. Cardona, Solid State Physics, Suppl. 11, edited by H. Ehrenreich, F. Seitz and D. Turnbull, (Academic Press, New York, 1969), p. 104.

91. M. Cardona, K. L. Shaklee, and F. H. Pollak, Phys. Rev. 154, 696 (1967).

92. M. Garfinkel, J. J. Tiemann, and W. Engeler, Phys. Rev. 148, 695 (1966).

93. M. Cardona, Solid State Physics, Suppl. 11, edited by. H. Ehrenreich, F. Seitz and D. Turnbull, (Academic Press, New York, 1969), p. 59.

94. B. O. Seraphin and N. Bottka, Phys. Rev. 145, 628 (1966).

95. B. Batz, Reference 21, p.338.

96. H. Ehrenreich and M. Cohen, Phys. Rev. 115, 786 (1959).

97. F. Stern, Solid State Physics, Vol. 15, Eds. F. Seitz and D. Turnbull, (Academic Press, New York, 1963), p. 299.

98. C. N. Berglund, J. Appl. Phys. 37, 3019, (1966).

99. Reference 20, p. 11.

100. R. A. Smith, Wave Mechanics of Crystalline Solids, (Chapman and Hall, London, 1961), p. 464.

101. H. Ehrenreich, Optical Properties of Solids, edited by J. Tauc (Academic Press, New York, 1966), p. 106.

102. L. van Hove, Phys. Rev. 89, 1189 (1953).

103. B. Batz, Thermoréflectivité du Germanium, Thesis. Free University of Brussels, 1967.

104. P. M. Morse and H. Feshbach, Methods of Theoretical Physics (McGraw-Hill, New York, 1953), p. 408.

105. Indalloy Intermediate Solder #1, Indium Corp. of America, New York, U.S.A.

106. Silicone Super Heat Sink Compound, DC-Z9, No. 8109-S, (white); Silicone Compound, Transistor Z-5, No. 8101, GC Electronics, Rockford, Illinois, 61101, U.S.A.

107. R. L. Powell, M. D. Bunch, and R. J. Corruccini, Cryogenics, 1, 139 (1961).

108. R. Glosser and B. O. Seraphin, Phys. Rev. 187, 1021 (1969); R. Glosser, J. E. Fischer, and B. O. Seraphin, Phys. Rev. B 1, 1607 (1970).

109. J. B. Arthur, A. C. Baynham, W. Fawcett, and E. G. S. Paige, Phys. Rev. 152, 740 (1966).

110. E. J. Johnson, Semiconductors and Semimetals, eds. R. K. Willardson and A. C. Beer, (Academic Press, New York, 1967), Vol. 3, p. 154.

111. T. P. McLean and E. G. S. Paige, Proc. Int. Conf. Physics of Semiconductors, Exeter, 1962, p. 450.

112. E. Matatagui, A. G. Thompson, and M. Cardona, Phys. Rev. 176, 950 (1968).

113. J. I. Pankove, Phys. Rev. 140 A2059 (1965).

114. R. J. Elliott, Polarons and Excitons, edited by C. G. Kuper and G. D. Whitfield (Oliver and Boyd, Edinburgh, 1963), p. 269.

115. A. Baldereschi and N. O. Lipari, Phys. Rev. Lett. 25, 373 (1970).

116. A. Baldereschi and N. O. Lipari, Phys. Rev. B 3, pp. 439 and 2497 (1971).

117. G. Dresselhaus, Phys. Chem. Solids 1, 14 (1956).

118. J. O. Dimmock, Ref. 110, p. 259.

119. R. S. Knox, Solid State Physics, Suppl. 5, edited by F. Seitz and D. Turnbull, (Academic Press, New York, 1963).

120. W. Kohn and J. M. Luttinger, Phys. Rev. 97, 1721 (1955); ibid 98, 915 (1955); W. Kohn, Solid State Physics, Vol. 5, eds. F. Seitz and D. Turnbull, (Academic Press, New York, 1957), p. 258.

121. Ref. 100, p. 348.

122. D. E. Aspnes and N. Bottka, Ref. 21, p. 457.

123. D. Bierens de Haan, Nouvelles Tables d'Integrals Definies (Hafner Publishing Company, New York, 1957), p. 143.

124. Reference 104, p. 422.

125. L. Petrakis, J. Chem. Education (USA) 44, 432 (1967).

126. G. E. Pake and E. M. Purcell, J. Chem. Phys. 16, 327 (1948); Phys. Rev. 74, 1184 (1948); Phys. Rev. 75, 534 (1949).

127. B. Lax and S. Zwerdling, Progr. Semicond. 5, 221 (1960).

128. M. V. Hobden, Phys. Chem. Sol. 23, 821 (1962).

129. S. Antoci, E. Reguzzoni, and S. Samoggia, Phys. Rev. Lett. 24 1304 (1970).

130. J. E. Rowe and D. E. Aspnes, Phys. Rev. Lett. 25, 162 (1970).

131. Kodak Photo Resist, Type 3, Eastman Kodak Co., Rochester, N.Y.

132. Mechanics and Bearing Blue, R. M. Hollingshead Corp., Camden, N.J.

133. J. G. Mavroides, Physics of Solids in Intense Magnetic Fields, ed. by E. D. Haidemenakis (Plenum Press, New York, 1969), p. 206.

134. J. B. Ubbink, Physica 13, 659 (1947).

135. Bausch and Lomb Light Polarizing Film, Catalogue #31-52-62-28, Rochester, N.Y., 14602, U.S.A.

136. Polaroid Optical Retarder 280 mμ (315 mμ).

137. Duzall flux, Allstate Welding Alloys Co. Inc., P. O. Box 350, White Plains, N.Y. 10602, U.S.A. (supplied by Canox in Canada).

138. S. H. Groves, C. R. Pidgeon, and J. Feinleib, Phys. Rev. Letts. 17, 643 (1966).

139. M. V. Hobden, Phys. Letters 16, 107 (1965).

140. E. J. Johnson and H. Y. Fan, Phys. Rev. 139, A1991 (1965).

141. W. D. Dreybrodt, F. Willmann, M. Bettini, and E. Bauser, Solid State Commun. 12, 1217 (1973).

142. Recent references in Phys Rev. B related to excitons in semiconductors:
Phys. Rev. B8 (1973): "Lifetimes of Free and Bound Excitons in High Purity GaAs", C. J. Huang, p. 646.
Phys. Rev. B7 (1973): "Polariton Reflectance and Photoluminescence in High Purity GaAs", D. D. Sell, S. E. Stokowski, R. Dingle, and J. V. DiLorenzo, p. 4568; "Construction of Wannier Functions and Applications to Energy Bands", W. Kohn, p. 4388; "Perturbation Theory Investigation of the Exciton Ground State of Cubic Semiconductors in a Magnetic Field", M. Atarelli and N. O. Lipari, p. 3798. "Exciton Thermoreflectance of GaTe", D. Gili-Tos, M. Grandolfo, and P. Vecchia, p. 2565.
Phys. Rev. 6, (1972): "Screening of Excitons in Semiconductors" J. G. Gay, p. 4884; "Calculations of 2-p Exciton States in Semiconductors with Degenerate Bands", N. O. Lipari and A. Baldereschi, p. 3764; "Electroreflectance Line Shape Analysis", J. D. Dow, F. C. Weinstein, and B. Y. Lao, p. 3148; "Effective Electron-Hole Interactions in Polar Semiconductors", S. D. Mahanti and C. M. Varma, p. 2209; "Effective Electron-Hole Interaction in Polar Semiconductors", J. Sak, p. 2226; "Excitonic Effects in Landau Transitions at the E_1 Edges in InSb and GaSb", S. O. Sari, p. 2304; "Optics of Polaritons in Bounded Media", J. L. Birman, p. 2482; "Local Field Effects on Electroreflectance Line Shapes", R. M. Martin, J. A. Van Vechten, J. E. Rowe, and D. E. Aspnes, p. 2500; "Role of Generalized Wannier Functions in the Effective Hamiltonian Formalism for Magnetic Fields", F. A. Butler and E. Brown, p. 148.

143. Ref. 56, p. 85.

144. H. S. Bennett and E. A. Stern, Phys. Rev. <u>137</u>, A448 (1965).

145. ~~L. M. Roth, Phys. Rev. 133, A542 (1964).~~

146. I. G. Austin, J. Electronics and Control <u>6</u>, 271 (1959).

147. Ref. 104, p. 368.

148. J. Tauc, <u>Proceedings of the International School of Physics</u> "Enrico Fermi", Course 34, edited by J. Tauc (Academic Press, New York, 1966), p. 63.

149. Ref. 44, p. 216.

150. Ref. 25, p. 106.

151. A. Messiah, <u>Quantum Mechanics</u>, (North-Holland Publishing Co., Amsterdam, 1963), Vol. II, p. 725.

Publications of material in this thesis

"Measurement and Fit of Thermoreflectance Data of Ge at E_0,"

Phys. Rev. Letters 27, 1563 (1971).

"Redetermination of the Effective Mass in Heavily-Doped n-Type InAs,"

phys. stat. sol. (b) 59, K35 (1973).

"Some Formulae Related to the Application of the Kane Conduction Band to Measurements on III-V Semiconductors,"

phys. stat. sol. (a) 19, 251 (1973).

"Thermoreflectance at the Fundamental Gap of Heavily-Doped n-Type InAs,"

Phys. Rev. B 8, No. 12 (December 15, 1973).

"Comment utiliser le modèle de Kane d'une façon exacte" and "Mesures de thermoréflectance dans InAs de type n, dopé de 10^{18} a 6 x 10^{19} porteurs par cc," given at the 41st meeting of l'Association Canadienne-Française pour l'Avancement des Sciences, Université de Montréal, May, 1973.

The authors of the above publications were R. R. Senechal and J. C. Woolley